



UNIVERSITÄT  
DES  
SAARLANDES

A Comparison of Synthetic Strategies  
for the Synthesis of Metal Oxide  
Nanoparticles: Reactive Milling and  
Microjet Reactor Process

Dissertation

Zur Erlangung des Grades des Doktors der  
Naturwissenschaften der Naturwissenschaftlich-Technischen  
Fakultät III, Chemie, Pharmazie, Bio- und  
Werkstoffwissenschaften der Universität des Saarlandes

vorgelegt von  
Annika Betke

Saarbrücken,  
Juni 2014

Tag des Kolloquiums:	08.09.2014
Dekan:	Prof. Dr. Volkhard Helms
Berichterstatter:	Prof. Dr. Guido Kickelbick Priv. Doz. Dr.-Ing. Guido Falk
Vorsitz:	Prof. Dr. Michael Springborg
Akademischer Mitarbeiter:	Dr. Andreas Rammo

Die vorliegende Arbeit entstand in der Zeit von November 2011 bis Juni 2014 im Institut für Anorganische Festkörperchemie an der Universität des Saarlandes im Arbeitskreis von Herrn Prof. Dr. G. Kickelbick.

## Kurzzusammenfassung

Die vorliegende Arbeit untersucht systematisch Synthesemethoden für anorganische Nanopartikel. Im Mittelpunkt steht der Einfluss von Prozessparametern (Mahldauer/-geschwindigkeit bzw. Druck/Temperatur) auf die resultierenden Partikel. Es wird ein *top-down* Verfahren zur Synthese von Metalloxid-Partikeln mit *in situ* Oberflächenfunktionalisierung beschrieben. Es handelt sich um die Methode der Reaktivvermahlung, durchgeführt in einer Hochenergie-Planetenkugelmühle. Es konnte oberflächenmodifiziertes TiO<sub>2</sub> erhalten werden. Als Funktionalisierungsreagenz wurden verschiedene Organophosphonsäuren eingesetzt. Neben der Partikelzerkleinerung und Funktionalisierung konnte eine tribochemische Phasenumwandlung des eingesetzten Anatas zu Rutil und hochdruck-TiO<sub>2</sub> beobachtet werden. Die resultierenden Partikel zeigen Größen von 100 - 300 nm. Es konnte ein Funktionalisierungsgrad von bis zu 1,4 mmol/g Partikel erreicht werden.

Des Weiteren wurde ein kontinuierliches, nasschemisches *bottom-up* Verfahren zur Synthese von anorganischen Nanopartikeln auf seine Eignung zur Herstellung oxidischer Nanopartikel systematisch untersucht. Mit Hilfe eines Microjet Reaktors ist es möglich, sehr kurze Mischzeiten und ein sofortiges Entfernen der bereits entstandenen Partikel aus der Reaktionszone zu erzielen, sodass gleichmäßig geformte Partikel mit einer schmalen Größenverteilung erhalten werden. Es wurden Zinkoxid und Magnetit mit Größen von 44 - 132 nm und plättchenförmiger Brushit hergestellt.

## Abstract

This work investigates systematically synthetic strategies for inorganic nanoparticles. The main focus is the investigation of different process parameters (milling time/-speed or pressure/temperature) on the resulting particles. A *top-down* approach for the synthesis of inorganic metal oxide particles with *in situ* surface-modification is described, which is an application of reactive milling and can be performed in a high-energy planetary ball mill. Surface functionalized titania particles are obtained using various organophosphonic acids as surface-modifying agents. The process of particle size reduction and surface functionalization was accompanied by a tribochemical phase transformation from the starting material anatase to rutile and a high-pressure modification of titania. The obtained particles show sizes between 100 nm and 300 nm. A degree of surface coverage of up to 1.4 mmol/g particle could be reached.

Furthermore, a wet chemical, *bottom-up* approach for the continuous production of inorganic nanoparticles was investigated for its suitability for the preparation of oxide nanoparticles. By means of a microjet reactor very short mixing times and the instant separation of already formed particles from the reaction zone can be achieved. As a result, uniform particles with a small size distribution can be obtained. Applying this method, zinc oxide and magnetite with particle sizes between 44 nm and 132 nm as well as flaky brushite were produced.

# Table of Contents

<b>1. Introduction</b>	1
<i>1.1 Synthesis of Nanoparticles</i>	5
1.1.1 Top-down approaches	6
1.1.2 Bottom-up approaches	7
1.1.3 Surface Functionalization	12
<i>1.2 Novel synthetic strategies</i>	16
1.2.1 Reactive Milling	16
1.2.2 Microjet Reactor Process	23
<b>2. Research Goals</b>	32
<i>2.1 Reactive Milling</i>	32
<i>2.2 Microjet Reactor Process</i>	35
<b>3. Results and Discussion</b>	38
<i>3.1 Reactive Milling</i>	38
3.1.1 Synthesis of Surface Functionalized Titania Particles with Organophosphorus Coupling Agents by Reactive Milling	40
3.1.2 Important Reaction Parameters in the Synthesis of Phenylphosphonic Acid Functionalized Titania Particle by Reactive Milling	50
3.1.3 Long Alkyl Chain Organophosphorus Coupling Agents for <i>in situ</i> Surface Functionalization by Reactive Milling	60

3.2 <i>Microjet Reactor Process</i> .....	75
3.2.1 Bottom-up, wet chemical Technique for the Continuous Synthesis of Inorganic Nanoparticles .....	76
<b>4. Summary</b> .....	93
<b>5. Outlook</b> .....	100
<b>6. Literature</b> .....	101
<b>7. Supporting Information</b> .....	106
7.1 <i>Synthesis of Surface Functionalized Titania Particles with         Organophosphorus Coupling Agents by Reactive Milling</i> .....	106
7.2 <i>Important Reaction Parameters in the Synthesis of Phenylphosphonic         Acid Functionalized Titania Particle by Reactive Milling</i> .....	119
7.3 <i>Long Alkyl Chain Organophosphorus Coupling Agents for in situ         Surface Functionalization by Reactive Milling</i> .....	127
<b>8. Acknowledgment</b> .....	135

## 1. INTRODUCTION

In chemistry and materials sciences exist several ideas for the classification of materials. For instance, materials can be distinguished according to their application or their chemical composition. Another possibility is the classification of materials with respect to their dimension, i. e. from bulk material to nanoparticles. Particles with a size in the range between 1 nm and 100 nm are called nanoparticles. The notation “nano” has its origin from the Greek and means “dwarf”.

Nanoparticles have elicited plenty of interest in the last decades due to their wide field of applications. They have been identified as important compounds for many different fields such as medicine, optics and electronics or materials sciences for example.[1–4] The properties of a material are highly dependent on the size in which the material is present. Bulk material or large particles have completely different physical and chemical properties than nanoparticles of the same compound. Nanoparticles manifest particular properties which are very interesting for the improvement of various materials with respect to their field of application. These changes of material properties are primarily a result of variations in particle size.

In contrast to large particles or bulk material nanoparticles have an extended specific surface area and thus a high proportion of surface atoms. As a result, they exhibit a high chemical reactivity and unique properties.[5] For example, elemental gold reveals catalytic activity in nanoparticulate form with respect to the oxidation of CO to CO<sub>2</sub>, which is not present for the bulk metal.[6] The second reason for the differences in properties due to variation of particle size is the so called quantum size effect (Figure 1):

In molecular compounds energy levels can be described using the molecular orbital (MO) theory: For each bond in the respective molecule one bonding as well as one anti-bonding molecular orbital is created by a linear combination of the respective atomic orbitals. The molecular orbitals represent the discrete energy levels in a given molecule. If the number of atoms in a system increases, the number of bonding and anti-bonding MOs increases as well. This results in decreasing distances between the discrete energy states.



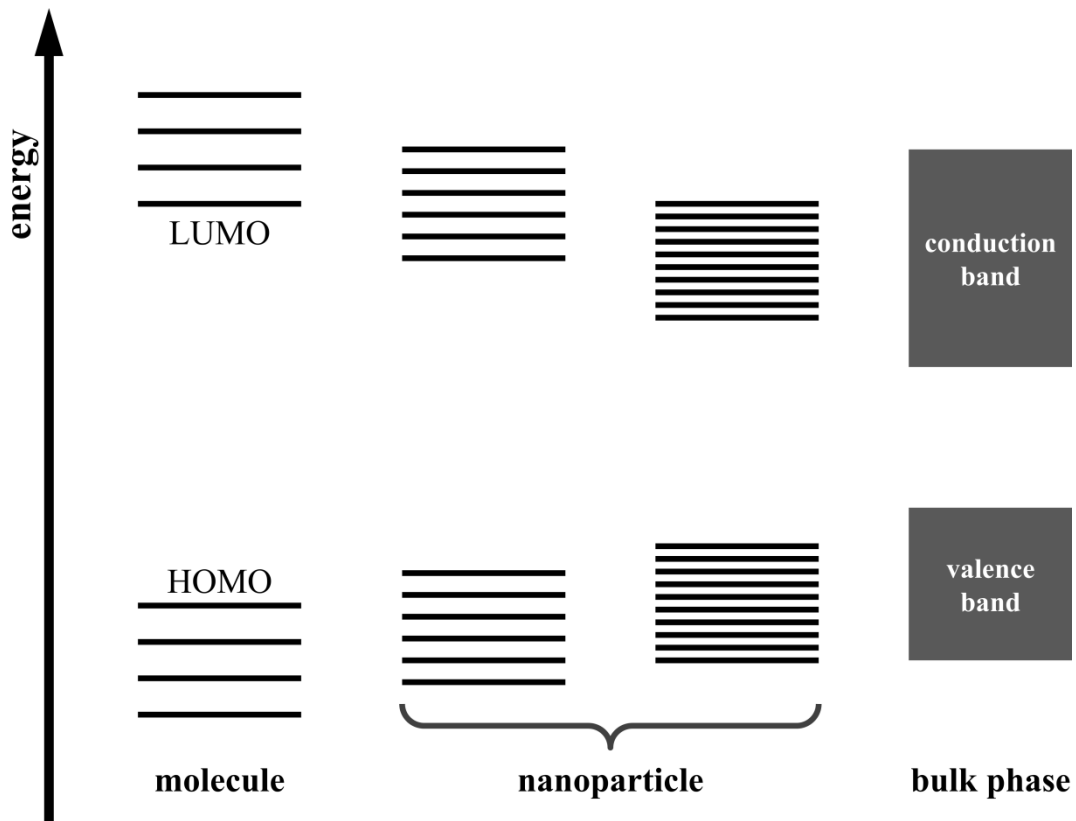


**Figure 1:** Quantum size effect: With increasing complexity in the respective system the number of molecular orbitals (MOs, dashes) increases and the energetic difference between them decreases. For bulk materials energy bands are formed by overlapping of the MOs. Nanoparticles are in the size range between bulk solids and molecules. They show discrete but densely packed energy levels as well as a size dependent gap between the highest occupied MO and the lowest unoccupied MO. For them the changes of material properties with decreasing particle size is caused by this relation of the energy gap in nanosized systems to its dimension.[7]

If the number of atoms in the system becomes large enough which is the case for bulk solid material, the distances between energy levels vanish by an overlap between the MOs. The overlapping bonding MOs form the valence band, the anti-bonding MOs form the conduction band. The electrons are delocalized over all bonding molecular orbitals. The distance between valence and conducting band is called “band gap” and has a major influence on the properties of a given solid compound.

Solids can be classified in three groups depending on their band gap and the resulting energetic difference between conduction and valence band: Isolators have a band gap of 4 eV or more (e. g. diamond 5.4 eV), electrons cannot be promoted into the conduction band therefore conduction of electric current is

impossible. For semiconductors the band gap ranges between 0.1 eV and 4 eV, electrons can be promoted into the conduction band by e. g. visible light or thermal energy. In case of metals there is no band gap, conduction band and valence band overlap.

The band gap equivalent (energy band model) for the MO theory is the distance of HOMO (highest occupied molecular orbital) and LUMO (lowest unoccupied molecular orbital) in molecular compounds.[8]

Nanoparticles are in the size range between bulk solids and molecular species. In contrast to bulk materials they exhibit discrete energy levels. However, the distance between them is rather small compared to molecular compounds, so the orbitals can almost be considered in terms of the energy band model. The changes of material properties with decreasing particle size is caused by a relation of the band gap in nanosized systems to its dimension.[5] This effect is only present if the size of the respective particle is below a critical point (~ 50 nm); in this case the band gap is size dependent and no material property anymore. This effect is nicely illustrated for CdS nanoparticles, which exhibit fluorescence in the visible light range. The emission wavelength can be tuned by the particle size. Consequently, the band gap structure which determines the energy needed for promoting electrons from valence to conducting band is dependent on the particle size.[9, 10]

In these days, nanoparticles are an indispensable part of everyday life. Many common products contain nanosized compounds already.

For example, nanosized titanium or zinc oxide is added to modern age sun creams. Due to their semiconducting behavior  $\text{TiO}_2$  and  $\text{ZnO}$  nanoparticles allow a conversion of hazardous UV radiation into visible light. Therefore, those creams show an improved sunprotection factor. In addition, sun creams containing nanosized particles do not deposit any white layer on the skin like conventional creams and show an improved spreadability.[11, 12]

Furthermore, the application of nanoparticles led to great advances in the area of renewable energies. For instance, solar cells can be produced based on  $\text{TiO}_2$ /dye composites at a lower price and better performance compared to silicon based modules.[13]

A further very important field of application for nanoparticles can be found in medicine. Particularly, gold nanoparticles are exposed to be very promising for various applications. Research is being conducted on their use for the treatment of cancer cells. Moreover, the use of nanoparticles as specific drug carrier is explored.[1, 14] As other examples magnetic nanoparticles lead to great advances in biomedical applications. For instance, uniformly sized iron oxide nanoparticles are investigated for their use as efficient magnetic resonance imaging contrast agent. Due to their biocompatibility, efficient contrast effects and versatile surface-modification capability they are suitable to increase the accuracy of magnetic resonance imaging.[15] Furthermore, magnetic nanoparticles lead to great progress in cancer therapy and diagnosis.[16]

A large field of application for nanoparticles is their use for the creation of nanocomposite materials.[17] Here nanosized inorganic particles are dispersed in an organic polymer matrix in order to improve the performance properties of the polymer. These materials have elicited plenty of interest in the automotive industry for example. Due to their lower rolling resistance, lower weight and superior performance in terms of fuel saving they entail a lot of beneficial properties. Furthermore, nanocomposites led to advances regarding to corrosion protection as well as fire resistance.[17]

There are many more possibilities for the construction of nanocomposites and therefore their field of applications if the nanoparticles surface is modified with suitable coupling agents.[18] Anti-fogging and self-cleaning applications are of great interest in various sectors. This has been made possible for instance by the modification of TiO<sub>2</sub> nanoparticles with polyethylglycol based coupling agents on silica.[19]

It becomes apparent that nanoparticles or rather nanotechnology have already allowed significant advances in various field of applications. For this reason there is a main focus on the synthesis of nanoparticles. Here, especially the control of particle size during particle synthesis is a major point of interest. Furthermore, economic and ecologic reasons are important incentives for the development of inexpensive and environmental friendly processes for nanoparticle synthesis.

## 1.1 SYNTHESIS OF NANOPARTICLES

There are two fundamental different strategies for the generation of nanoparticles (Figure 2). On the one hand, in *top-down* approaches nanoparticles are generated starting from a macroscopic structure. On the other hand, in *bottom-up* approaches nanoparticles are build up starting from molecular compounds.[20]

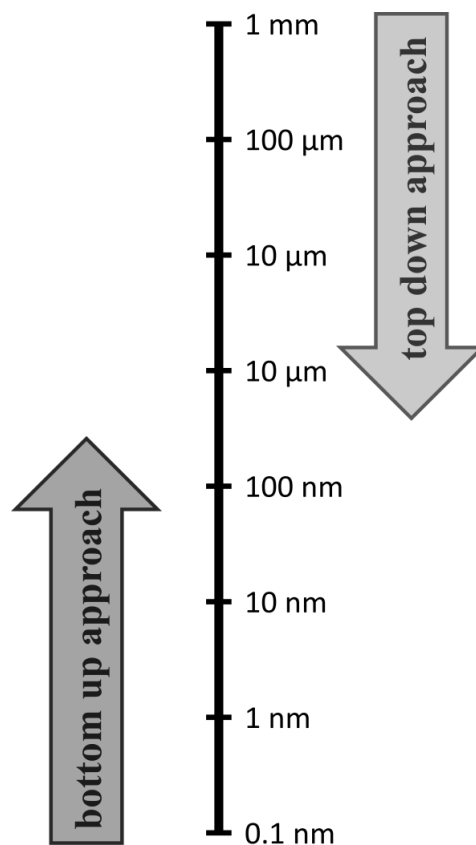


**Figure 2:** The two principles for the synthesis of nanoparticles: In case of *top-down* approaches nanoparticles are generated starting from a macroscopic structure. In contrast, *bottom-up* approaches build up nanoparticles starting from molecular precursors.

Not only has the synthesis of nanoparticles elicited plenty of interest but also their surface functionalization. Due to the surface functionalization particles interact less with each other but more with their environment. For instance, this is important for avoiding particle agglomeration or tuning the interactions between particle and dispersion medium. As a result, many more material combinations and applications are provided.[18]

### 1.1.1 TOP-DOWN APPROACHES

Synthetic strategies where nanoparticles are generated starting from a macroscopic structure are known as *top-down* approaches. The most common *top-down* approaches are the generation of nanoparticles by mechanical grinding or by laser ablation methods. Further possibilities for the use of *top-down* techniques are lithographic processes. Here no nanoparticles but rather nanostructures are generated, for example this approach can be used for the fabrication of modern electronic devices (computer chips).[21, 22]

*Mechanical grinding* induces a comminuting of particles to very small sizes by the input of mechanical energy and is limited to those materials which are not degraded due to the high-energy impact which is usually necessary. In addition, the obtained particles have a broad size distribution and often structure defects which are consequences of the mechanical treatment.

There are several types of milling devices, in which mechanochemical processes can be carried out, for example shaker mills, planetary mills, drum mills or vibratory mills. Each mill type offers variable milling efficiencies and capacities. However, in all mills the main acting forces are the same (Figure 3) but their combination is different.[23] Grinding of the material is conducted by three main processes: Impact of milling balls to a) each other and b) to the wall of the bowl results in a comminution of the material. Further grinding is achieved by shearing forces between milling balls and friction on the bowl wall.

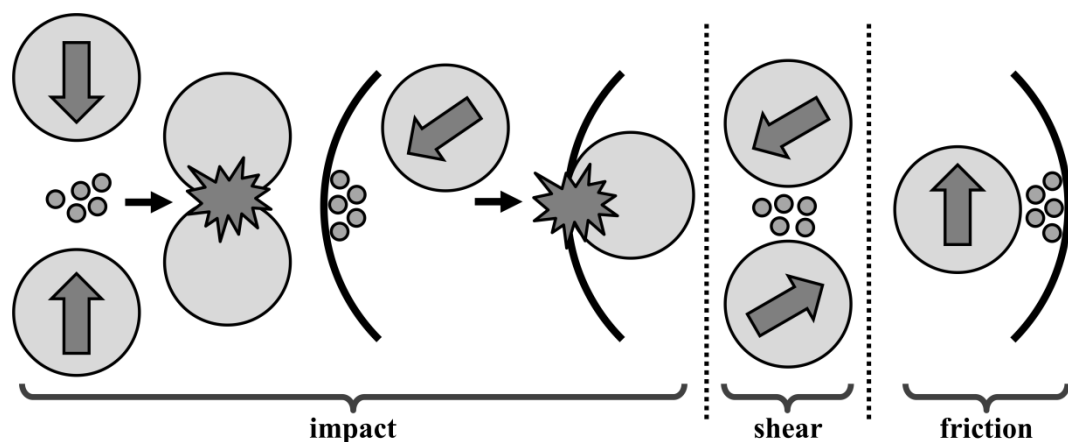


**Figure 3:** Main forces that act in a ball mill: Due to the course of movements of the mill there are impact, shear as well as friction forces which perform energy input on the sample.[23]

*Laser ablation* means removing material from a surface using a laser beam. Due to the absorbed laser energy the material is heated and evaporates or sublimates. An example for the field of application is the preparation of silver nanoparticles (Figure 4). A silver plate (>99.99% purity) is vertically placed in a beaker filled with acetone. The silver plate is irradiated with a pulsating laser operating at 10 Hz. The power of the laser is adjusted at 600 mJ/pulse. As a result, ablation occurs and nanoparticles of silver suspended in acetone are obtained. The obtained particles are spherical shaped with dimensions of about 100 nm.[24]

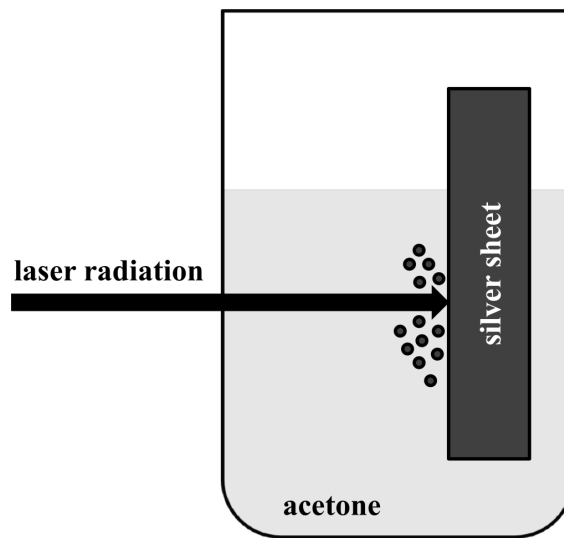


**Figure 4:** Generation of silver nanoparticles using laser ablation. A silver plate is placed in a beaker filled with acetone. The silver plate is irradiated with a laser and ablation occurs. As a result, nanoparticles of silver suspended in acetone are obtained.[24]

### 1.1.2 BOTTOM-UP APPROACHES

A great advantage of *bottom-up* approaches compared to *top-down* techniques is reaching a better size control as well as an improved size distribution. The most common *bottom-up* approaches are sol-gel, precipitation and hydrothermal processes. Furthermore, there are flame spray pyrolysis and hot-injection methods.

In case of *bottom-up* approaches the growth of the nanoparticles can be described using a kinetic theory which was formulated in 1950 by *LaMer* (Figure 5).[25] In the preparation of monodispersed hydrosols *LaMer* discovered that upon exceeding a critical concentration spontaneously nucleation to nanoparticles

occurs. Due to this supersaturation the nucleation rate is high enough that equal nuclei are formed in the whole reaction solution. A reduction of the supersaturation occurs till the nucleation rate has decreased to zero. The remaining supersaturation is degraded due to diffusion of the precursor to the nuclei which involves an increase in size of the resulting particles.

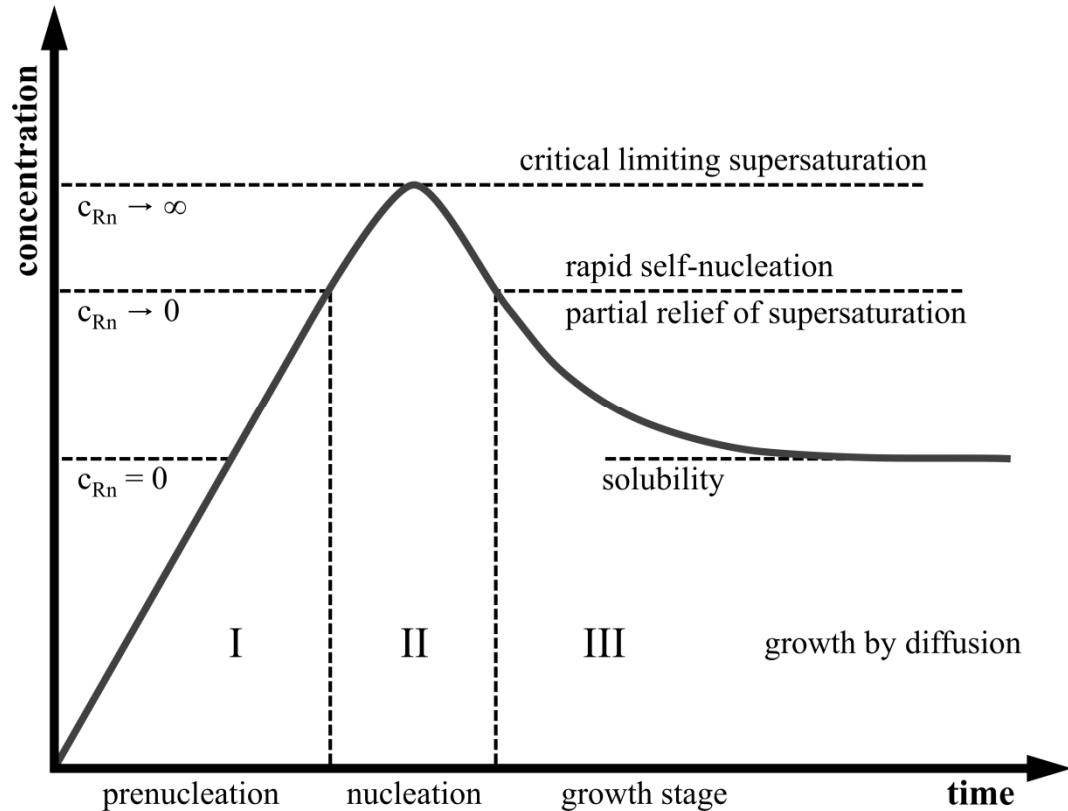


**Figure 5:** *LaMer* model: Kinetic theory for the description of the growth of nanoparticles. Particle generation can be separated in prenucleation, nucleation and growth stages. Above a critical concentration nucleation starts and reduces supersaturation. This process ends when the supersaturation reaches a critical point at which the rate of nucleation  $C_{Rn}$  drops to zero. From this point supersaturation is only further reduced to solubility level by growing of existing nuclei.[25]

However, the thermodynamic theory for the description of the growth of nanoparticles, the so called *Ostwald ripening*, signifies that the larger particles grow at the expense of the little ones (Figure 6).[26, 27] *Ostwald* ripening and the *LaMer* model have in common that particle generation starts with the nucleation of numerous nuclei. These small nuclei exhibit a large surface area which is unfavorable from a thermodynamic point of view. In *Ostwald's* theory a part of these nuclei dissolve again and the dissolved species are transported to other a little larger nuclei and crystallize there forming larger particles. Another

possibility is the agglomeration of smaller nuclei to larger particles. In the *LaMer* model the initial formation of numerous nuclei leads to a reduction of the supersaturation which decreases the rate of nucleation. When the supersaturation decreased enough no new nuclei are formed and the remaining supersaturation is dissipated by growing of the present nuclei until the solubility concentration of the respective material is reached. The thermodynamic instability of smaller particles compared to larger ones leading to higher dissolution rates for smaller particles is not considered in the *LaMer* theory.

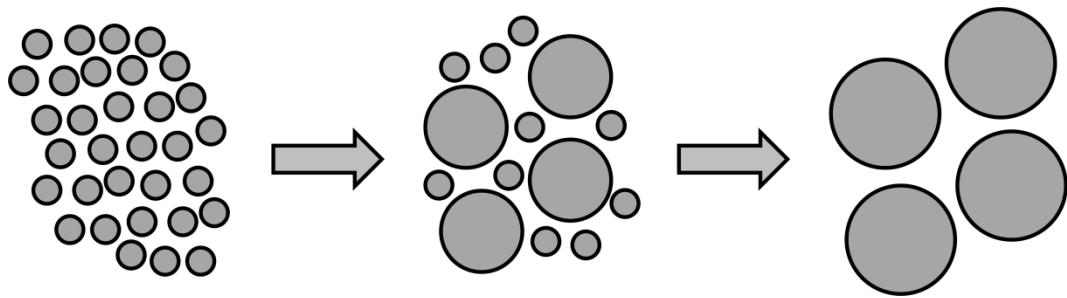
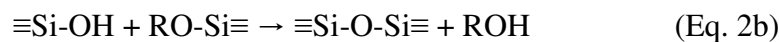
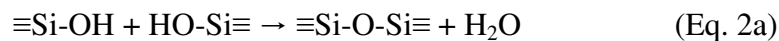
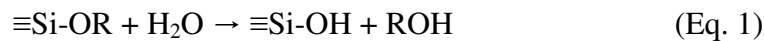


**Figure 6:** *Ostwald* ripening: Thermodynamic theory for the description of the growth of nanoparticles which signifies that the larger particles grow at the expense of the little ones.

The *sol-gel process* consists of two steps: The hydrolysis and condensation of a precursor. Here, usually metal alkoxides are used. A colloidal solution is formed (sol) which further condensates to an integrated network (gel). A typical application is the synthesis of SiO<sub>2</sub> nanoparticles, known as the *Stöber*-process. Monodisperse silica nanoparticles are obtained by the hydrolysis of tetraethylorthosilicate (Equation 1) followed by condensation of the formed silanol species (Equation 2a and b).

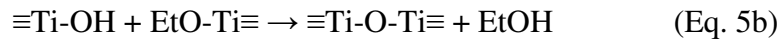
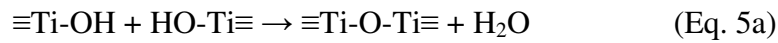
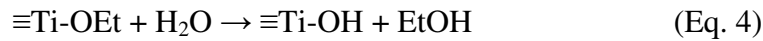
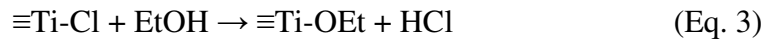


Ammonia is used as catalyst causing the formation of spherical particles. Dependent of the process parameters particles with sizes between 5 nm and 200 nm and a narrow size distribution are obtained. The particle size could be

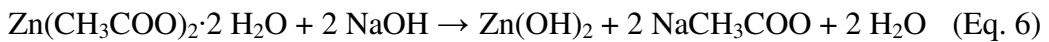


regulated by means of the final pH of the reaction solution as well as the used solvents and the ratio of the used components.[28]

Another example is the preparation of nanosized titania in the anatase phase. Titanium tetrachloride in ethanol is used as precursor solution, which is gelatinized for several days to form a  $\text{TiO}_x(\text{OH})_{4-2x}$  gel (Equation 3-5). This hydrogel solution is then dried at 80 °C to a xerogel. Finally, the xerogel can be calcined to a  $\text{TiO}_2$  nanopowder. The obtained particles reveal grain sizes about 10 nm.[29]



*Hydrothermal synthesis* can be described as the preparation of nanoparticles from an aqueous precursor solution. The reaction takes place at elevated temperature in a sealed autoclave under autogenous pressure. A typical application is the synthesis of ZnO nanoparticles using zinc acetate dihydrate as precursor (Equation 6, 7). Therefore zinc acetate dihydrate and sodium hydroxide were dissolved in methanol respectively. The NaOH solution was added under continuous stirring to the  $\text{Zn}(\text{CH}_3\text{COO})_2 \cdot 2\text{H}_2\text{O}$  solution. This reaction mixture was then transferred into a teflon lined sealed stainless steel autoclave. The particle size and morphology can be adjusted by the reaction temperature and the precursor concentration.[30]



*Flame spray pyrolysis* is a continuous approach for the synthesis of nanoparticles. A well known application is the AEROSIL process (Evonik), the industrial production of  $\text{SiO}_2$  nanoparticles. A solution containing silicon tetrachloride as precursor is sprayed into a hot zone containing the reaction gas (oxyhydrogen gas) and reacts with the  $\text{H}_2\text{O}$  formed from  $\text{H}_2$  combustion (Equation 8) to silica and

hydrogenchloride (Equation 9) (Figure 7). The size of the obtained particles can be controlled by the droplet size.[31]

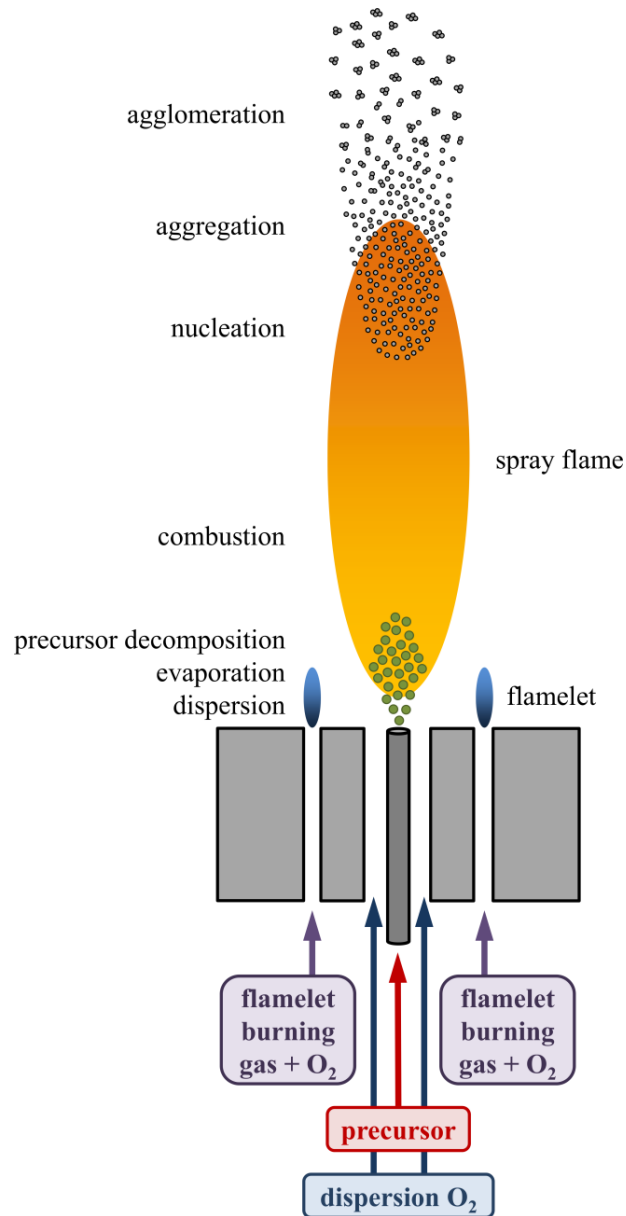


**Figure 7:** Principle setup for the generation of nanoparticles using flame spray pyrolysis. A precursor solution is sprayed into a hot zone containing the reaction gas. After combustion of the precursor particles are formed by subsequent nucleation, aggregation and agglomeration processes. A crucial influence on the final particle size is attributed to the droplet size of the precursor solution.[32]

The *hot-injection method* for the synthesis of nanoparticles enables the separation of the nucleation stage from the growth steps which benefits the generation of monodisperse particles. This approach is based on the thermal decomposition of an organometallic precursor in the presence of an organochalcogen compound and stabilizers. The organometallic precursor and the stabilizer are heated in a high boiling solvent. If the reaction temperature has reached values between 100 °C and 300 °C the organochalcogen compound is added. As a result, the reaction solution becomes supersaturated and colloidal nanoparticles are precipitated. The particle size can be adjusted by the reaction time. If the desired size is reached the reaction mixture is cooled.

A typical example for the use of the hot-injection method is the generation of CdS or CdSe nanocrystals. Cd-salts are heated in high boiling solvents in presence of organosulfur or organoselenium compounds as chalcogenide source and phosphines or long chain carboxylic acids as stabilization agents for the obtained particles of CdS/CdSe. Using this method, CdS/CdSe nanocrystals with sizes between 1.2 nm and 12 nm can be obtained.[33]

### 1.1.3 SURFACE FUNCTIONALIZATION

In these days, the requirements on a specific material are more and more demanding, for example with respect to decreasing weight with maintaining mechanical stability. In order to fulfill these requests it is necessary to develop composite materials which combine the beneficial properties of two or multiple material classes in one composite material. Properties of polymer based materials can be improved by the inclusion of inorganic compounds in (nano)particular form, e. g. for increasing the index of refraction or gas permeability.[34] The unique properties of composites result from the amount of interface between inorganic and organic phase. Therefore, the use of compounds in nanoparticluar form is preferable against bulk material or large particles due to the enhanced amount of surface area. In general it is important that the inorganic particles are dispersed homogenously and formation of clusters and agglomerates has to be avoided.

For the preparation of organic-inorganic composite materials the surface functionalization of the respective inorganic particles is an important parameter in

order to enable the combination of polar inorganic (nano)particles with unpolar organic polymer matrices. The goal is to decrease the interactions between the particles in order to avoid agglomeration or aggregation, as the benefit of nanoparticles is only apparent if they are dispersed uniformly in the polymer matrix. Simultaneously, an increase of the interaction between the particles and their environment is preferable.

The most common method of particle functionalization is the post-modification approach where nanoparticles are treated with a coupling agent independent of their synthesis. The nanoparticles are dispersed in an appropriate solvent and then mixed with a coupling agent at room temperature or under reflux.[35–37]

Particles can be modified with many different coupling agents. Such surface-modifying agents typically consist of an anchor group, a spacer moiety and a functional group (Figure 8).

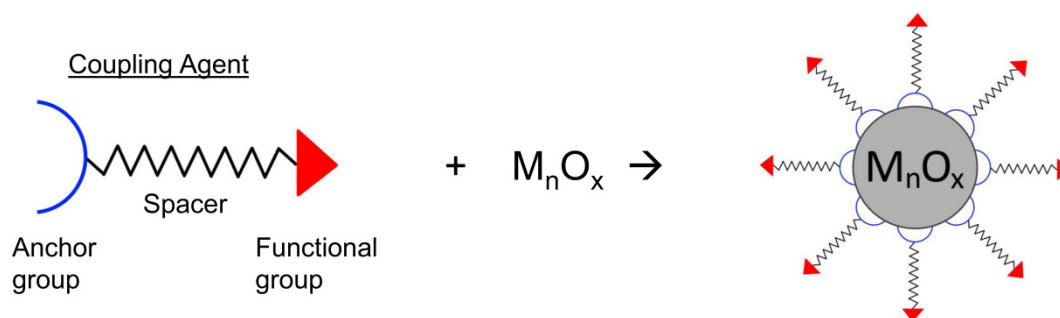
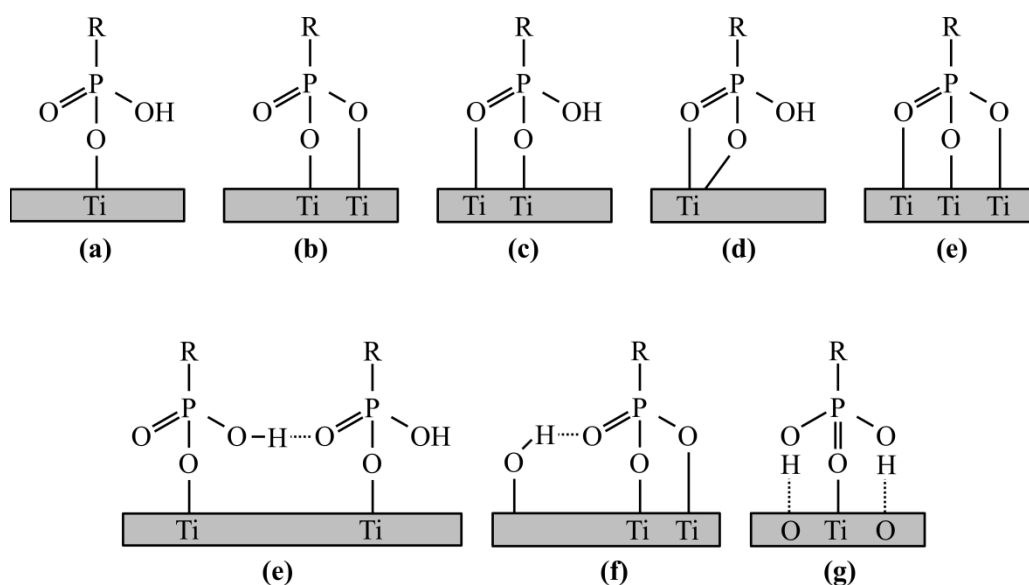


**Figure 8:** Principle of surface functionalization: A surface-modifying agent consisting of an anchor group, a spacer and a functional group is bonded at the surface of a particle.

The anchor group is responsible for a stable attachment of the surface-modifying agent to the surface of the inorganic particles. The spacer which is in most cases an alkyl chain is responsible for the polarity of the coupling agent and influences the interaction with the polymer medium for example. The functional group allows further chemical reactions, e.g. taking part in polymer crosslinking reactions for additional fixing of the particle in the polymer matrix. However, it also can be just an inert end group.[38]

Popular surface-modifying agents are organophosphorus species. They are known to form strong covalent bonds to many oxides, especially for transition metal oxides, e. g.  $TiO_2$  and  $ZrO_2$ . [39] A widely used model system is the functionalization of titania surface with organophosphonic acids. The chemical character of the binding between organophosphonic acids and titania surface has

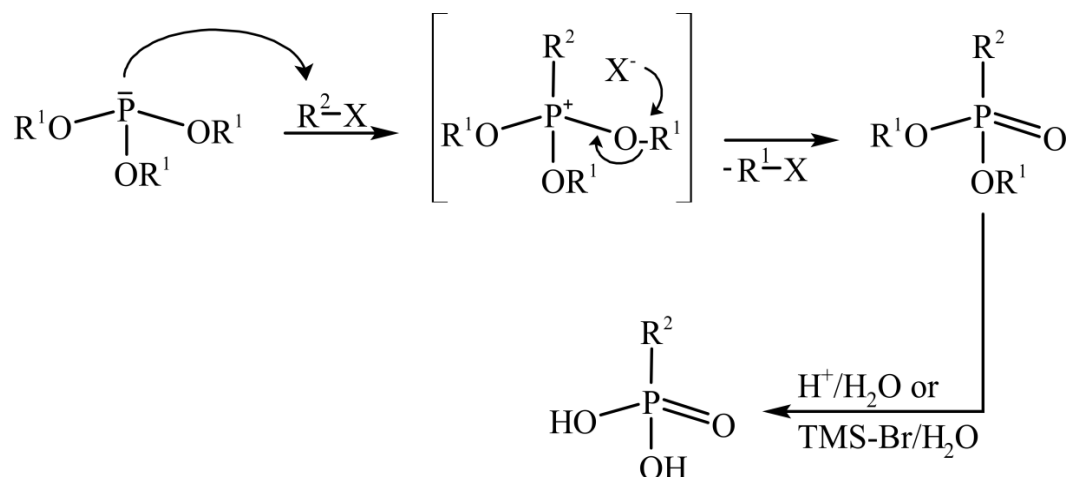
been studied already. Organophosphonates can bind towards the oxide surface utilizing a variety of binding modes: monodentate, bidentate, tridentate as well as numerous binding modes with additional hydrogen-bonding interactions (Figure 9).[40] This diversity of possible coordination modes is manifest in the  $^{31}\text{P}$  solid state NMR spectra of phosphonate functionalized particles. Usually, several bands can be observed related to the different binding modes. For the formation of the Ti-O-P bond surface hydroxyl groups are necessary due the fact that this bonding is a result of a condensation reaction between those Ti-OH groups and the P-OH moieties of the coupling agent.



**Figure 9:** Possible binding modes of phosphonates: (a) monodentate, (b, c) bridging bidentate, (d) chelating bidentate, (e) bridging tridentate, (f-h) additional hydrogen-bonding interactions.[40]

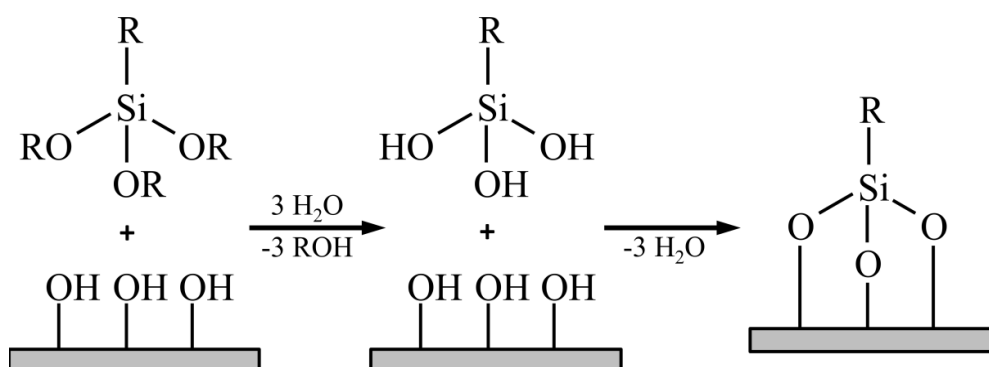
The synthesis of organophosphonic acids can be performed using the *Michaelis-Arbusov* rearrangement which is the reaction of a trialkyl phosphite,  $\text{P}(\text{OR}^1)_3$ , with an organic halide,  $\text{R}^2\text{X}$ . The organic group of the halide gets attached to the phosphorus atom forming an intermediate of the type  $[\text{R}^2\text{P}(\text{OR}^1)_3]^+\text{X}^-$ . Subsequently, the halide ion attacks one of the alkoxy moieties forming a new alkyl halide  $\text{R}^1\text{X}$  and the respective organophosphonic acid dialkyl ester  $\text{R}^2\text{PO}(\text{OR}^1)_2$ . The *Michaelis-Arbusov* reaction can be performed with a variety of organic halides (e. g.  $\text{R}^1 = \text{alkyl-}, \text{alkenyl-}, \text{aryl-}$ ), for halides of lower reactivity (aryl halides) the presence of a catalyst (e. g. Ni-salts) is necessary.[41]

The corresponding phosphonic acid is generated from the organophosphonic acid dialkyl ester by acidic hydrolysis. If the newly introduced organic moiety  $R^2$  is not inert under these conditions the phosphonate ester can be reacted with trimethylsilyl bromide followed by an aqueous hydrolysis of the intermediately formed trimethylsilyl phosphonate (Figure 10).[42]



**Figure 10:** *Michaelis-Abruzov* rearrangement: A trialkyl phosphite,  $\text{P}(\text{OR}^1)_3$ , reacts with an organic halide,  $\text{R}^2\text{X}$ , forming an intermediate of the type  $[\text{R}^2\text{P}(\text{OR}^1)_3]^+\text{X}^-$ . The halide ion attacks one of the alkoxy moieties forming a new alkyl halide  $\text{R}^1\text{X}$  and the respective organophosphonic acid dialkyl ester  $\text{R}^2\text{PO}(\text{OR}^1)_2$ . Afterwards the resulting ester is hydrolyzed to form the corresponding phosphonic acid.

Another example for a surface-modifying agent of wide ranging application are organosilanes  $\text{R-SiX}_3$  ( $\text{X}$  = reactive functional group, e. g.  $\text{Cl}$  or alkoxide). They are often used for the modification of  $\text{SiO}_2$  particles. Here, strong covalent  $\text{Si-O-Si}$  bonds are formed by the condensation of  $\text{Si-OH}$  moieties on the particle surface with reactive anchor groups of the coupling agent molecule. Surface hydroxyl groups are required for this attachment (Figure 11).[43]

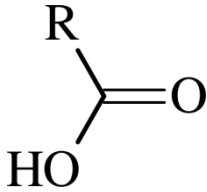
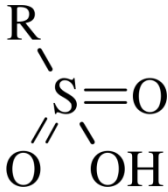
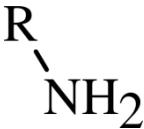


**Figure 11:** Attachment of an organosilane coupling agent on the surface of  $\text{SiO}_2$  particles. Surface hydroxyl groups are required to form strong  $\text{Si-O-Si}$  bonds.[43]

Organosilane coupling agents are also used for the functionalization of transition metal oxides but in this case the Si-O-M bond is usually not very stable against hydrolysis. For this reason in such cases nowadays organophosphorus coupling agents are preferred against the silanes.[39]

Further potential coupling agents especially for metal oxides are carboxylic acids, sulfonic acids or amines, to mention only three out of many. The following table (Table 1) gives an overview on their structure and applications.

**Table 1:** Overview on selected surface-modifying agents and examples for typically substrates for their application.

	carboxylic acids	sulfonic acids	amines
Structure			
Substrates	Ag <sub>2</sub> O[44], Al <sub>2</sub> O <sub>3</sub> [44]	Fe <sub>2</sub> O <sub>3</sub> [45], SiO <sub>2</sub> [46]	SiO <sub>2</sub> [46], Pd[47]

However, the attachment of these molecules to the particle surface is usually performed by electrostatic interactions and covalent bonds are formed to a lesser extent.[48] This results in a more labile binding of these coupling agents to the particles. Therefore, modification of inorganic oxide particles is usually performed with silanes or organophosphorous compounds.

## 1.2 NOVEL SYNTHETIC STRATEGIES

### 1.2.1 REACTIVE MILLING

Mechanical grinding not only means the reduction of particle sizes but also the generation of large surfaces, phase transformations and chemical reactions. Once a chemical reaction occurs during the mechanical grinding the process is called reactive milling.

In most cases a high-energy ball mill is used. The notation has its origin in the movements which are like those of planets (Figure 12). The grinding bowl is fixed at a plate and rotates around its own center in opposite direction to the rotation of the plate. As a result, centrifugal forces are generated which are responsible for

the movements of the milling balls. The milling balls first move along the grinding bowl wall, then freely fall through the grinding bowl and bounce to the opposite container wall. Thus, a high-energy impact to the sample can be reached. The energy impact can be controlled by means of various process parameters. Milling time as well as the rotational speed have a crucial influence on the overall energy impact. In addition, here it is to consider that the temperature increases with enhanced milling time and rotational speed. The required milling time for a mechanochemical reaction is reduced with increasing temperature as the diffusivity in the system is enhanced. Other parameters which influence the energy input are the grinding bowl material and the kind of grinding balls. The higher the density of these materials the higher is the energy impact on the sample due to higher collision energy. As a result, the reaction time is reduced. Furthermore, the ball to powder ratio and the filling level of the grinding bowl play an important role with respect to the resulting energy input. In addition, the mechanochemical process can be influenced by the use of a process control agent. This additive can slow down the reaction rate and therefore make the reaction more controllable. A further point that has to be considered is the contamination of the sample during the milling process. Such impurities can have their origin due to abrasion of the grinding sphere material but also the use of a process control agent can entail impurities.[49]

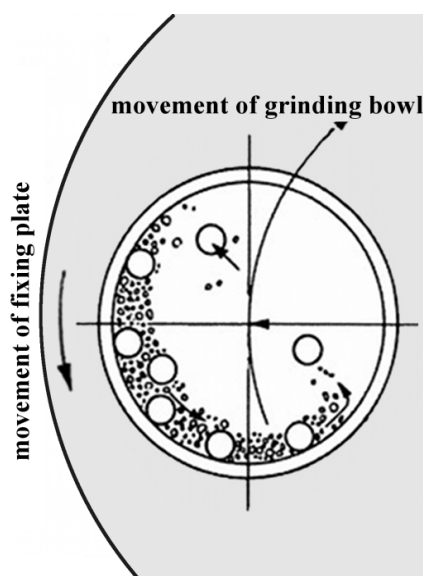


**Figure 12:** Characteristic movements in a planetary ball mill. The grinding bowl is fixed on a plate and rotates around its own center of gravity in opposite direction to the rotation of the plate. As a result, centrifugal forces are generated which are responsible for the movements of the milling balls.[49]



Reactive milling has elicited plenty of interest particularly due to the fact that it is a solvent free and therefore environmentally friendly approach.[50–53] Previously, it was mainly used for inert oxide compounds and the synthesis of multicomponent oxides.[23] For example, the dielectric material  $\text{ZrTiO}_4$  can be obtained by milling an equimolar mixture of  $\text{TiO}_2$  and  $\text{ZrO}_2$ . The reaction was performed in air using a vial and balls made of zirconia. The balls had a diameter of 1 cm and a powder-to-ball weight ratio of 1:10 was used. The milling time was varied between 10 min and 10 h with a rotational speed of 500 rpm. The results show that milling times shorter than 2 h induce no reaction between  $\text{TiO}_2$  and  $\text{ZrO}_2$  but a phase transition from anatase  $\text{TiO}_2$  to a high-pressure modification. Milling times between 2 h and 5 h lead to a formation of solid solutions. After milling for 5 h or longer the reaction between  $\text{TiO}_2$  and  $\text{ZrO}_2$  takes place and  $\text{ZrTiO}_4$  is formed. Due to the strong forces that act in a ball mill, the resulting products may be characterized by their small particle sizes as well as the presence of inconvenient metastable phases or structure defects.[54]

Another example is the mechanochemical synthesis of  $\text{BiFeO}_3$  nanoparticles. As starting materials  $\text{Bi}_2\text{O}_3$  and  $\alpha\text{-Fe}_2\text{O}_3$  were used in stoichiometric proportions. The milling chamber and balls used were made of tungsten carbide. The balls had a diameter of 10 mm and a ball-to-powder weight ratio of 22:1 was used. The milling time was varied up to 12 h with a rotational speed of 600 rpm. Milling the starting materials up to 1 h just lead to a broadening of the starting material reflections in the XRD pattern. An increase of the milling time induces a consistent decrease of the diffraction reflections corresponding to the starting materials. Simultaneously new diffraction reflections corresponding to  $\text{BiFeO}_3$  arise. After milling 12 h the mechanochemical induced reaction is complete and nanostructured  $\text{BiFeO}_3$  with particle sizes between 5 nm to 40 nm was obtained.[55]

Meanwhile, reactive milling has been used for a couple of different reaction types. For instance, reactive milling can be used for the production of metal nanoparticles by the reduction of their chlorides. Dry milling of metal chlorides  $\text{M}^*\text{Cl}_n$  together with an electropositive metal M leads to nanoparticles of the corresponding metal  $\text{M}^*$  (Equation 10). The metal chloride  $\text{MCl}_n$  formed as side-product can be easily leached from the nanoparticles. The following equation demonstrates the general reaction process.

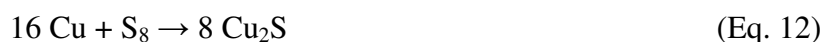


This approach has been shown to be successful for  $M = \text{Na, Mg, Ca, Al, Si, Ti, Ni}$  and  $M^* = \text{Ti, V, Zr, Cr, Fe, Co, Ni, Cu, Zn, Ta, Sm, Gd, Er}$ .<sup>[56]</sup> A typical example is the generation of magnetic samarium nanoparticles by milling samarium chloride with sodium:



The reaction was carried out in a sealed hardened steel vial and corresponding milling balls. The balls had a diameter of 10 mm and a ball-to-powder weight ratio of 10:1 was used. The starting materials were transferred into the milling media in a high purity argon glovebox. The reductant was used in a 15% excess. The milling process was carried out for 16 h. The influence of the milling time has not been investigated.<sup>[57]</sup>

Another field of application of reactive milling is the generation of metal sulfides by milling metals and sulfur. The S-S bonds can be broken upon milling and different oxidation states of the metal can be reached depending on the stoichiometry of the starting materials. A typical example is the milling of sulfur with copper:

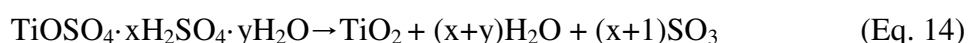


The reaction occurs rapidly and quantitatively. By variation of the stoichiometry between Cu metal and sulfur the sulfides of  $\text{Cu}^{\text{I}}$  as well as  $\text{Cu}^{\text{II}}$  can be prepared (Equation 12, 13).<sup>[58]</sup>

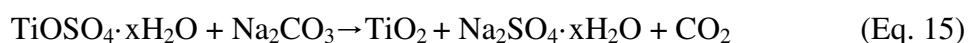
An example for the preparation of an organometallic compound is the mechanochemical synthesis of *ortho*-functionalized triarylbismuthanes which are difficult to access by conventional wet routes. Milling *o*-substituted aryl iodides with bismuth in the presence of Cu and CuI as catalysts *tris*-(2-*R*-aryl)bismuthanes are obtained. The reaction was carried out at room temperature in a laboratory ball mill and a reaction time of 6 h or 12 h was used. After milling for 12 h the yield was higher than after milling for 6 h. However, no further optimization of the milling parameters with respect to a complete conversion of the starting materials was performed.<sup>[59]</sup>

Futhermore, reactive milling has been used for the preparation of quite sensitive materials like metal hydrides. Calcium hydride could be obtained by milling calcium and phenylphosphonic acid under an inert atmosphere. A 50 ml milling vial and 200 milling balls with a diameter of 5 mm both made of tungsten carbide were used. The milling was performed with 250 rpm for 24 h or 48 h. After milling for 24 h the reaction was not complete but this was the case after milling for 48 h. The obtained small particles are highly efficient for the uptake and release of hydrogen, which has attracted attention for the storage of hydrogen.[60]

The main focus of this work was reactive milling of titania. The mechanochemical synthesis of titania nanoparticles has been reported in literature already. As starting material titanyl sulfate was used and sodium chloride was added as inert diluent phase. The reaction was performed in a planetary ball mill under argon atmosphere with a rotational speed of 400 rpm for 4 h. The milling balls were made of stainless-steel. Milling balls with a diameter of 20 mm and 10 mm and a ball-to-powder ratio of 10:1 were used. After the milling process the obtained powder was annealed at temperatures between 600 °C to 900 °C. The final particles exhibit sizes in a range of 15 nm to 50 nm. The mechanochemical formation of TiO<sub>2</sub> during the milling process is described in the following equation:



Prior the annealing step the as milled powder is not crystalline. The annealing temperature influences the crystalline phase of the obtained titania. An annealing temperature of 600 °C lead to the formation of the anatase phase of titania. Annealing temperatures of 700 °C or higher result in the formation of the thermodynamically more stable rutile phase.[61] Another possibility for the mechanochemical synthesis of titania nanocrystals is the use of TiOSO<sub>4</sub> · xH<sub>2</sub>O and Na<sub>2</sub>CO<sub>3</sub> as starting materials:



The reaction was carried out in a high-energy ball mill with grinding vials and balls made of steel or corundum. To obtain the final product the milling process was followed by an annealing step. Using the milling media made of steel an

annealing temperature of 300 - 600 °C lead to anatase. The stability of the anatase phase is increased up to 700 °C when the corundum milling media was used. Milling in the corundum vial followed by annealing at 600 and 700 °C results in final particle with sizes in the range of 20 - 50 nm.[62]

The behavior of titania during high-energy milling has been studied already as well. The experiments were performed in a modified Szegvari attritor. Milling balls made of tungsten carbide with a diameter of 4.76 mm and a ball-to-powder weight ratio of 60:1 was used. The milling process was conducted with a speed of 600 rpm and the milling canister was cooled with circulation water during the milling processes. As starting material anatase TiO<sub>2</sub> particles with a diameter of about 0.2µm were used. After milling for 1.5 h the crystallite size of anatase is in the nanometer range already. It has been observed that the crystallite size decrease constantly with increasing milling time. Furthermore, a phase transformation of anatase TiO<sub>2</sub> to rutile and srilankite is described taking place due to the energy impact during the milling process. This phase transition is dependent on the milling time: The degree of phase transition increases with increasing milling time. In addition, the milling process induces an amorphization of titania but at once a crystallization of the amorphous phase. Furthermore, the effect of the addition of graphite was investigated. Due to lubrication effects the addition of graphite results in a decrease of phase transformation as well as amorphization. After the milling process the samples show nanocrystalline dimensions, large specific surface areas as well as a high amount of structure defects.[63]

Further studies have been conducted regarding to the ball mill induced phase transformation in anatase TiO<sub>2</sub>. The effects of the milling time and the powder to ball weight ratio as well as the influence of the nature of the grinding media have been investigated. The experiments were performed in a planetary ball mill. The rotational speed was adjusted at 710 rpm for the disc and 1420 rpm for the vials. Grinding vials (45 cm<sup>3</sup>) and balls (diameter = 15 mm) made of steel or alumina were used. The powder-to-ball weight ratio was varied from 1:40 to 1:10. As starting material anatase TiO<sub>2</sub> was used. These particles were monocrystalline with a bimodal size distribution which reveal sizes around 0.15 µm and 0.9 - 1 µm. It turned out that the particle sizes as well as shapes are stable up to a milling time of 15 min. Applying longer milling times the particles tend to

agglomerate and there are slight changes in the shape. The milling process induces a phase transformation from anatase to high-pressure TiO<sub>2</sub> and rutile. After milling 90 min or longer rutile is the only species remaining. The diffraction pattern corresponding to high-pressure TiO<sub>2</sub> is observable after milling for 5 min already but their intensity passes through a maximum. First the amount of high-pressure TiO<sub>2</sub> increases with the milling time but further enhancement of the milling time lead to a decrease of the high-pressure TiO<sub>2</sub> fraction. Independent of the milling time the high-pressure phase shows nanometric crystallite sizes. However, it was observable that the phase transformation occurs without fracturing of the particles. Furthermore, the studies reveal that the powder-to-ball weight ratio influence only the reaction rate but not the yields. In addition, it turned out that the reaction kinetics are faster when grinding vial and balls made of alumina instead of steel are used.[64]

Regarding to the phase transformation similar findings has been obtained in another study. Here ceramic milling vials and balls were used. A ball-to-powder weight ratio of 2:1 with a single 4 g ball was applied. The results of this study reveal a conversion of the starting material anatase to high-pressure TiO<sub>2</sub> and rutile. The amount the high-pressure phase first increases with inceasing milling times but then again decreases. After the milling process the main phase of the sample consist of rutile.[65]

Mechanical ball milling of TiO<sub>2</sub> powder not only leads to a phase transformation but also to an improvement of the photocatalytic activity. For the experiments a conventional ball mill was used and the photocatalytic activity was investigated using the decomposition of methylene blue. The TiO<sub>2</sub> powder was milled for 24 h. The milling process leads to a decrease of the particle size from 555 nm to 122 nm. There were no changes in the crystal structure. Non-milled TiO<sub>2</sub> powder decomposes 61% of the methylene blue solution under irradiation. In contrast, the TiO<sub>2</sub> powder milled for 24 h lead to a dye decomposition of 94% under the same conditions.[66]

Futhermore, milling processes can lead to the formation of oxygen vacancies and additives can be introduced into particles. An example is the co-milling of titania nanoparticles with poly(tetrafluoroethylene) (PTFE). The milling process was carried out in a planetary mill with grinding bowl and balls made of zirconia. The

process was carried out at 720 rpm for 3 h. Afterwards the obtained powder was annealed at 300 °C for 1 h. The described procedure causes a significant amount of oxygen vacancies and an incorporation of fluorine into the applied titania nanoparticles.[67]

### **1.2.2 MICROJET REACTOR PROCESS**

Despite the long mixing times and thus hard to control nucleation and growth processes stirred tank batch reactors techniques are still the most employed wet chemical systems.[68] There are several studies which indicate that the effect of mixing has an important influence on the particle size and particle size distribution. [69, 70]

For this reason, there is a lot of interest in the development of improved synthesis techniques which fulfill this requirement. In addition, it would be a great benefit if the synthesis could be performed continuously because this would eliminate differences in nanoparticle properties from batch to batch.

For wet chemical synthesis of nanoparticles precipitation reactions play a major role besides sol-gel or hydrothermal processes. Many nanosized compounds can be prepared by precipitation from a solution of the respective metal salt with a suitable precipitation agent (e. g. a base). For reaching a sharp size distribution the precipitation process has to be complete in a short time. Otherwise nucleation and particle growth occurs simultaneously leading to polydisperse particles. In order to reach a fast precipitation reaction a high rate of nucleation is desired. Therefore techniques were developed which allow a fast and thoroughly mixing of the starting materials.

The easiest and oldest way to perform a rapid mixing is the double-jet precipitation. In a stirred tank batch reactor the starting materials are charged through small tubings in short proximity to a fast rotating stirrer. This allows a fast mixing of the components. This process was established for the preparation of silver halides with controllable size for photographic applications.[71] The formation of unstable nuclei occurs in close proximity to the jets/stirrer. Nuclei formation runs simultaneously with the particle growth. For preparation of monodisperse particles these nuclei have to be removed continuously by agglomeration or Ostwald ripening forming stable particles.

The nucleation as well as crystallization rate and agglomeration process can be controlled by adding polyelectrolytes or surfactants to the precipitation vessel. Zinc oxide for example can be prepared by precipitation of  $\text{Zn}^{2+}$  with NaOH in form of star-like agglomerates built by 30 nm ZnO primary particles.[72] If sodium dodecylsulfate (SDS) is added, ellipsoidal agglomerates are obtained. SDS forms micelles in the precipitation bath which influence the agglomeration behavior of the primary particles. Another example is the precipitation of  $\text{Pb}(\text{SO}_4)$  in presence of polyethyleneimine (PEI) by a double jet precipitation technique.[73] Addition of PEI leads to a drastic reduction of particle size from several micrometers (precipitation in distilled water) to 400 nm for precipitation in presence of PEI. As the reason for this behavior a complexation of the  $\text{Pb}^{2+}$  ions by the polyethyleneimine is discussed.

Drawbacks of the double-jet precipitation result from the utilization of a tank batch reactor which complicates scale-up due to difficult control of heat- and mass transfer. Furthermore, a continuous production is complicated. Therefore, other techniques have been developed which are based on the rapid mixing of the starting materials in microchannel reactors, for example tee-shaped mixers.[74] These devices allow a more efficient transfer of heat and mass resulting in more uniform temperature and concentration profiles.[75] The efficiency of mixing is generally influenced by the flow rate and the corresponding Reynolds number.[76] A great advantage of the micromixer approach is that a continuous process is possible.

In recent studies the influence of process parameters, for example the flow rate, has been studied. Palanisamy and Paul demonstrated the effect of the flow rate and therefore the Reynolds number applied to the tee-mixer on the particle size and size distribution of  $\text{CeO}_2$  particles.[77] Optimal conditions were found for Reynolds numbers above 300. Here,  $\text{CeO}_2$  particles with a size of 15 nm were obtained. The influence of the tee-mixer geometry was studied for preparation of magnetite nanoparticles.[78] Optimal results were obtained for a mixer with staggered inlet tubings. Applying this synthesis route pure magnetite particles with a size of 6 nm were obtained. Furthermore, it was demonstrated that the particle size decreases for longer mixing tubes after the tee-mixer due to longer nucleation times.

The general applicability of the microchannel mixer technology was demonstrated recently by the successful combination of hydrothermal syntheses in tee-shaped mixers. For example,  $\text{LiFe}(\text{PO}_4)$  nanoparticles were prepared in supercritical water at 400 °C by mixing the starting materials in a tee-mixer.[79] The effect of mixer geometry on the electrochemical properties of the  $\text{LiFe}(\text{PO}_4)$  obtained was studied. Optimal conditions were found for a mixer with staggered inlets which allows a swirling of the reaction solution.

A further variation of the precipitation method for producing nanoparticles is the application of ultrasound to the reaction mixture during the precipitation process. Ultrasound produces gas bubbles in the reaction medium which collapse and generate very high thermal energy over a short period of time, less than 1 ns. This results in cooling rates up to  $10^{11}$  K/s.[80] These high cooling rates hinder the organization and crystallization of the obtained products. Ultrasonication has been successfully performed on many sulfides and selenides ( $\text{PbS}$ ,  $\text{HgS}$  [81];  $\text{CdS}$ ,  $\text{CdSe}$  [82, 83];  $\text{CuSe}$  [84];  $\text{WS}_2$  [85]) as well as oxides ( $\text{Al}_2\text{O}_3$  [86];  $\text{Eu}_2\text{O}_3$  [87];  $\text{TiO}_2$ ,  $\text{V}_2\text{O}_5$ ,  $\text{WO}_3$  [88]).

Ultrasonication can also be combined with microchannel reactors. Studies at a  $\text{Ba}(\text{SO}_4)$  reference system showed that sonication can improve mixing, especially at low flow rates.[89] For barium sulfate a reduction in particle size from 2  $\mu\text{m}$  to 200 nm was reached by additional ultrasound treatment. Another example is the formation of  $\text{BaTiO}_3$  nanoparticles by sonication of a  $\text{BaCl}_2/\text{TiCl}_4/\text{NaOH}$  mixture in ethanol/ $\text{H}_2\text{O}$ .[90] Here, ultrasound alters the particle growth mechanism by forcing preliminary formed nanocrystals into an oriented aggregation to larger particles.

In the last decades tee-shaped mixers were succeeded by confined impinging jet reactors which have been found to be more efficient.[91] An example of an impinging jet reactor is the microjet reactor developed by the Synthesechemie company which was used in parts of this work.[92]

The microjet reactor technique is a *bottom-up*, wet-chemical approach for the continuous synthesis of inorganic nanoparticles. It enables a continuous synthesis route involving a very fast mixing of the starting material solutions. The major improvement over the tee mixers is that the reagents solutions are forced with high-pressure through a narrow cone (100 - 300  $\mu\text{m}$ ) in a reactor chamber that is



constantly flushed with a gas flow (Figure 13). As a result, the obtained product is removed directly from the reaction chamber so that clogging is avoided.[93] This additional gas flow distinguishes the microjet reactor process from conventional tee mixers. In these devices the reaction products are removed from the vessel by the flow of the starting material solutions.

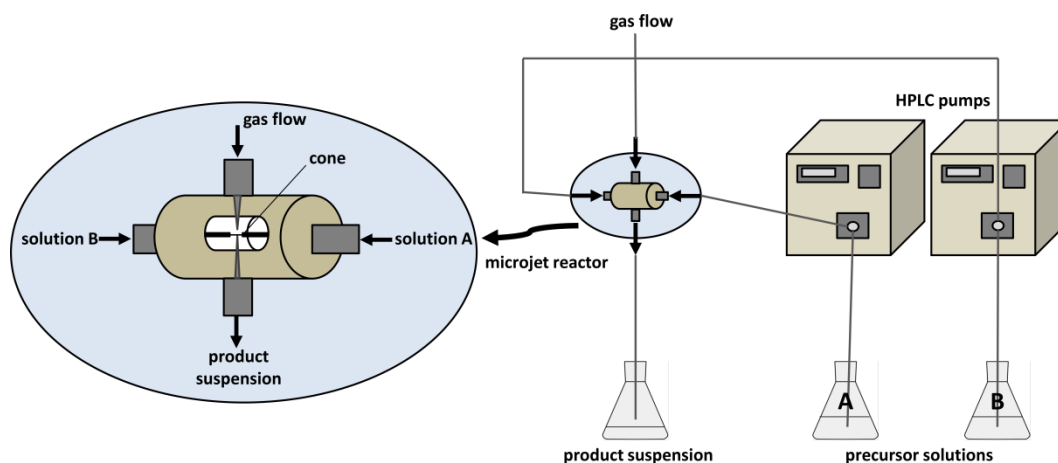


**Figure 13:** Schematic set up of the microjet reactor approach. The reagents solutions are forced with high-pressure through a narrow cone in a reactor chamber that is constantly flushed with a gas flow.[93]

Two HPLC pumps are used to transport the solutions containing the starting materials as dissolved substances to the microjet reactor. The collision takes place in a confined reaction chamber, which is defined by the dimensions of the microjet reactor.

Due to the fluid dynamics in the microjet reactor, there is a very short mixing time. Consequently, there is a maximum number of nuclei in an absolutely homogeneous environment. In addition the nucleation rate is increased compared to the nucleus growth.[92, 94] Directly after the nuclei are formed, they are transported from the reaction chamber to a tubing where the particle growth occurs. A great advantage is that the particles are obtained in suspension, which can be used for a direct application, e. g. in spray coating or inkjet printing.

The described technique has been used already for the production of barium sulfate and titania.

For the preparation of barium sulfate, precursor solutions of barium chloride dihydrate and potassium sulfate were used.[95] The starting materials were applied stoichiometrically with concentrations between 0.2 and 0.4 mol/L. The

diameter of the cone of the microjet reactor was 100  $\mu\text{m}$  and flow rates between 750 and 1050 mL/h were used. The precipitated particles were stabilized using the commercial available dispersing agent MelPers 0030 (Fa. BASF Construction) which was added to the potassium sulfate precursor solution. The particle sizes were determined using dynamic light scattering. The particle sizes can be measured to be 60 and 150 nm depending on the process parameters.

Phase content controlled titania nanoparticles were produced using the microjet reactor technology and titanium tetraethylate and nitric acid as precursor solutions.[96] The diameter of the cone of the microjet reactor was 50  $\mu\text{m}$ . The flow rate was varied between 4 and 14 mL/min at temperatures between room temperature and 210  $^{\circ}\text{C}$ . Dynamic light scattering was used to determine the particle size of the obtained products. The phase composition was analyzed by X-ray diffraction. The results reveal that the reaction temperature influences the content of anatase which increases with increasing reaction temperature. In contrast, the flow rate did not influence the phase composition. There was no correlation between the reaction temperature and the particle size. The particle size was influenced by the flow rate but no trend was observable.

In this work the microjet reactor process should be investigated whether it is suitable for the synthesis of zinc oxide, magnetite and brushite. In the following conventional wet chemical synthesis routes based on precipitation reactions for these kinds of particles are introduced.

Zinc oxide can be obtained using a simple wet chemical precipitation route starting from a 1.0 M aqueous solution of  $\text{ZnCl}_2$  and a 0.5 M aqueous solution of NaOH. The  $\text{ZnCl}_2$  solution is added drop-wise to the NaOH solution under mechanical stirring using a magnetic stirrer at room temperature. The reaction solution was stirred for 2 h. Afterwards the white precipitate was filtered and washed with de-ionized water. Finally, the precipitate was annealed at 150  $^{\circ}\text{C}$ . The result of this synthesis route are crystalline disc-like ZnO submicrometer structures in the wurtzite structure with diameters between 300 nm and 500 nm.[97]

Zinc oxide can also be obtained using zinc acetate dihydrate and potassium hydroxide. These starting materials were dissolved in methanol respectively and then mixed together. The reaction mixture was stirred for 72 h at 60  $^{\circ}\text{C}$ . The

obtained precipitate was isolated by centrifugation and washed with de-ionized water. Finally, the sample was dried at 40 °C under vacuum. XRD analysis reveal that mainly zinc oxide in the wurtzite structure is obtained. The sample contains a slight amount of basic zinc acetate which has its origin in a hydrolysis of zinc acetate in the methanol solution. TEM images show that the ZnO particles are rod shaped with uniform morphology. These ZnO nanorods have an average length of 69 nm, the average diameter has found to be 18 nm. The basic zinc acetate appear as thin flake-like films.[98]

A further possibility for the synthesis of zinc oxide is the use of zinc nitrate and sodium hydroxide as starting materials and an additional use of starch as a stabilizing agent. At 27 °C to 100 ml of distilled water containing 0.3 g starch 10 ml of a 0.1 M zinc nitrate were added. After this mixture was stirred for 2 h 10 ml of 0.2 M sodium hydroxide solution was added drop-wise, being complete after 2 h. The obtained precipitate was isolated by centrifugation and washed with ethanol. The sample was dried at 100 °C for 2 h. The as prepared particles are highly crystalline and show the wurtzite structure. The average crystallite size has found to be about 19 nm. TEM images reveal that the particles are spherical shaped with a size of around 40 nm.[99]

Zinc oxide can also be synthesized applying controlled double-jet-precipitation. This approach allows good control of the nucleation and growth of the resulting particles. As starting materials aqueous solutions of ZnCl<sub>2</sub> and NaOH were used and applied stoichiometricly. The reaction was performed at 70 °C. Primary particles with diameters between 20-30 nm are obtained but they tend to agglomerate and form ellipsoidal particles with sizes of a few hundred nanometers.[100]

The described possibilities for the synthesis of zinc oxide have in common that they cannot be performed continuously. An alternative continuous synthetic strategy is described in literature using a microfluidic reactor. The reactor was prepared based on a silicon substrate which was treated with deep reactive ion etching and consists of 200 µm wide and 200 µm deep microchannels including two inlets and one outlet as well as a preheating, a mixing and a synthesis region. As starting materials solutions of sodium hydroxide (30 mM) and zinc acetate (10 mM) were applied. They were injected to the reactor using a syringe pump. The reaction was performed at 60 °C. The obtained ZnO nanoparticles are highly

crystalline with diameters between 3 - 5 nm. They show better preservability and dispersibility than ZnO nanoparticles synthesized by a conventional batch approach.[101] Another continuous synthesis route for zinc oxide nanoparticles is their synthesis in supercritical water using a flow type apparatus which offers rapid heating of the precursor solutions. Aqueous solutions of zinc nitrate and potassium hydroxide were applied as starting materials. The obtained particles are characterized to be single phase zinc oxide with particle sizes in the range of 30 - 50 nm.[102]

Magnetite can be synthesized using a co-precipitation technique applying ferrous and ferric salts and potassium hydroxide as starting materials. Aqueous solutions of  $\text{FeCl}_3 \cdot 6\text{H}_2\text{O}$  and  $\text{FeSO}_4 \cdot 7\text{H}_2\text{O}$  were mixed. The ferrous species must be applied in excess as the experiments were performed at open atmosphere where  $\text{Fe}^{2+}$  ions tend to oxidize and form  $\text{Fe}^{3+}$ . Afterwards a KOH solution was added rapidly under stirring. XRD analysis reveals that  $\text{Fe}_3\text{O}_4$  in the cubic spinel structure with grain sizes of 7 nm was obtained.

For this synthesis route the effect of organic additives has been investigated. The results reveal that the use of such additives favors the formation of single crystalline nanoparticles.[103] A similar synthetic route uses ferrous and ferric chloride and ammonium hydroxide as starting materials. Therefore a 0.2 M aqueous solution of ferrous and ferric chloride as well as 4 M ammonia were prepared. An equal volume of both solutions was transferred into two syringes which were implemented to a mixture unit including two jets with diameters of 0.19 mm. In this manner a fast mixing of the starting material solutions occur. The resulting reaction mixture was directed into a vial which was then kept at various temperatures. XRD studies reveal that the obtained particles consist of highly crystalline magnetite and maghemite. The particle size can be adjusted by the temperature. Particles with sizes from 3.8 nm to 10.9 nm can be obtained.[104]

Another synthetic strategy for the synthesis of magnetite nanoparticles uses iron acetate as precursor. 0.006 mmol of iron acetate were dissolved in 100 ml of a mixture of oleylamine and 1-octadecene (8:2). This solution was heated up to 180 °C for 24 h. Subsequently, the reaction mixture was cooled down and  $\text{Fe}_3\text{O}_4$  nanoparticles were precipitated by adding an excess amount of ethanol. The obtained precipitate was washed several times with a mixture of ethanol and

toluene and was then dried at 80 °C for 8 h under vacuum. The resulting particles are uniformly shaped and show good crystallinity with particle sizes of around 10 nm. The mixture of oleylamine and 1-octadecene serves not only as solvent but also as ligand and surfactant.[105]

The synthesis of magnetite nanoparticles can be performed continuously in supercritical methanol using a continuous flow reactor apparatus. The reaction was carried out at 30 MPa and 400 °C applying a residence time of 38 s. Iron(III)-nitrate was used as precursor applying a 0.05 M solution. There was no need of a reducing agent. The obtained magnetite particles show crystalline structure and have an average particle size of 22 nm. In this context performed studies reveal that magnetite is only obtained by the use of supercritical methanol. In case that supercritical water was applied hematite is obtained.[106]

The synthesis of calcium phosphate particles can be performed using a simple one-step approach starting from a 0.1 M aqueous solution of calcium nitrate tetrahydrate and a 0.1 M aqueous solution of di-ammonium hydrogen phosphate. The resulting phase can be defined by the pH of the reaction solution. If the pH of the starting material solutions is adjusted to 5 the resulting phase is brushite, to obtain hydroxyapatite the pH has to be adjusted to 11. To 10 ml of the di-ammonium hydrogen phosphate solution 20 ml of the calcium nitrate tetrahydrate solution were added drop-wise with a rate of 1 ml per minute. The resulting reaction solution was stirred at room temperature for 4 h. Finally, the particles were washed with distilled water and then freeze-dried. The obtained particles are crystalline and reveal hydrodynamic diameters of  $139.1 \pm 15.4$  nm for brushite and  $145 \pm 19.8$  nm for hydroxyapatite.[107]

Furthermore, the precipitation of brushite has been performed in a cylindrical stirred tank reactor with a diameter of 12 cm. The bottom of this tank was rounded in order to eliminate regions at low turbulence. The set up was equipped with a thermocouple as well as a pH probe. The experiments were performed at room temperature and a solution pH below 7. Solutions of sodium hydrogen phosphate, calcium chloride and sodium hydroxide were used as starting materials. The reactants were supplied from the top of the reactor. Initial phosphate and calcium concentrations were varied. In order to avoid the uptake of carbon dioxide the reaction solution was constantly flushed with nitrogen gas. The resulting

precipitate was characterized to be crystalline brushite. SEM images reveal plate-like morphology. The crystal size and crystal size distribution did not show any dependence to the varied process parameters.[108]

Brushite has also been synthesized using a reverse microemulsion technique. Aqueous solutions of calcium nitrate tetrahydrate and di-ammonium hydrogen phosphate were used as precursor. Additionally a mixture of surfactants (trioctylmethylammonium chloride and polyoxyethylene 20 sorbitan monolaurate) was applied as template directing agents. Kerosene was used as the oil phase. The precursor concentrations as well as the reaction temperature were varied. The general procedure was to prepare microemulsions by stirring kerosene, the surfactants and an aqueous solution of calcium nitrate or di-ammonium hydrogen phosphate for 4 h.

The phosphate containing microemulsion was added to the calcium containing microemulsion under stirring. Depending on the reaction temperature particle formation starts after 30 - 45 min (room temperature), 10 min (60 °C) or two days (6 °C). However, the final precipitate was isolated by centrifugation, washed with methanol and then dried at 80 – 100 °C for 6 h. The final particles were characterized to be brushite with diameters between 23 nm and 87 nm. The particle size can be adjusted by the precursor concentrations. The reaction temperature had an influence on the particle morphology. Monodisperse and spherical shaped particles were obtained at a reaction temperature of 60 °C. If the reaction was performed at 6 °C nanoflakes were formed.[109]

A similar procedure is reported using aqueous solutions of calcium nitrate tetrahydrate and di-ammonium hydrogen phosphate as starting materials. Surfactin was applied as surfactant and n-hexane was used to provide the oil phase. Two microemulsions were prepared and then mixed together by rigorous shaking. The reaction takes place for four days. Afterwards the resulting product was isolated by centrifugation, washed with methanol and dried at 50 °C. The resulting crystalline brushite particles are spherical formed with an average diameter of 16 nm or needle-like (diameter: 8 - 14 nm and length: 80 - 100 nm) depending on the water to surfactin ratio.[110]

## 2. RESEARCH GOALS

In both fields for the synthesis of nanoparticles, *top-down* and *bottom-up*, a lot of methods and techniques have been developed, but there are still needs for improvements. In the last decades nanoparticles have elicited plenty of interest and they have been identified as major compounds for a wide field of applications. For this reason, there is a lot of interest in new synthetic strategies.

The aim of this work was to investigate novel synthetic approaches using a *top-down* technique as well as a *bottom-up* technique. Systematic studies on the influence of different process parameters should help to define the possibilities and limitations of both new approaches.

### 2.1 REACTIVE MILLING

Reactive milling has elicited significant interest for its application in various fields. Particularly the fact that reactive milling can be performed solvent-free and therefore environmental friendly is a great benefit of this technique. Reactive milling has been shown already to be suitable for many synthetic pathways to powdered materials. An interesting question is whether organically surface-functionalized (nano)particles can be synthesized by this approach. For this reason one of the research goals of this work was to investigate reactive milling for the synthesis of particles with *in situ* surface functionalization. Titania is used as inorganic pigment and different organophosphonic acids as surface-modifying agents.

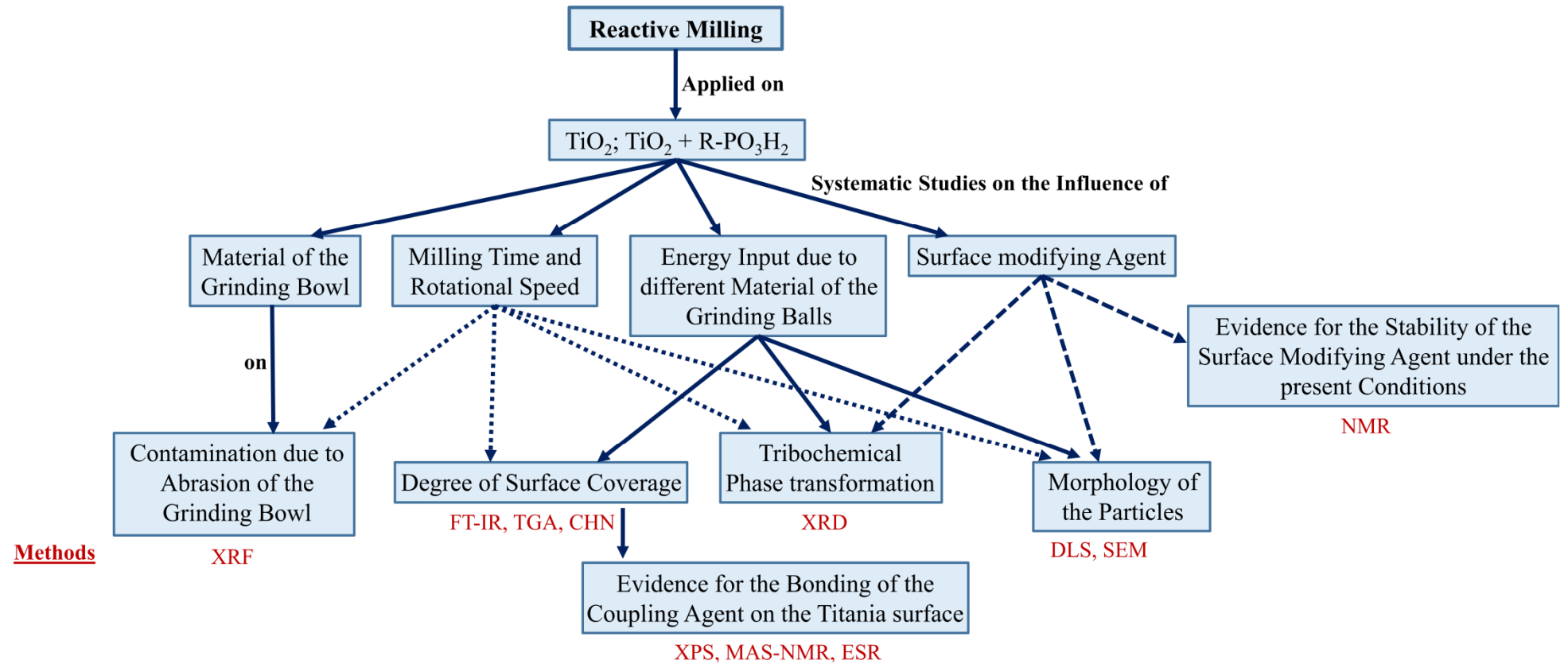
Titania was selected for the use as inorganic pigment due to the fact that it has several crystallographic phases that can be converted into each other depending on the energy input to the system. Consequently, the ration between the different crystallographic phases is an indicator for the energy applied to the sample. The influence of the milling time, rotational speed as well as the grinding sphere material has to be analyzed with respect to the surface coverage, the composition of the samples as well as the particle morphology. In addition, it must be verified that the coupling agent used is not degraded due to the strong forces which acts in

a ball mill. Several methods will be used for the characterization of the obtained particles.

As surface-modifying agents phenylphosphonic acid, dodecylphosphonic acid and octadecylphosphonic acid are used. The evidence for the stability of these agents under the harsh reaction conditions in a ball mill is conducted using nuclear magnetic resonance (NMR) spectroscopy. The degree of surface coverage of the obtained functionalized particles is investigated using fourier-transform-infrared (FT-IR) spectroscopy, thermo gravimetric analysis (TGA) as well as elemental analysis (CHN). The evidence for the bonding of the surface-modifying agent on the titania surface is performed using magic-angle spinning nuclear magnetic resonance (MAS-NMR) spectroscopy as well as X-ray photoelectron spectroscopy (XPS) and electron spin resonance (ESR) measurements. X-ray diffraction (XRD) is used to analyze the samples regarding to their phase composition and crystallite sizes. The particle size and morphology is studied by the use of dynamic light scattering (DLS) as well as scanning electron microscopy (SEM). X-ray fluorescence spectroscopy (XRF) is used to analyze the samples with respect to contaminations due to abrasion of the grinding sphere material. The following diagram gives an overview of the proposed research project regarding to reactive milling.



**Overview on the proposed research project regarding to reactive milling**



## 2.2 MICROJET REACTOR PROCESS

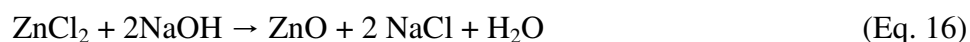
A great benefit in nanoparticle synthesis would be to perform it continuously. This would eliminate differences in nanoparticle properties from batch to batch. There are continuous techniques already, but they all require an improvement with respect to the mixing time. The microjet reactor technology fulfills fast mixing and has shown to be promising for nanoparticle synthesis already. One of the research goals of this work was to verify the suitability of the microjet reactor process for nanoparticle synthesis.

In order to demonstrate the wide field of application the microjet reactor technique has to be investigated for the synthesis of various nanoparticles. Zinc oxide (ZnO), magnetite (Fe<sub>3</sub>O<sub>4</sub>) and brushite (CaHPO<sub>4</sub>·2H<sub>2</sub>O) should be used. These particles were selected because they are not only interesting for academic reason but also have applications in optoelectronics, clinical and biomedical devices.

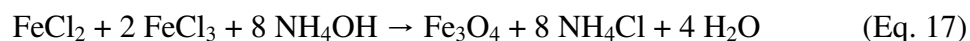
Zinc oxide has elicited plenty of interest in the area of renewable energies. Due to its semiconductor properties it has found to be useful for the production of solar cells with improved performance. Magnetite is of particular interest for biomedical applications. For instance, it could lead to great advances in cancer treatment. Also brushite is of interest for clinical and biomedical devices. For example, it is a promising candidate for the use as gene delivery carrier. For this reason, the improvement of synthesis routes for these particles has attracted great attention.

It has to be analyzed if the particle size is controllable by means the process parameters flow rate and reaction temperature. Furthermore, the influence of the composition of the precursor solution has to be investigated.

The synthesis of zinc oxide is performed using zinc chloride and sodium hydroxide as starting materials:



The synthesis of magnetite was conducted based on ferrous and ferric chloride as well as ammonia:



Different to the stoichiometric reaction equation ferrous chloride is applied in excess as the synthesis is performed under air where  $\text{Fe}^{2+}$  ions tend to oxidize and form  $\text{Fe}^{3+}$  ions.

Brushite is synthesized using calcium nitrate and di-ammonium hydrogen phosphate as starting materials:

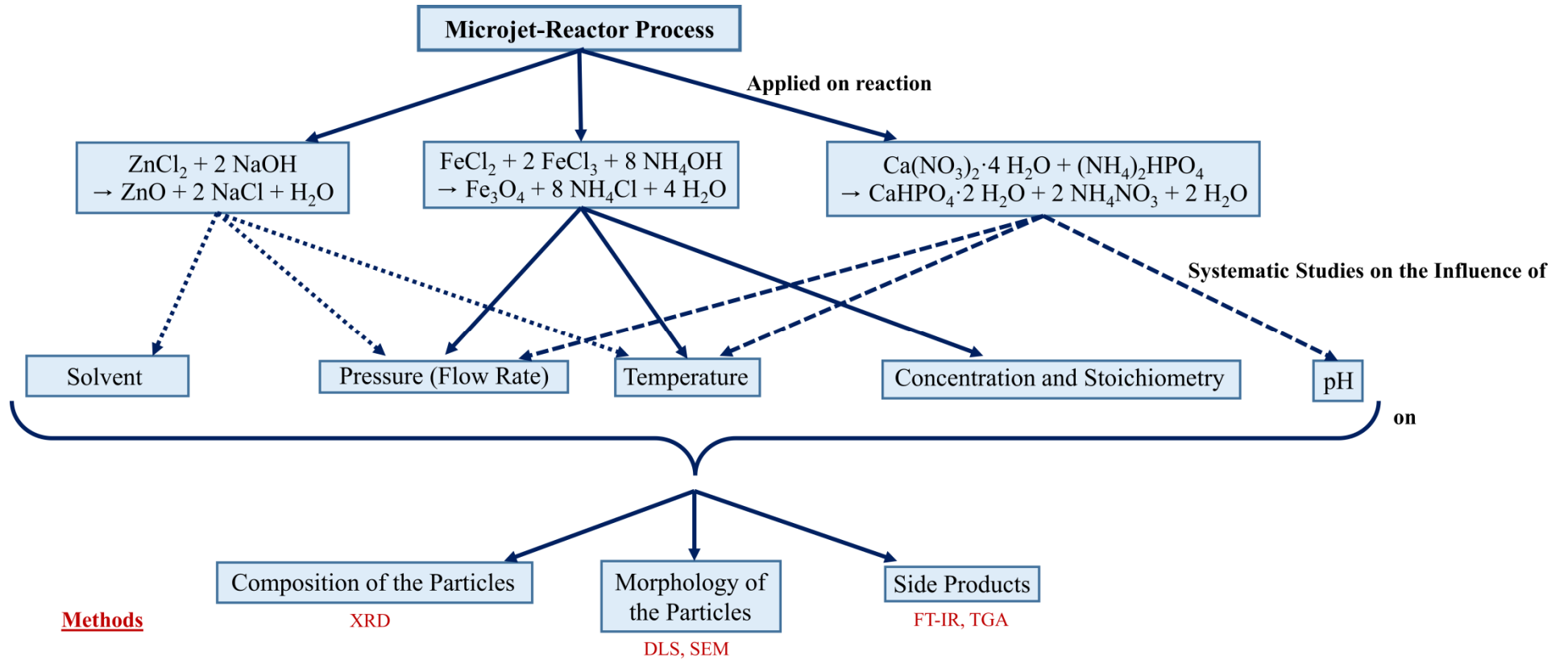


To obtain calcium phosphate in the brushite phase the pH of the precursor solutions is adjusted to 5.

X-ray diffraction (XRD) was applied to characterize the samples regarding to their phase composition and crystallite sizes. The particle sizes and morphology are analyzed using dynamic light scattering (DLS) and scanning electron microscopy (SEM). Fourier-transform-infrared (FT-IR) spectroscopy and thermo gravimetric analysis (TGA) are used to identify possible side products.

The following diagram gives an overview of the proposed research project regarding to the microjet reactor process.

**Overview on the proposed research project with respect to the microjet reactor process**



### 3. RESULTS AND DISCUSSION

The results of this work have been published.

#### 3.1 REACTIVE MILLING

Reactive milling is a solvent free and therefore environmental friendly approach. Due to this benefit against conventional synthetic strategies it has elicited plenty of interest for various fields of applications. Reactive milling has been investigated already for many synthetic pathways for powdered materials but not for the surface functionalization of inorganic pigments with surface-modifying agents. The studies in this work regarding to reactive milling have been performed in order to proof the suitability of reactive milling for the synthesis of organically surface-modified particles. In order to have an indicator for the energy applied into the system titania was used as inorganic pigment. Titania has several crystallographic phases which can be converted into each other depending on the energy applied to the system. Consequently, from the ratio of these phases in the sample after the milling process conclusions can be drawn with respect to the amount of energy input. As surface-modifying agent phenylphosphonic acid was used as it is a common model molecule.

Systematic studies on the influence of the milling time as well as the milling speed were performed in order to optimize the milling conditions with respect to the properties of the obtained samples. The milling time was varied between 12 h and 48 h whereas milling speeds of 200 rpm, 250 rpm and 300 rpm were applied. The samples were analyzed with respect to the stability of the surface-modifying agent, their phase composition, surface coverage, particle size and morphology as well as impurities due to abrasion of the grinding sphere material. These results have been published in a first publication.

A further parameter which is of special interest regarding to reactive milling processes is the influence of the grinding sphere material. In the previous studies a grinding bowl and milling balls made of WC/Co-hard metal were used. These experiments were conducted again but with the use of a grinding bowl and milling balls made of zirconia. Systematic studies regarding to the effect of milling time and rotational speed were performed. The obtained products were characterized

with respect to the stability of the surface-modifying agent, their phase composition, surface coverage, particle size and morphology as well as impurities due to abrasion of the grinding sphere material. These results were then compared to the findings of the experiments with the WC/Co hard metal grinding sphere. The results of these studies have been published in a second publication.

The results of the performed studies reveal that reactive milling is a promising method for the synthesis of inorganic particles with *in situ* surface functionalization without the use of any solvent. Now an interesting question was whether this approach is suitable for the surface functionalization of inorganic particles with long alkyl chain organophosphorus surface-modifying agents as well. The previous studies showed that lower impurity concentrations due to abrasion of the grinding sphere material are obtained in case of using grinding sphere material made of zirconia. For this reason, the further experiments were conducted using this type of grinding bowl and milling balls.

Again titania was used as inorganic pigment and dodecylphosphonic acid was used as surface-modifying agent. Systematic studies on the influence of the milling time and milling speed were performed in order to optimize these milling parameters with respect to the properties of the obtained samples. The samples were analyzed regarding to the stability of the surface-modifying agent, their phase composition, surface coverage, particle size and morphology as well as impurities due to abrasion of the grinding sphere material. The results showed that reactive milling is also suitable for the production of particles with *in situ* surface functionalization using dodecylphosphonic acid as surface-modifying agent. Consequently, it was of crucial interest if this approach is assignable on other long alkyl chain organophosphorus surface-modifying agents as well. To clarify this question octadecylphosphonic acid was applied as surface-modifying agent. It turned out that the approach can be successfully performed with octadecylphosphonic acid as well. The findings of these studies have been published in a third publication.

### **3.1.1 SYNTHESIS OF SURFACE FUNCTIONALIZED TITANIA PARTICLES WITH ORGANOPHOSPHORUS COUPLING AGENTS BY REACTIVE MILLING**

The first publication describes the systematic investigation of a *top-down* approach for the synthesis of metal oxide particles with *in situ* surface functionalization. The experiments were performed in a high-energy planetary ball mill using a grinding bowl and milling balls made of WC/Co-hard metal. As inorganic pigment titania was used as it has various crystallographic phases which can be converted into each other depending on the energy input to the system. As a result, the phase composition of the milled samples is an indicator for the applied energy.

As surface-modifying agent phenylphosphonic acid was used. Systematic studies of the influence of milling time and rotation speed were conducted in order to optimize these process parameters. NMR studies were performed to verify that the surface-modifying agent is not degraded due to the high-energy input during the milling process. Furthermore, FT-IR spectroscopy was applied to show that a surface functionalization has taken place and solid state NMR spectroscopy was carried out to investigate the binding mode of the surface-modifying agent on the titania surface.

The results reveal that the surface-modifying agent is not degraded during the milling process and that it is bound covalently to the titania surface using different binding modes (mono-, bi-, tri-dentate). The degree of surface coverage was determined using TG as well as CHN analysis. The studies reveal that the degree of surface coverage is dependent on the milling time as well as the milling speed. The amount of surface functionalization increases with the increase of these parameters. Applying a milling time of 48 h at 300 rpm a surface coverage of 1.4 mmol phosphonate per gram particle could be obtained.

X-ray diffraction was used to investigate the phase composition of the samples after the milling process. A tribochemical phase transition from the starting material anatase to rutile and high-pressure titania was observed. The amount of phase transition increases with increasing milling time and increasing milling speed. The addition of the surface-modifying agent inhibits the overall phase transition but concurrently seems to stabilize the high-pressure phase. The high-

pressure phase arises in nanocrystalline dimensions with crystallite sizes of 5 - 6 nm independent of the milling parameters. Granular crystalline anatase with crystallite sizes above 300 nm was used as starting material. Due to the milling process there is a crystallite size reduction but the anatase remains in the granular crystalline dimension with crystallite sizes around 100 nm.

The particle size and morphology were determined using dynamic light scattering and scanning electron microscopy. Both methods reveal that there are two fractions with different sizes, approximately 100 nm and 300 nm. This can be explained by the different crystallographic phases present in the samples.

In order to determine impurities due to abrasion of the grinding sphere material X-ray fluorescence spectroscopy was conducted. The concentration of impurities increases with increasing milling time and speed thus with increasing energy input. Milling 12 h at 200 rpm lead to impurities of 0.046 wt-% tungsten. Increasing the energy input by milling 48 h at 300 rpm results in an impurity concentration of 0.277 wt-%. However, in each case the impurities are insignificant small.

The samples after the milling process show a grey discoloration which can have its origin either in the impurities of tungsten or the presence of subvalent Ti atoms. The performed XPS analyses give no clear results wheter  $Ti^{3+}$  species are present in the sample or not. For this reason, ESR measurements are performed in following work. Furthermore, it would be interesting whether the grinding sphere material has an influence on the milling process as well.

In conclusion, it was shown that reactive milling is a promising technique for the synthesis of inorganic particles with *in situ* surface functionalization. Titania could be surface-modified with phenylphosphonic acid applying this high-energy milling process. The supporting information (see chapter 7.1) belonging to this publication contains tables summarizing the phase composition of all samples and IR spectra as well as XRD pattern of all samples are shown. Furthermore, the liquid- and solid-state NMR spectra are presented.

The results have been published in the *European Journal of Inorganic Chemistry*:

A. Fischer, C. Ney, G. Kickelbick, Synthesis of Surface-Functionalized Titania Particles with Organophosphorus Coupling Agents by Reactive Milling, *Eur. J. Inorg. Chem.*, **2013**, 33, 5701-5707.



Christoph Ney is mentioned as author as well because he carried out preliminary studies on this research topic during his time in the working group of Prof. Dr. Kickelbick. The publication was written by Annika Betke (nee Fischer) and all experiments and characterizations presented were performed by her. Guido Kickelbick has contributed suggestions for improvements and is mentioned as corresponding author as he is the working group leader and Ph.D. supervisor.

DOI:10.1002/ejic.201300589

# Synthesis of Surface-Functionalized Titania Particles with Organophosphorus Coupling Agents by Reactive Milling

Annika Fischer,<sup>[a]</sup> Christoph Ney,<sup>[a]</sup> and Guido Kickelbick\*<sup>[a]</sup>

**Keywords:** Milling processes / Titania / Phosphonates / Nanoparticles / Phase transitions / Surface chemistry

We describe a top-down approach for the synthesis of metal oxide particles with simultaneous surface modification. Functionalized titania particles were obtained by reactive milling together with phenylphosphonic acid in a high-energy planetary ball mill. This process was accompanied by a tribochemical phase transition from the starting material anatase to the thermodynamically more stable rutile and a high-pressure modification of titania, which was influenced by the presence of the coupling agent. The obtained products were

characterized by X-ray powder diffraction, IR and X-ray fluorescence spectroscopy, thermal and elemental analysis as well as by scanning electron microscopy. The analysis showed final particle sizes of 100 to 300 nm, depending on the milling time and speed (rpm). Furthermore, the prepared particles showed a high degree of surface coverage with organophosphorus coupling agent, up to 1.4 mmol per gram. Coordination of the coupling agent to the surface resulted in a stabilization of the high-pressure phase.

## Introduction

Over the last decades there has been significant interest in mechanochemical syntheses.<sup>[1,2]</sup> Particularly the fact that reactive milling is a solvent-free and therefore environmentally friendly alternative to conventional synthetic strategies has elicited plenty of interest in academia and industry.<sup>[3,4]</sup> Although mainly applied for inert oxide compounds, reactive milling can also be used for the synthesis of quite sensitive materials, such as metal hydrides, which has attracted recent attention for the storage of hydrogen. The obtained small particles are highly efficient for the uptake and release of hydrogen. Recently, we developed a route for the preparation of calcium hydride by milling of calcium and phenylphosphonic acid (PPA) under an inert atmosphere.<sup>[5]</sup> Another example for the advantageous use of reactive milling is the synthesis of multicomponent oxides. For example, the dielectric material ZrTiO<sub>4</sub> can be obtained by milling an equimolar mixture of TiO<sub>2</sub> and ZrO<sub>2</sub>. Due to the strong forces that act in a ball mill, the resulting products may be characterized by their small particle sizes, inconvenient metastable phases or structure defects.<sup>[6]</sup> Nevertheless, reactive milling has been used for the preparation of various alloys and in a limited number of organic syntheses.<sup>[3,7,8]</sup>

One of the drawbacks of reactive milling is the often limited control over the size, shape and composition of the sample. An interesting question is whether organically sur-

face-functionalized (nano)particles can be synthesized by this approach. Such surface-functionalized (nano)particles are important building blocks for various applications in materials science,<sup>[9]</sup> optics,<sup>[10]</sup> electronics,<sup>[11]</sup> and in the biomedical field.<sup>[12]</sup> Most of the particles are prepared by bottom-up approaches due to the advantages of higher control of morphology and composition of the particles. Such materials with tunable properties are in great demand but their preparation is still very complex and is often not amenable to scaling up to industrial dimensions.<sup>[13]</sup> Reactive milling procedures have been described for the activation of inorganic compounds prior to the surface modification step but, to the best of our knowledge, it has not been used directly for in situ surface modification. For example, zirconia powder was milled prior to functionalization with stearic acid; this treatment by ball milling resulted in an increase in the number of hydroxyl groups on the surface of the zirconia, which is important for functionalization because stearic acid binds through esterification with these groups.<sup>[14]</sup>

In this study we investigated reactive milling processes by applying strongly surface-binding phosphonates as additives and titania as inorganic pigment. The goal was the in situ surface functionalization of the final products with an organophosphorus coupling agent.

## Results and Discussion

Reactive milling was carried out by using commercially available titania powder in a high-energy planetary ball mill under a range of reaction conditions such as milling time and rotational speed. Titania was used because it has several crystallographic phases that can be converted into each

[a] Saarland University, Inorganic Chemistry,  
Am Markt Zeile 3, 66125 Saarbrücken, Germany  
E-mail: guido.kickelbick@uni-saarland.de  
<http://www.uni-saarland.de/lehrstuhl/kickelbick.html>

Supporting information for this article is available on the WWW under <http://dx.doi.org/10.1002/ejic.201300589>.

other depending on the energy put into the system, thus, the ratio between the different crystallographic phases is an indicator of the energy applied to the sample. As surface active reagent, PPA was added to the powder before milling. After the milling procedure, the obtained material was thoroughly washed and the resulting compound was characterized by applying various techniques. The final products were analyzed with respect to changes in the composition depending on the reaction parameters. FTIR analyses of the prepared materials showed that bonding between the PPA and the titania phase occurred during the milling process. The titania starting material revealed no absorption in the region typical for organic molecules. In contrast, samples after the milling process displayed bands that were characteristic for aromatic C–C oscillation ( $1600\text{ cm}^{-1}$ ), C–H deformation ( $1440\text{ cm}^{-1}$ ), P–phenyl ( $1150\text{ cm}^{-1}$ ), and P–O ( $1000\text{ cm}^{-1}$ ) vibrations, as well as aromatic C–H oscillation ( $3050\text{ cm}^{-1}$ ) (Figure 1). A broad band at approximately  $1000\text{ cm}^{-1}$  indicated covalent bonding of PPA on the surface of the titania particles; the wide width of this band being due to different bonding types (e.g., bi- and tridentate bonding) of PPA on the titania surface.<sup>[15]</sup> The intensity of the bands varied with the different process parameters, but there was no linear correlation between the intensities and milling time or the speed (revolutions per minute, rpm).

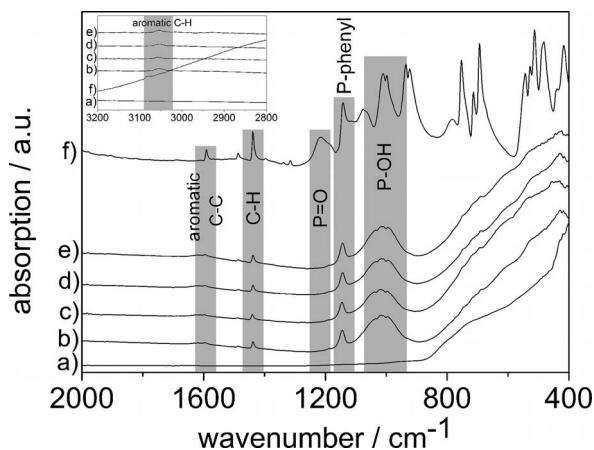


Figure 1. FTIR spectra: (a) starting material titania; (f) coupling agent PPA and samples after the milling process: (b) 300 rpm/12 h; (c) 300 rpm/24 h; (d) 300 rpm/36 h; (e) 300 rpm/48 h; surface modification occurred after the milling process, which is indicated by the characteristic bands for aromatic C–C oscillation ( $1600\text{ cm}^{-1}$ ), C–H oscillation ( $1440\text{ cm}^{-1}$ ), P–phenyl vibrations ( $1150\text{ cm}^{-1}$ ), the wide band at  $1000\text{ cm}^{-1}$  (P–O region) and the aromatic C–H oscillation at  $3050\text{ cm}^{-1}$ .

An important parameter was the extent to which the organophosphorus coupling agent was attached to the surface, i.e., the surface coverage. To establish this value, thermal gravimetric (TGA) as well as elemental (CHN) analyses were applied after washing the material and the results were correlated with the milling parameters (Figure 2).

Two parameters can influence the size and the composition of the obtained material, i.e., the rotational speed (in rpm) and the milling time. Both are expected to decrease particle size, increase the number of defects on the particle

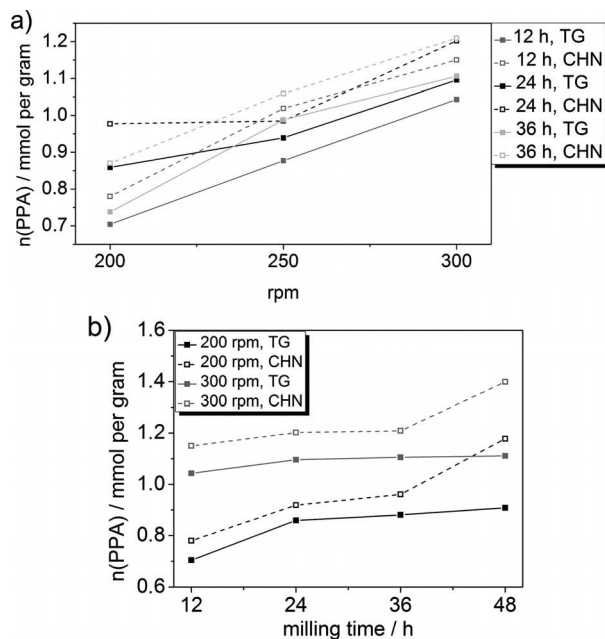


Figure 2. Surface modification dependence on (a) the milling speed or (b) the milling time; results calculated on the basis of TGA (solid line) and CHN analyses (dashed line).

surface and thus also increase the extent of surface functionalization. It was observed that the degree of surface modification increases with increasing milling speed as well as increasing milling time. A linear correlation between the milling speed applied and the surface coverage was observable, which can have two reasons. Either the size of the particles decrease, which increases their surface area and thus leads to a higher portion of coupling agent bound to the surface, or the increasing energy input leads to a better binding of the organic groups to the surface. Furthermore, the correlation between the surface coverage and the milling time is linear. In each case, the TGA and CHN results show similar development between the samples. CHN analysis generally indicates a slightly higher degree of surface coverage than TGA analysis; a discrepancy that is due to measuring inaccuracies of both methods.

Solid-state NMR spectroscopy was performed to study the binding modes of PPA to the titania surface (Figure 3). The results confirmed that PPA was bonded to the titania surface. The  $^{31}\text{P}$  solid-state NMR spectrum of pure PPA revealed a signal at  $\delta = 21.8\text{ ppm}$ , whereas the sample after the milling process showed a signal at  $\delta = 13.3\text{ ppm}$ . This chemical shift agrees well with reported NMR spectroscopic data for covalently bonded PPA on a titania surface.<sup>[16]</sup> Furthermore,  $^{13}\text{C}$  NMR spectroscopy revealed that the phenyl ring was completely intact and no chemical modification occurred during the high-energy milling process (see the Supporting Information).

X-ray powder diffraction was used to study the dependence of the phase composition on the milling parameters. The results reveal a tribochemical phase transition occurring from the starting material anatase to the thermodynamically more stable rutile and a high-pressure modifica-

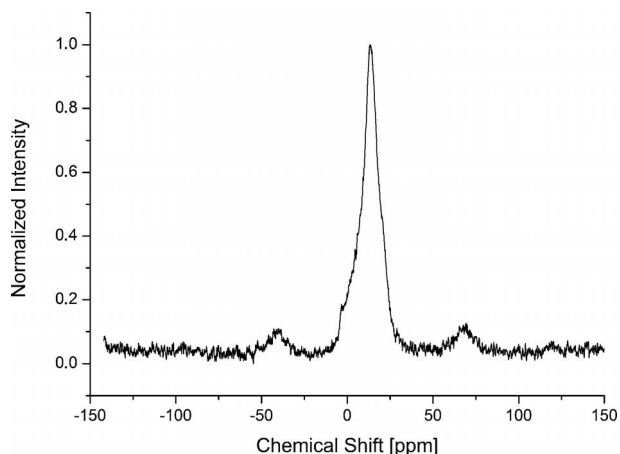


Figure 3.  $^{31}\text{P}$  CP-MAS NMR spectrum of titania milled with PPA at 300 rpm for 48 h.

tion of titania (Figure 4). A high-pressure phase of titania was first published in 1962 and its structure type was reported in 1967.<sup>[17,18]</sup> The difference between rutile and high-pressure titania is manifested in the orientation of the vertex-connected  $\text{TiO}_6$ -octahedra along the *c*-axis. In the case of the rutile structure, the octahedra form straight columns in the crystal structure but in the case of high-pressure titania they arrange in zigzag chains. It is known that the high-pressure phase can be obtained by high-energy impact vibrational ball milling.<sup>[19]</sup>

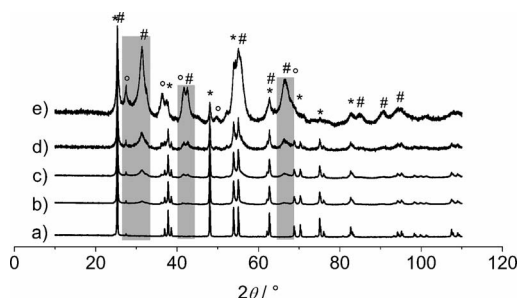


Figure 4. XRD patterns of (a) the starting material anatase (\*) and samples after milling titania with PPA: (b) 200 rpm/12 h; (c) 200 rpm/48 h; (d) 300 rpm/12 h; (e) 300 rpm/48 h. The selection indicates the main differences in the reflections: the presence of high-pressure  $\text{TiO}_2$  (#) ( $2\theta = 31^\circ$ ,  $42^\circ$ , and  $66^\circ$ ) and rutile (°) ( $2\theta = 27^\circ$ ) indicated by additional reflections.

The XRD patterns show that both the milling time and speed influence the phase formation of the sample. With increasing milling time and increasing speed, the reflections for high-pressure  $\text{TiO}_2$  ( $2\theta = 31^\circ$  and  $66^\circ$ ) as well as rutile ( $2\theta = 27^\circ$ ) become more intense. It is qualitatively apparent that samples contain more rutile and high-pressure  $\text{TiO}_2$  with increasing milling time and increasing speed. Quantitative Rietveld phase analysis was also conducted. It cannot be excluded that an amorphous phase also develops, but the proportion of this phase is very small (less than 5%). In the Rietveld analysis, the development of the background provides no evidence for the presence of an amorphous

phase. Selected results are listed in Table 1 and the results of the quantitative Rietveld phase analysis are summarized in Figure 5.

Table 1. Titania milled with PPA, phase composition of selected samples.

Process parameters	Anatase [wt.-%]	Rutile [wt.-%]	hp- $\text{TiO}_2$ [wt.-%]
0 h/0 rpm	98.2 ± 0.1	1.8 ± 0.1	0
12 h/200 rpm	73.0 ± 0.2	2.5 ± 0.1	24.5 ± 0.2
48 h/200 rpm	49.3 ± 0.2	4.4 ± 0.1	46.3 ± 0.2
12 h/300 rpm	32.6 ± 0.3	4.1 ± 0.2	63.3 ± 0.3
48 h/300 rpm	7.6 ± 0.1	7.0 ± 0.2	85.4 ± 0.2

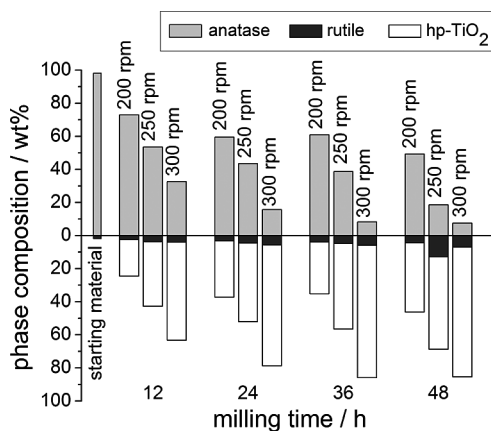


Figure 5. Titania milled with PPA; phase composition of the samples after milling, determined by X-ray powder diffraction. Phase composition changes from the starting material anatase to rutile and high-pressure (hp)  $\text{TiO}_2$ .

Titania was also milled without addition of PPA to verify the influence of the coupling agent on the phase transition; the main results are listed in Table 2. Figure 6 gives an overview of all results. The results show that a phase transition also occurs but in a different way. When anatase was milled together with PPA there was rarely rutile in the product but more of the high-pressure  $\text{TiO}_2$  phase. When anatase was milled without any coupling agent the overall phase conversion of anatase was higher and there was more rutile in the resulting product. Consequently, PPA inhibits the overall phase conversion but, simultaneously, benefits the formation of the high-pressure modification. An explanation for this behavior could be that, on the one hand, PPA stabilizes the anatase modification as a result of surface functionalization and, on the other hand, PPA favors the surface of the high-pressure titania for functionalization, which consequently stabilizes this modification in comparison to rutile.

Table 2. Titania milled without any additives, phase composition of selected samples.

Process parameters	Anatase [wt.-%]	Rutile [wt.-%]	hp- $\text{TiO}_2$ [wt.-%]
0 h/0 rpm	98.2 ± 0.1	1.8 ± 0.1	0
12 h/200 rpm	39.8 ± 0.3	5.1 ± 0.2	55.1 ± 0.4
48 h/200 rpm	31.3 ± 0.3	13.3 ± 0.4	55.4 ± 0.5
12 h/300 rpm	6.1 ± 0.1	44.2 ± 0.6	49.7 ± 0.7
48 h/300 rpm	4.2 ± 0.1	52.3 ± 0.6	43.5 ± 0.7

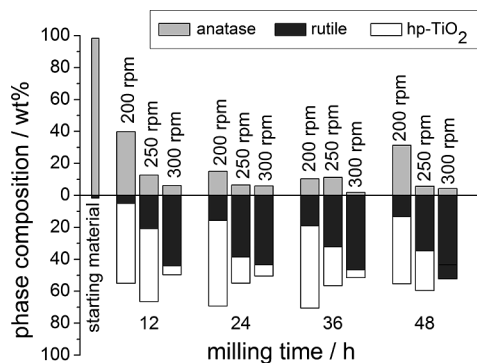


Figure 6. Titania milled without any additives; phase composition of the samples after the milling process, determined by X-ray powder diffraction. Phase composition change occurs from the starting material anatase to rutile and high-pressure (hp) TiO<sub>2</sub>.

In addition to the tribochemical phase transition, crystallite sizes were also analyzed. Granular crystalline anatase with crystallite sizes above 300 nm was used as starting material. Crystallites corresponding to the resulting high-pressure phase were significantly smaller, with sizes of 5–6 nm, irrespective of the milling speed or milling time. The residual anatase phase remained in the granular crystalline dimensions. Due to the grinding process, the size decreased to ca. 100 nm. Consequently, the milling speed and milling time have most influence on the phase transition. In each case, the resulting high-pressure titania is nanocrystalline and the residual anatase remains granular crystalline.

The particle morphology was determined by means of scanning electron microscopy (Figure 7). These images show that the samples are agglomerated and not uniformly shaped. The particle size was in the range of 100–300 nm. It was observed that the particle size decreased with increasing milling time and milling speed.

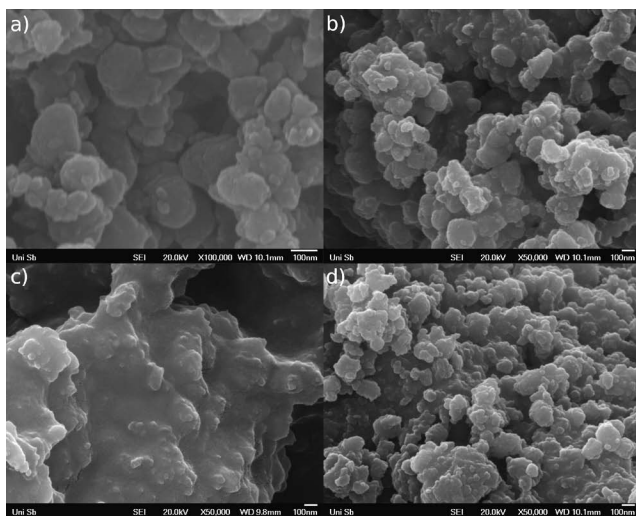


Figure 7. SEM images of selected samples: (a) 200 rpm/12 h; (b) 200 rpm/48 h; (c) 300 rpm/12 h; (d) 300 rpm/48 h. All the samples are agglomerated and not uniformly shaped; the size of the particles decreases slightly with increasing milling time and increasing milling speed.

The surface-functionalized particles were directly dispersed in organic solvent to determine the radius of the particles by dynamic light scattering (DLS). The samples were dispersed in cyclohexane by exposure to ultrasound for 30 min. The particle size of the starting material was also determined to obtain information on the effect of milling; however, because pristine titania particles are not dispersible in cyclohexane due to their hydrophilic surface, the titania starting material was dispersed in water. The results show that the starting material has particle diameters of 500 nm or larger. After the milling process there was a significant reduction in particle size. The samples exhibit two distinct particle-size fractions: particles with sizes of approximately 120 nm and particles of around 400 nm. The influence of the milling speed and the duration of the milling process were not clear, with the difference between samples milled for 48 h at 300 rpm and for 12 h at 200 rpm being negligible (Figure 8).

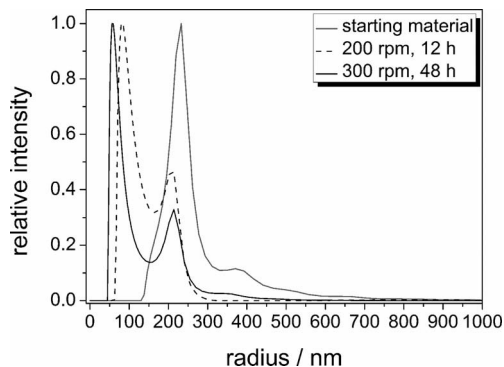


Figure 8. Particle size determined by dynamic light scattering. The starting material was dispersed in water, whereas the functionalized particles were dispersed in cyclohexane; all samples were dispersed by exposure to ultrasound for 30 min.

All samples were analyzed by X-ray fluorescence spectroscopy to investigate potential contamination due to abrasion of the grinding bowl (Figures 9 and 10).

When titania was milled with the coupling agent, the results show that the level of contamination increased with increasing milling speed as well as with increased milling time. After milling for 12 h at 200 rpm the sample contained 0.046 wt.-% W. An extension of the milling time to 48 h gave rise to a contamination of 0.196 wt.-% W. Increasing the milling speed to 300 rpm led to an abrasion of 0.071 wt.-% W by milling for 12 h. A process time of 48 h at 300 rpm resulted in an impurity level of 0.277 wt.-% W. In each case, the impurities were insignificantly small. Milling titania without any coupling agent led to significantly higher impurity levels; impurity levels up to 0.957 wt.-% compared with 0.277 wt.-% when the coupling agent was present. These results indicate that the energy input into the sample is higher when milling without any coupling agent, which means that the coupling agent absorbs a certain part of the emerged energy.

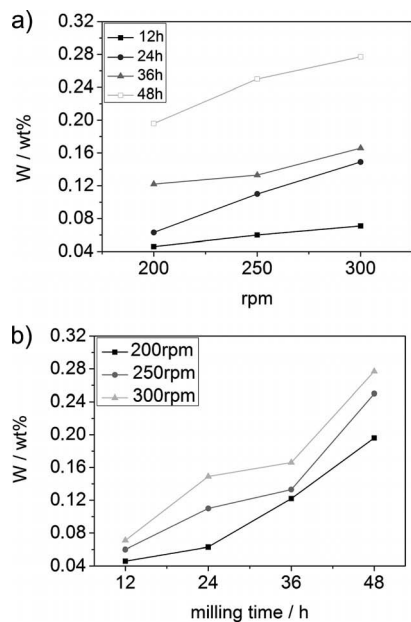


Figure 9. Impurities introduced by the grinding bowl according to (a) milling speed, or (b) milling time determined by X-ray fluorescence spectroscopy; titania milled with the coupling agent.

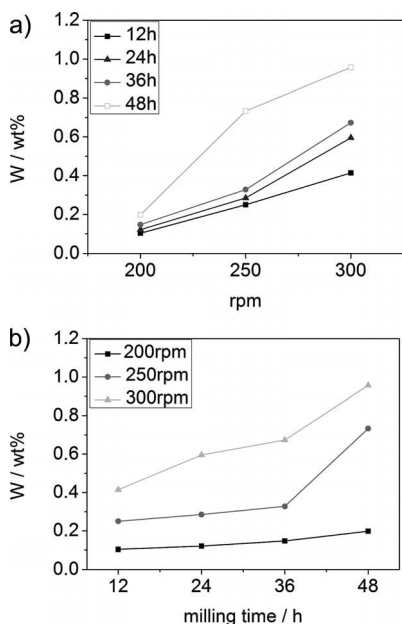


Figure 10. Impurities introduced by the grinding bowl according to (a) milling speed, or (b) milling time determined by X-ray fluorescence spectroscopy; titania milled without any coupling agent.

The samples change their color during the milling process. Whereas the starting materials  $\text{TiO}_2$  and PPA are white or colorless, samples after the milling process show a grey discoloration that increases with increasing milling time and milling speed (Figure 11).

The change in color can have two origins; either impurities or the presence of subvalent Ti atoms leading to a dark-

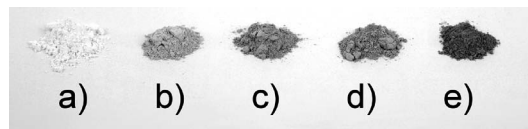


Figure 11. Images of selected samples: (a)  $\text{TiO}_2$ , (b) 200 rpm/12 h; (c) 200 rpm/48 h; (d) 300 rpm/12 h; (e) 300 rpm/48 h.

ening of the samples. When a zirconia grinding bowl was employed under similar conditions a grey discoloration was also observed, although to a much lesser extent. Since it is unlikely that zirconia contaminations lead to the same discoloration, it seems more likely that the discoloration stems from a reduction of  $\text{Ti}^{4+}$  to  $\text{Ti}^{3+}$ .<sup>[20]</sup> We attempted to confirm the existence of  $\text{Ti}^{3+}$  by undertaking XPS analysis of samples milled in the WC grinding bowl. Although there was no indication of  $\text{Ti}^{3+}$  species originating from the milling process on the particle surface, it is not clear whether there was any in the bulk.  $\text{Ti}^{3+}$  species were observed on the surface but these were also found in the untreated samples, therefore, their formation can be the result of Ar-bombarding during XPS measurements as previously described.<sup>[21,22]</sup> An appropriate method to clarify whether  $\text{Ti}^{3+}$  is formed in bulk is the use of electron spin resonance (ESR) spectroscopy, which will be conducted in future work.

The high energy impacts that occur during the reactive milling process leads to temperatures that can exceed  $200^\circ\text{C}$  in the milling bowl, resulting in decomposition reactions such as oxidation of the coupling agents on the surface. Therefore, the washing solution was analyzed to clarify whether side reactions occurred to the PPA.  $^1\text{H}$ ,  $^{13}\text{C}$  and  $^{31}\text{P}$  NMR spectra confirm that PPA was the only species present in the washing solution. Because no decomposition products were detected (see the Supporting Information, Figures S9–S20), it can be assumed that the coupling agent is not degraded due to the high energy impacts during the milling process.

## Conclusions

It was shown that reactive milling is a promising top-down technique for the synthesis of particles with in situ surface modification. Titania surfaces can be modified with a suitable coupling agent such as PPA. Systemic studies on the influence of milling speed and milling time revealed that increasing energy input results in increasing surface coverage of the particles. Contamination of the prepared samples as a result of abrasion from the grinding bowl can be neglected. A tribochemical phase transition from the starting material anatase to the thermodynamically more stable rutile and a high-pressure modification of titania was observed, which depends of the specific process parameters. Particularly, the presence of a surface modifying molecule seems to stabilize the high-pressure phase.

## Experimental Section

**Materials:** Titanium(IV) oxide powder, anatase and phenylphosphonic acid were purchased from Sigma Aldrich. All chemicals were used without further purification.

**Instruments and Characterization:** FTIR measurements were performed under ambient air (40 scans at a resolution of  $4\text{ cm}^{-1}$ ) in attenuated total reflectance (ATR) mode with a Bruker Vertex 70 spectrometer. X-ray powder diffraction was carried out with a Panalytical X'Pert and a Bruker D8 Advance-system, Bragg–Brentano geometry, and  $\text{Cu-K}_\alpha$  radiation was used in both cases. Quantitative phase analysis was carried out by using the Rietveld method with the program TOPAS<sup>[23]</sup> and crystallographic data for the modifications of titania (anatase,<sup>[24]</sup> rutile,<sup>[25]</sup> high-pressure  $\text{TiO}_2$ <sup>[26]</sup>). The same program package was used to determine crystallite sizes, applying the Pawley method. X-ray fluorescence spectroscopy measurements were performed with an Eagle EDAX and an EDAX II instrument. Thermogravimetric analysis (TGA) was carried out with a Netzsch Iris TG 209 instrument. The sample was placed in an alumina crucible, which was then heated from room temperature to  $700\text{ }^\circ\text{C}$  under a nitrogen atmosphere followed by heating to  $800\text{ }^\circ\text{C}$  under an oxygen atmosphere with a rate of  $20\text{ K min}^{-1}$ . The mass loss during the thermal analysis was used to calculate the amount of coupling agent on the surface of the titania particles. Here one has to consider that the residue is not only titania, because the phosphonate groups are oxidized to phosphate, which remain on the surface of the particles. Equation (1) gives the molar amount of coupling agent per gram particles.

$$C_{CA} = \frac{\Delta m \cdot 10}{M_{\Delta m}} \quad (1)$$

where  $C_{CA}$  is the molar concentration of coupling agent per gram [ $\text{mmol g}^{-1}$ ],  $\Delta m$  is the mass loss during thermal analysis [%], and  $M_{\Delta m}$  is the molar mass of the molecule that leaves during thermal analysis [ $\text{g mol}^{-1}$ ].

Elemental analysis was carried out with a Leco CHN-900 analyzer. The amount of coupling agent on the surface of the titania particles was calculated by using the percentage of carbon from elemental analysis. The molar amount of coupling agent per gram of particles can be calculated by using Equation (2).

$$C_{CA} = \frac{m_C \cdot 10}{M_C \cdot N_C} \quad (2)$$

where  $C_{CA}$  is the molar concentration of coupling agent per gram [ $\text{mmol g}^{-1}$ ],  $m_C$  is the mass of carbon from elemental analysis [%],  $M_C$  is the molar mass of carbon [ $\text{g mol}^{-1}$ ], and  $N_C$  is the number of carbon atoms per coupling agent.

Liquid-state NMR spectra were recorded with a Bruker Avance 300 spectrometer operating at  $300.13\text{ MHz}$  for  $^1\text{H}$ ,  $75.47\text{ MHz}$  for  $^{13}\text{C}$ , and at  $121.49\text{ MHz}$  for  $^{31}\text{P}$ . Scanning electron microscopy (SEM) images were recorded with a JEOL SEM-7000 microscope. The SEM samples were prepared by placing some grains on a specimen stub with attached carbon adhesive foil followed by deposition of a gold layer. Dynamic light scattering (DLS) measurements were carried out with an ALV/CGS-3 compact goniometer system with an ALV/LSE-5003 multiple  $\tau$  correlator at a wavelength of  $632.8\text{ nm}$  (He-Ne Laser) and at a  $90^\circ$  goniometer angle. The particle radius was then determined by analysis of the correlation function through the  $g_2(t)$  method followed by a logarithmic number-weighting (n.w.) of the distribution function. Solid-state CP-MAS NMR spectra were recorded with a Bruker DSX Avance

NMR spectrometer operating at  $125.78\text{ MHz}$  for  $^{13}\text{C}$  and at  $202.48\text{ MHz}$  for  $^{31}\text{P}$ .

**Synthesis:** The following experiments were performed in a high-energy planetary ball mill Retsch PM 100. The material of the grinding bowl was WC/Co-hard metal. We used a  $50\text{ mL}$  grinding bowl and 200 corresponding milling balls with a diameter of  $5\text{ mm}$ . Systematic studies on the effect of the milling time and speed on the milling process were carried out. The milling time was varied between 12 and 48 h and the milling speed had values of 200, 250, and 300 rpm. In each case,  $4\text{ g}$  of titania (anatase) and  $1\text{ g}$  of the coupling agent PPA were placed in the grinding bowl and milled at the specified parameters. After the milling process, the product was washed with ethanol (three times) and distilled water (three times). Finally, the functionalized particles were separated by centrifugation ( $13000\text{ rpm}$ ) and dried at  $100\text{ }^\circ\text{C}$ .

**Supporting Information** (see footnote on the first page of this article): IR spectra and XRD patterns of all samples. Liquid- and solid-state NMR spectra. Tables summarizing the phase composition of all samples.

## Acknowledgments

We thank Dr. Robert Haberkorn for assistance in the analysis of the X-ray powder patterns, and Susanne Harling for the elemental analyses. Furthermore, we thank Dirk Schaffner (University of Kaiserslautern) for the solid-state NMR spectroscopy and Dr. Frank Müller as well as Samuel Grandthyll (Physics Department, Saarland University) for the XPS measurements and for fruitful discussions.

- [1] J. F. Fernández-Bertran, *Pure Appl. Chem.* **1999**, *71*, 581–586.
- [2] A. L. Garay, A. Pichon, S. L. James, *Chem. Soc. Rev.* **2007**, *36*, 846–855.
- [3] G. Kaupp, *CrystEngComm* **2006**, *8*, 794–804.
- [4] S. L. James, C. J. Adams, C. Bolm, D. Braga, P. Collier, T. Friščić, F. Grepioni, K. D. M. Harris, G. Hyett, W. Jones, A. Krebs, J. Mack, L. Maini, A. G. Orpen, I. P. Parkin, W. C. Shearouse, J. W. Steed, D. C. Waddell, *Chem. Soc. Rev.* **2012**, *41*, 413–447.
- [5] C. Ney, H. Kohlmann, G. Kickelbick, *Int. J. Hydrogen Energy* **2011**, *36*, 9086–9090.
- [6] A. F. Fuentes, L. Takacs, *J. Mater. Sci.* **2013**, *48*, 598–611.
- [7] G. Kaupp, *CrystEngComm* **2011**, *13*, 3108–3121.
- [8] D. Braga, F. Grepioni, *Angew. Chem.* **2004**, *116*, 4092–4102.
- [9] K. C.-F. Leung, S. Xuan, X. Zhu, D. Wang, C.-P. Chak, S.-F. Lee, W. K.-W. Ho, B. C.-T. Chung, *Chem. Soc. Rev.* **2012**, *41*, 1911–1928.
- [10] S. Hameed, P. Predeep, M. R. Baiju, *Rev. Adv. Mater. Sci.* **2012**, *26*, 30–42.
- [11] W. Chen, Y. Qiu, S. Yang, *Phys. Chem. Chem. Phys.* **2012**, *14*, 10872–10881.
- [12] A. J. Mieszawska, W. J. M. Mulder, Z. A. Fayad, D. P. Cormode, *Mol. Pharm.* **2013**, *10*, 831–847.
- [13] C. Queffélec, M. Petit, P. Janvier, D. A. Knight, B. Bujoli, *Chem. Rev.* **2012**, *112*, 3777–3807.
- [14] W. Liu, Z. Xie, X. Yang, Y. Wu, C. Jia, T. Bo, L. Wang, *J. Am. Ceram. Soc.* **2011**, *94*, 1327–1330.
- [15] P. H. Mutin, G. Guerrero, *Chem. Mater.* **2001**, *13*, 4367–4373.
- [16] P. H. Mutin, G. Guerrero, *Chem. Mater.* **2008**, *20*, 5191–5196.
- [17] F. Dachille, R. Roy, *Am. Ceram. Soc. Bull.* **1962**, *41*, 225.
- [18] P. Y. Simons, F. Dachille, *Acta Crystallogr.* **1967**, *23*, 334–336.
- [19] J. Chaudhuri, M. L. Ram, B. K. Sarkar, *J. Mater. Sci.* **1994**, *29*, 3484–3488.
- [20] U. Diebold, *Surf. Sci. Rep.* **2003**, *48*, 53–229.

- [21] F. Zhang, S. Jin, Y. Mao, Z. Zheng, Y. Chen, X. Liu, *Thin Solid Films* **1997**, *310*, 29–33.
- [22] J. T. Mayer, U. Diebold, T. E. Madey, E. Garfunkel, *J. Electron Spectrosc. Relat. Phenom.* **1995**, *73*, 1–11.
- [23] *Topas V4.2*; General profile and structure analysis software for powder diffraction data, User Manual, Bruker AXS, Karlsruhe, Germany, **2008**.
- [24] D. W. Kim, N. Enomoto, Z. Nakagawa, K. Kawamura, *J. Am. Ceram. Soc.* **1996**, *4*, 1095–1099.
- [25] R. J. Hill, C. Madsen, *Z. Kristallogr.* **1991**, *196*, 73–92.
- [26] S. K. Fulatov, N. A. Bendeliani, B. Albert, J. Kopf, T. I. Dyuzheva, L. M. Lityagina, *Dokl. Phys.* **2007**, *52*, 195–199.

Received: May 6, 2013

Published Online: September 25, 2013



### **3.1.2 IMPORTANT REACTION PARAMETERS IN THE SYNTHESIS OF PHENYLPHOSPHONIC ACID FUNCTIONALIZED TITANIA PARTICLES BY REACTIVE MILLING**

The second publication deals with the influence on the grinding bowl and grinding sphere material on the synthesis and *in situ* surface functionalization of titania with phenylphosphonic acid. This process parameter is often overseen but it is assumed to have a crucial influence on the energy input during the milling process as well. For this reason, systematic studies were performed in order to investigate the influence of the grinding sphere material. The experiments were performed in a high-energy planetary ball mill. In contrast to the previous studies where a WC/Co-hard metal grinding bowl and corresponding milling balls were used here grinding sphere material made of zirconia is applied.

Again titania was used as inorganic pigment as the phase composition of the samples after the milling process is an indicator for the energy input to the system. Phenylphosphonic acid is applied as surface-modifying agent. Systematic studies on the effect of milling time and rotational speed were performed with respect to the optimization of these process parameters.

In order to reveal that the surface-modifying agent is not degraded due to the high-energy impact during the milling process NMR studies were conducted. FT-IR spectroscopy was applied to show that a surface functionalization has taken place. The binding modes of the surface-modifying agent were investigated using solid state NMR spectroscopy. The degree of surface coverage was determined by the use of TG and CHN analyses. X-ray diffraction was applied in order to characterize the phase composition of the samples and X-ray fluorescence spectroscopy was performed to identify impurities due to abrasion of the milling process. The particle size and morphology were analyzed applying dynamic light scattering and scanning electron microscopy.

The results of these studies were compared to the findings of the experiments with the WC/Co-hard metal grinding sphere material. Just as in the experiments with the WC/Co-hard metal grinding bowl and balls there is no degradation of the surface-modifying agent when zirconia grinding bowl and balls are used. Here a surface functionalization takes place as well with different binding modes of the

phenylphosphonic acid on the titania surface. The degree of surface coverage increases with increasing energy input but it is slight smaller than in the prior experiment with the WC/Co-hard metal grinding sphere material. On average it is possible to achieve a surface-modification with the WC/Co grinding bowl increased by approximately 0.2 mmol phosphonate per gram particle compared to the ZrO<sub>2</sub> grinding equipment.

Even the amount of phase transition decreases in case of the zirconia grinding sphere material. However, in both cases the addition of the surface-modifying agent inhibits the overall phase transition but concurrently seems to stabilize the high-pressure phase. The grinding sphere material seems to have no influence on the crystallite sizes as well as particle sizes and morphology.

The great advantage of the zirconia grinding equipment against the WC/Co one is the fact that lower impurity concentration in the final material was achieved due to the better abrasion behavior of the zirconia grinding bowl. For the WC/Co grinding bowl impurities of 0.05 wt-% up to 0.28 wt-% tungsten were found. Milling in the zirconia grinding bowl results in impurities between only 0.03 wt-% and 0.15 wt-%. However, in both cases the impurity concentration increases with increasing energy input.

Just as in case of the WC/Co grinding bowl the samples obtained with the ZrO<sub>2</sub> grinding bowl show a grey discoloration which origin was not identified clearly. Now ESR measurements were performed which clarify that the samples contain Ti<sup>3+</sup> ions which most likely lead to a darkening of the obtained powders. The supporting information (see chapter 7.2) belonging to this publication contains tables summarizing the phase composition of all samples and IR spectra as well as XRD pattern of all samples are shown. Furthermore, the liquid- and solid-state NMR spectra as well as the ESR spectra are presented.

These results have been published in the *New Journal of Chemistry*:

A. Betke, G. Kickelbick, Important reaction parameters in the synthesis of phenylphosphonic acid functionalized titania particles by reactive milling, *New J. Chem.*, **2014**, 38, 1264-1270.

Reproduced by permission of The Royal Society of Chemistry (RSC) for the Centre National de la Recherche Scientifique (CNRS) and the RSC.

<http://pubs.rsc.org/en/content/articlelanding/2014/nj/c3nj01291c#!divAbstract>

The publication was written by Annika Betke and all experiments and characterizations presented were performed by her. Guido Kickelbick has contributed suggestions for improvements and is mentioned as corresponding author as he is the working group leader and Ph.D. supervisor.

# Important reaction parameters in the synthesis of phenylphosphonic acid functionalized titania particles by reactive milling†

Cite this: *New J. Chem.*, 2014, **38**, 1264

Annika Betke and Guido Kickelbick\*

Surface functionalized titania particles are obtained using a high energy planetary ball mill. A parameter that is often overseen while applying this technique is the grinding bowl and grinding sphere material which has a crucial influence on the energy impact in the milling process. In this paper we describe the influence of the grinding bowl focusing on a zirconia ceramic material and comparing the results with experiments performed using a WC/Co-hard metal grinding bowl. The degrees of surface coverage as well as tribochemical phase transitions are dependent on the grinding bowl material. Due to the lower density of ZrO<sub>2</sub>-ceramic the overall energy input is lower. As a result the surface coverage and amount of phase transition decreased when using a zirconia ceramic grinding bowl instead of the WC/Co-hard metal grinding bowl. Lower impurity concentration in the final material was achieved due to the better abrasion behavior of the zirconia grinding bowl.

Received (in Montpellier, France)  
17th October 2013,  
Accepted 13th January 2014

DOI: 10.1039/c3nj01291c

[www.rsc.org/njc](http://www.rsc.org/njc)

## Introduction

Reactive milling is a solvent-free and therefore environmentally friendly alternative to conventional synthetic strategies. For this reason there is increasing interest for several applications.<sup>1,2</sup> Reactive milling can not only be applied to inert oxide compounds but also for the synthesis of quite sensitive materials, such as metal hydrides. Here small particles show a large efficiency in the uptake and release of hydrogen, as a result these compounds have received great attention in the last few years for the storage of hydrogen. Ney *et al.* reported that it is possible to obtain calcium hydride by milling calcium and phenylphosphonic acid under an inert atmosphere.<sup>3</sup> Furthermore, reactive milling was already used for the preparation of various alloys and a couple of organic synthesis.<sup>1,4,5</sup> Another example of the advantageous use of reactive milling is the synthesis of multicomponent oxides. Due to the strong forces which act in a ball mill the resulting products distinguish themselves through small particle sizes, inconvenient metastable phases and structure defects.<sup>6</sup> Many research fields are very interested in surface-functionalized (nano)particles, because they are important building blocks for various applications for example in material science,<sup>7</sup> optics,<sup>8</sup> electronics<sup>9</sup> or in

the biomedical field.<sup>10</sup> Such materials with tunable properties are in great demand but their preparation is still very complex. While previously most of those particles were prepared by bottom-up approaches due to the advantages of higher control of morphology and composition of the particles, we showed recently that reactive milling is suitable for the preparation and *in situ* surface functionalisation of inorganic nanoparticles. We investigated reactive milling processes applying phenylphosphonic acid as an additive and titania as an inorganic pigment. It was possible to create functionalized particles using a high energy planetary ball mill and a WC/Co-hard metal grinding bowl.<sup>11</sup> In this study we investigate the effect of the grinding bowl on this synthesis route. The goal was to clarify the influence of the grinding bowl on the synthesis and *in situ* surface functionalization of titania with phenylphosphonic acid in a planetary ball mill.

## Results and discussion

Reactive milling was carried out using a high energy planetary ball mill with a ZrO<sub>2</sub>-ceramic grinding bowl at varying hours of milling time and revolutions per minute (rpm). Titania was used as an inorganic pigment and phenylphosphonic acid as a surface reactive reagent. Due to the fact that titania has different crystallographic phases which are dependent on the energy put into the system, the ratio between these phases indicates the energy input to the sample during the milling process. The obtained material was thoroughly washed before it

*Inorganic Chemistry, Saarland University, Am Markt Zeile 3, 66125 Saarbrücken, Germany. E-mail: [guido.kickelbick@uni-saarland.de](mailto:guido.kickelbick@uni-saarland.de); Web: <http://www.uni-saarland.de/lehrstuhl/kickelbick.html>*

† Electronic supplementary information (ESI) available: IR spectra and XRD patterns of all samples, tables summarizing the phase composition of all samples and solid state NMR as well as ESR spectra. See DOI: 10.1039/c3nj01291c

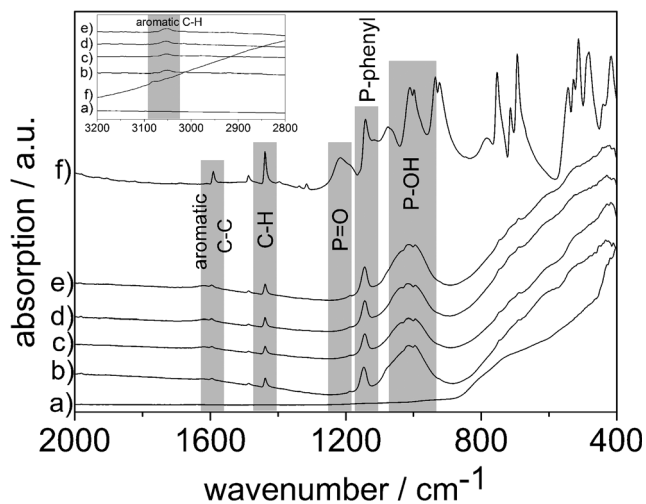


Fig. 1 FTIR-spectra: (a) starting material titania, (f) coupling agent phenylphosphonic acid and samples after the milling process: (b) 300 rpm/12 h, (c) 300 rpm/24 h, (d) 300 rpm/36 h, (e) 300 rpm/48 h; surface modification has taken place after the milling process, which is indicated by the characteristic bands for aromatic C–C oscillation ( $1600\text{ cm}^{-1}$ ), the C–H oscillation ( $1440\text{ cm}^{-1}$ ), P-phenyl vibrations ( $1150\text{ cm}^{-1}$ ), the wide band at  $1000\text{ cm}^{-1}$  (P–O region) and the aromatic C–H oscillation at  $3050\text{ cm}^{-1}$ .

was characterized applying various techniques focusing on changes in the composition depending on the reaction parameters. FTIR-analysis showed that the phenylphosphonic acid was attached to the surface of the titania. Instead of the starting material, which reveals no absorption in the typical region for organic molecules, the samples after the milling process display such characteristic bands. There are typical bands for the aromatic C–C oscillation ( $1600\text{ cm}^{-1}$ ) and the aromatic C–H stretching vibration ( $3050\text{ cm}^{-1}$ ) as well as the C–H ( $1440\text{ cm}^{-1}$ ) deformation, P-phenyl ( $1150\text{ cm}^{-1}$ ) and the P–O ( $1000\text{ cm}^{-1}$ ) vibration. The covalent binding of the phenylphosphonic acid to the surface of the titania particles is indicated by the broad band at approximately  $1000\text{ cm}^{-1}$ . The different bonding types *e.g.* bi- and tridentate of the phenylphosphonic acid on the titania are responsible for the width of this band.<sup>12</sup> The different process parameters yield in a variation of the intensity of the bands (Fig. 1). These results show that the synthesis of particles with *in situ* surface modification occurs not only using a WC/Co grinding bowl but also by using a  $\text{ZrO}_2$  grinding bowl.

Beside the proof that the organophosphorous coupling agent was attached to the surface it is important to determine the amount of surface coverage using thermal (TGA) and elemental (CHN) analysis. These methods were applied to the obtained products and the results were associated with the milling time and the rotational speed (Fig. 2). With increasing values both parameters are expected to decrease the particle size as well as the number of defects on the particle surface which is accompanied by an increase of surface coverage, which was observed for the treated samples. It is noticeable that there is only a small difference between milling times of 12 h or 24 h at 200 rpm. Apart from that the increase of surface coverage correlates almost linearly with milling time (Fig. 2a).

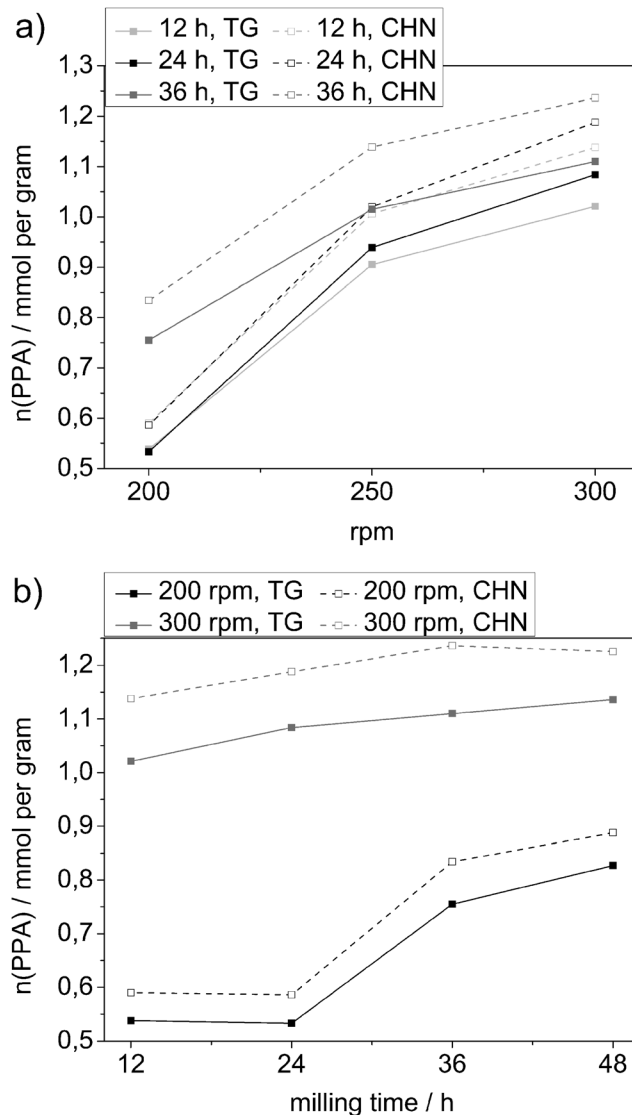


Fig. 2 Surface modification independent of (a) the rpm or (b) the milling time, results calculated from TGA analyses (straight line) and from CHN analyses (dashed line).

CHN analysis generally results in a slightly higher amount of surface coverage than TGA analysis which is due to experimental errors of both methods. Comparing these achievements to the outcome resulting from the experiments with the WC/Co-hard metal grinding bowl it becomes apparent that in the case of using the  $\text{ZrO}_2$ -ceramic grinding bowl the overall surface coverage is lower. The reason for this is the difference in the density of the material of the grinding bowl. Due to the lower density of the  $\text{ZrO}_2$ -ceramic in comparison to the WC/Co-hard metal the overall energy input during the milling process is lower. On the average it is possible to achieve approximately  $0.2\text{ mmol per gram}$  more surface modification with the WC/Co grinding bowl than with the  $\text{ZrO}_2$  grinding bowl.

The so far applied characterization methods indicate that a surface modification has taken place during the milling process. Beside this fact and the information on the amount of surface

coverage it would be interesting to know in which way the phenylphosphonic acid has bound on the surface of the titania. For this reason solid state NMR spectroscopy was performed. The results reveal that covalent bonding occurs. Pure phenylphosphonic acid shows a signal at  $\delta = 21.8$  ppm in the solid state  $^{31}\text{P}$  NMR spectrum.  $^{31}\text{P}$  solid state NMR spectra of the samples after the milling process show a broad signal between  $\delta = 0$  ppm and  $\delta = 16$  ppm (ESI,† S8–S10) which is characteristic for covalent bonding of phosphonic acid on the surface.<sup>13</sup> The  $^{13}\text{C}$  solid state NMR spectra of the samples after the milling process show overlapping signals between  $\delta = 121$  ppm and  $\delta = 125$  ppm which indicates that a phenyl ring is present.

X-ray powder diffraction shows that the milling process was accompanied by a tribochemical phase transition which occurs from the starting material anatase to the thermodynamically more stable rutile and a high pressure modification of titania (Fig. 3). The difference between rutile and the high pressure titania appear in the orientation of the vertex-connected  $\text{TiO}_6$ -octahedra along the *c*-axis. In the case of the rutile phase they form straight lines but in the case of high pressure titania they build zigzag chains. Such a phase formation was observed when using the WC/Co grinding bowl as well. In both cases the reflections for high pressure  $\text{TiO}_2$  ( $2\theta = 31^\circ$ ,  $42^\circ$  and  $66^\circ$ ) and rutile ( $2\theta = 27^\circ$ ) become more intensive when the milling time or the rotational speed are enhanced.

In addition to the qualitatively visible change in the reflection intensity a quantitative Rietveld phase analysis was performed. The presence of an amorphous phase cannot be excluded but the development of the background gives no evidence for it. In case that an amorphous phase is present its proportion is estimated to be less than 5%. The summarized results are presented in Fig. 4 and some results are listed in Table 1. These results confirm the assumption established based on the reflection intensity which revealed that there is

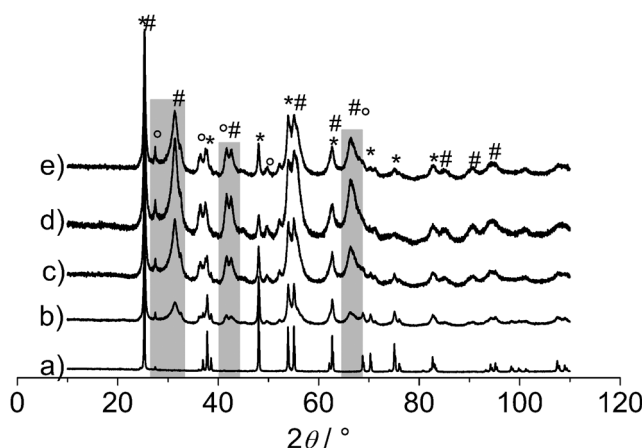


Fig. 3 XRD patterns of (a) the starting material anatase (\*) and some samples after the milling process titania with phenylphosphonic acid: (b) 300 rpm/12 h, (c) 300 rpm/24 h, (d) 300 rpm/36 h, (e) 300 rpm/48 h. The selection indicates the main differences in the reflections: the presence of high pressure  $\text{TiO}_2$  (#) ( $2\theta = 31^\circ$ ,  $42^\circ$  and  $66^\circ$ ) and rutile (°) ( $2\theta = 27^\circ$ ) is indicated by additional reflections.

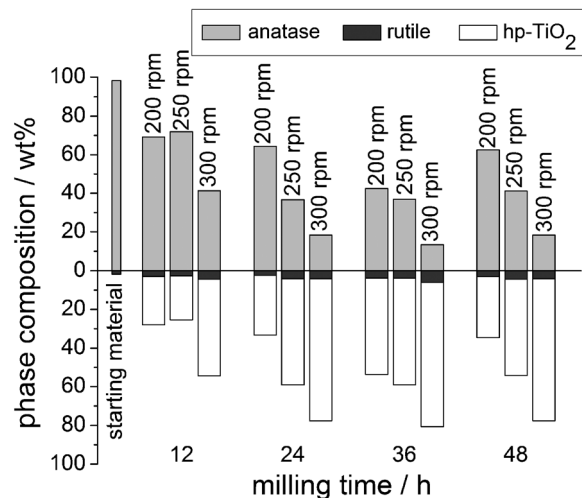


Fig. 4 Titania milled with phenylphosphonic acid: phase composition of the samples after the milling process determined by X-ray powder diffraction. Phase composition occurs from the starting material anatase to rutile and high pressure (hp)  $\text{TiO}_2$ .

Table 1 Titania milled with phenylphosphonic acid, phase composition of some selected samples

Process parameter	Anatase/wt%	Rutile/wt%	hp- $\text{TiO}_2$ /wt%
0 h/0 rpm	98.2 ± 0.1	1.8 ± 0.1	0
12 h/200 rpm	69.1 ± 0.2	2.9 ± 0.1	28.0 ± 0.2
48 h/200 rpm	62.4 ± 0.2	3.0 ± 0.1	34.6 ± 0.2
12 h/300 rpm	41.3 ± 0.2	4.3 ± 0.2	54.4 ± 0.2
48 h/300 rpm	18.3 ± 0.2	4.1 ± 0.1	77.6 ± 0.2

increase in the amount of rutile and high pressure  $\text{TiO}_2$  in the samples with increasing milling time and rpm.

Comparing these results with the findings of the WC/Co grinding bowl it is apparent that there is less phase transition during the milling process in the  $\text{ZrO}_2$  grinding bowl. This confirms the assumption that the overall energy input into the system is lower if a  $\text{ZrO}_2$  grinding bowl is used (Table 2).

The influence of the coupling agent on the tribochemical phase transition was discovered by milling titania without any addition. Some results are listed in Table 3 and Fig. 5 gives an overview of all results.

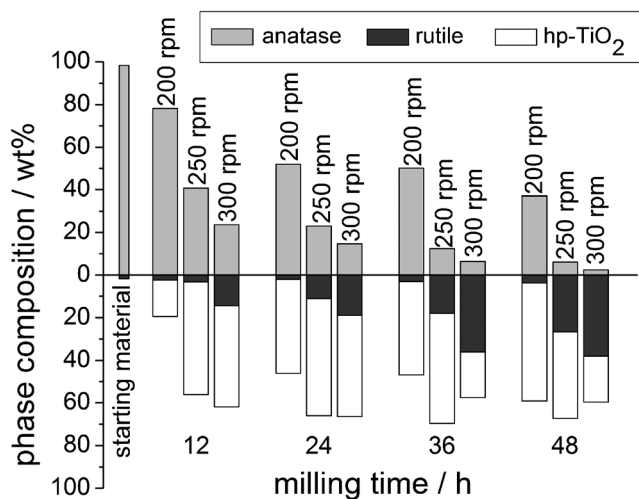
It turned out that the phase transition behaves differently when titania was milled without an additive. In the case of milling titania without the addition of the coupling agent phenylphosphonic acid the overall phase transition is higher and more rutile is generated.

Table 2 Overall phase transition of titania particles milled with phenylphosphonic acid at various process parameters in different grinding bowls

Process parameters	WC/Co-hard metal grinding bowl	$\text{ZrO}_2$ -ceramic grinding bowl
	Anatase/wt%	Anatase/wt%
12 h/200 rpm	73.0 ± 0.2	69.1 ± 0.2
48 h/200 rpm	49.3 ± 0.2	62.4 ± 0.2
12 h/300 rpm	32.6 ± 0.3	41.3 ± 0.2
48 h/300 rpm	7.6 ± 0.1	18.3 ± 0.2

**Table 3** Titania milled without any additives, phase composition of some selected samples

Process parameter	Anatase/wt%	Rutile/wt%	hp-TiO <sub>2</sub> /wt%
0 h/0 rpm	98.2 ± 0.1	1.8 ± 0.1	0
12 h/200 rpm	78.1 ± 0.3	2.4 ± 0.2	19.5 ± 0.3
48 h/200 rpm	37.1 ± 0.4	3.8 ± 0.2	59.1 ± 0.4
12 h/300 rpm	23.6 ± 0.2	14.5 ± 0.4	61.9 ± 0.4
48 h/300 rpm	2.4 ± 0.1	38.0 ± 0.6	59.6 ± 0.6

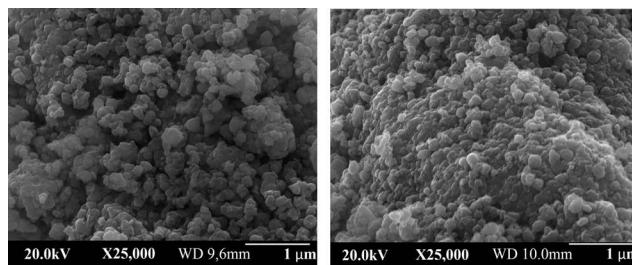
**Fig. 5** Titania milled without any additives: phase composition of the samples after the milling process determined by X-ray powder diffraction. Phase composition occurs from the starting material anatase to rutile and high pressure (hp) TiO<sub>2</sub>.

This behavior was also found when the experiments were performed in the WC/Co grinding bowl. Hence, the phenylphosphonic acid inhibits the phase transformation of anatase; a reason for this could be that anatase becomes more stable against phase transition due to the surface modification. Concurrently the phenylphosphonic acid enhances the formation of high pressure TiO<sub>2</sub> which could be explained by the assumption that the phenylphosphonic acid favors the surface of the high pressure titania for functionalization which consequently stabilizes this modification in comparison to rutile. Also in the case of milling titania without any additive the overall phase transition is higher when milling in a WC/Co than in a ZrO<sub>2</sub> grinding bowl (Table 4).

An important characteristic of the obtained samples beside the surface functionalization and phase transition are the crystallite

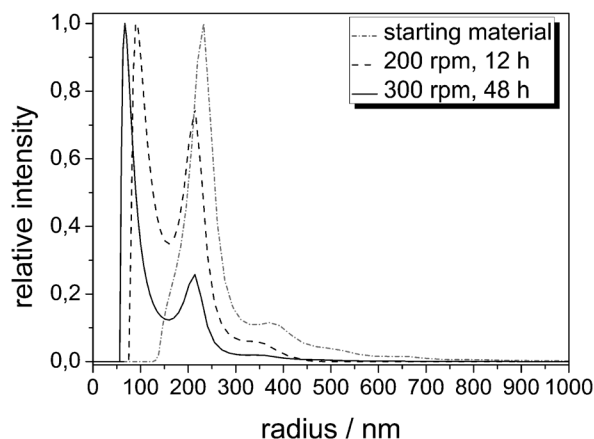
**Table 4** Overall phase transition of titania particles milled without any additive at various process parameters in different grinding bowls

Process parameters	WC/Co-hard metal grinding bowl	ZrO <sub>2</sub> -ceramic grinding bowl
	Anatase/wt%	Anatase/wt%
12 h/200 rpm	39.8 ± 0.3	78.1 ± 0.3
48 h/200 rpm	31.3 ± 0.3	37.1 ± 0.4
12 h/300 rpm	6.1 ± 0.1	23.6 ± 0.2
48 h/300 rpm	4.2 ± 0.1	2.4 ± 0.1

**Fig. 6** SEM images of two selected samples: titania milled with phenylphosphonic acid at 300 rpm for 12 h (left) and for 48 h (right). Both samples are agglomerated and not uniformly shaped, the size of the particles decreases with increasing milling time.

as well as the particle sizes. The crystallite sizes were derived from XRD pattern applying the Pawley method. The results show that the milling process yields in a slight decrease of the crystallite size. As starting material granular crystalline anatase with crystallite sizes above 300 nm was used. In contrast the resulting high pressure TiO<sub>2</sub> has sizes around 5 nm to 6 nm. The residual anatase phase remains in the granular crystalline dimension, there is only a reduction of about 100 nm compared to the starting material. The milling time and the rotational speed mostly influence the phase transition but not the particle size. Independent of these parameters the resulting high pressure TiO<sub>2</sub> is nano crystalline but the residual anatase remains granular crystalline. SEM images of the obtained powders show that the samples are not uniformly shaped and agglomerated (Fig. 6). Particle sizes are in a range of 100 nm to 300 nm and decreases with increasing milling time.

The radius of the particles was determined by dynamic light scattering (DLS) (Fig. 7 and 8). The surface functionalized particles can be directly dispersed in cyclohexane by the exposition of ultrasound for 30 minutes. The starting material and the unmodified samples can be dispersed in water. The starting material has sizes of 500 nm or larger but it is apparent that

**Fig. 7** Particle size determination by dynamic light scattering, titania milled with phenylphosphonic acid. The starting material was dispersed in water while the functionalized particles were dispersed in cyclohexane, both by the exposition to ultrasound for 30 minutes. Particle size decreases slightly with increasing milling time and increasing rpm.

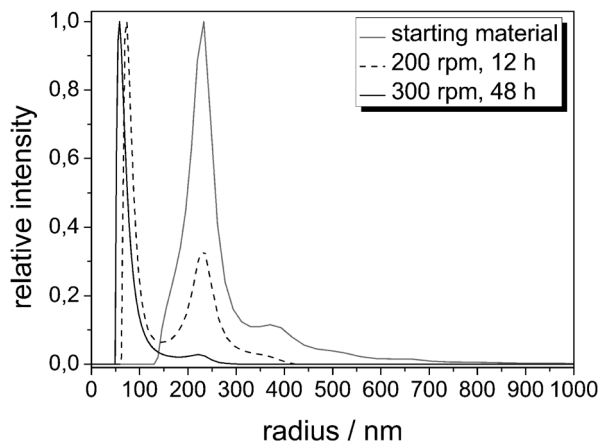


Fig. 8 Particle size determination by dynamic light scattering, titania milled without any additive. All samples were dispersed in water by the exposition to ultrasound for 30 minutes. Particle size decreases slightly with increasing milling time and increasing rpm.

after the milling process there is a significant reduction of the particle size. The samples after the milling process exhibit two distinctly sized particle fractions which is in agreement to the results of XRD that there are different phases of titania. Firstly there are particles with sizes about 400 nm and secondly there are some which show sizes around 140 nm (300 rpm, 48 h) and 200 nm (200 rpm and 12 h). In the case of milling titania without any additive the reduction of the particle size is advanced due to the milling process. There are two different fractions as well but the smaller one show sizes about 110 nm and 160 nm. In addition the fraction with particle sizes around 400 nm is smaller.

The contamination of the samples due to abrasion of the grinding bowl was analyzed by applying X-ray fluorescence spectroscopy (Fig. 9). As expected there is more contamination with increasing milling time and rotational speed. Compared to the results obtained by using the WC/Co grinding bowl the impurities are smaller. In the case of the WC/Co grinding bowl impurities of 0.05 wt% up to 0.28 wt% tungsten were found. Milling in the  $ZrO_2$  grinding bowl results in impurities between only 0.03 wt% and 0.15 wt% Zr.

Whereas the starting materials  $TiO_2$  and PPA are white the samples after the milling process show a grey discoloration which becomes more intensive with increasing milling time and speed (Fig. 10). This discoloration was observed as well when a WC/Co-hard metal grinding bowl was used. We assumed that this discoloration has its origin in impurities due to the abrasion of the grinding bowl which is likely to be grey in the case of tungsten. The experiments with the zirconia grinding bowl results in a grey discoloration as well. Here it is unlikely that the zirconia impurities lead to a grey discoloration. An explanation for the change in color beside the contamination with impurities could be the presence of subvalent Ti species which could be formed during the milling process due to reduction of  $Ti^{4+}$  to  $Ti^{3+}$ . To clarify the reason for this aspect electron paramagnetic resonance was applied. The results confirm the presence of  $Ti^{3+}$  in the samples where

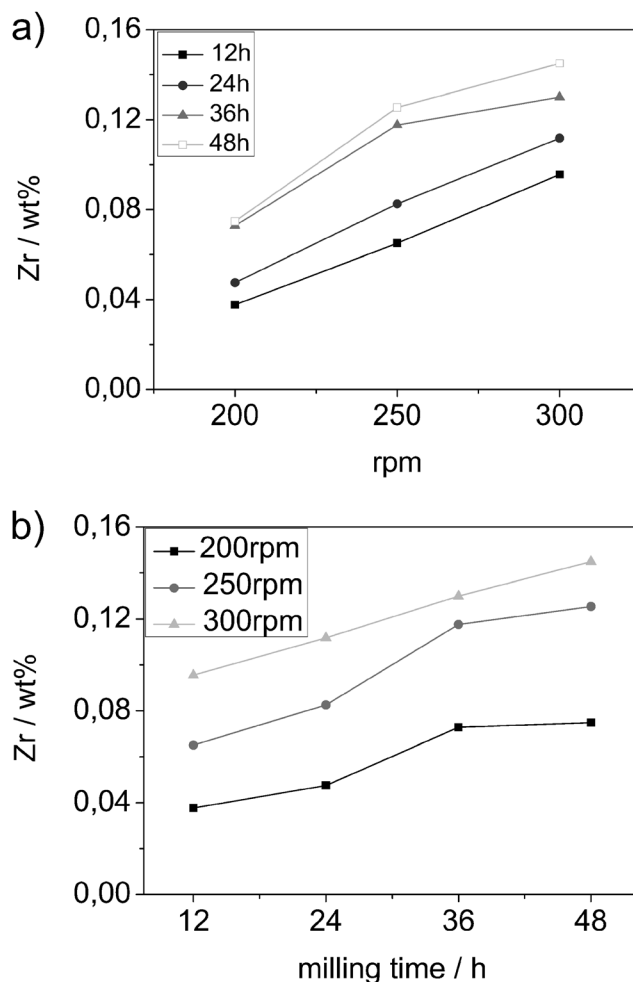


Fig. 9 Impurities by the grinding bowl according to (a) the rpm or (b) the milling time determined by X-ray fluorescence spectroscopy, titania milled with the coupling agent.

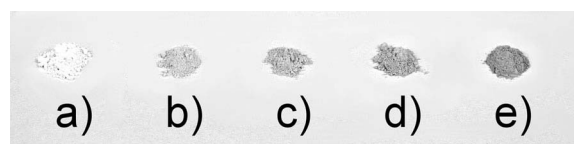


Fig. 10 Images of some selected samples of titania milled with the coupling agent: (a)  $TiO_2$ , (b) 200 rpm/12 h, (c) 200 rpm/48 h, (d) 300 rpm/12 h, (e) 300 rpm/48 h. The contamination due to abrasion of the grinding bowl is visible to the naked eye. With increasing revolutions per minute as well as increasing milling time the samples show increasing grey discoloration.

titania was milled with a coupling agent. These samples show the characteristic ESR signal for  $Ti^{3+}$ .<sup>14</sup> In the case of milling titania without any additive there was no signal associated with  $Ti^{3+}$  (ESI,† S11). In this case the grey discoloration has its origin in the contamination with tungsten if a WC/Co-grinding bowl was used. When a zirconia grinding bowl was used the samples milled without any additive show nearly no discoloration (Fig. 11). Consequently, in the case of using a WC/Co-hard metal grinding bowl the grey discoloration has two origins. On the one hand the impurities due to abrasion and on the other hand the



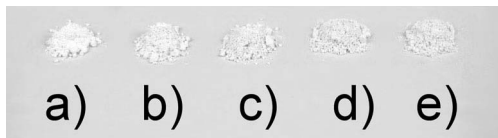


Fig. 11 Images of some selected samples of titania milled without any additive: (a)  $\text{TiO}_2$ , (b) 200 rpm/12 h, (c) 200 rpm/48 h, (d) 300 rpm/12 h, (e) 300 rpm/48 h.

presence of subvalent Ti species which lead to darkening of the samples. When a zirconia grinding bowl is used the grey discoloration is attributed only to the presence of subvalent Ti ions. The presence of  $\text{Ti}^{3+}$  is only appropriate in the case of milling titania with a coupling agent because it acts as a reducing agent as well.

## Conclusions

In summary, reactive milling is shown to be a promising environmentally friendly technique for the synthesis of particles with *in situ* surface functionalization. The systematic study on the influence of the different process parameters shows that increasing milling time and increasing rotational speed results in an increasing degree of surface modification as well as an increasing phase transition of the starting material anatase to rutile and high pressure  $\text{TiO}_2$ . This observed tribochemical phase transition is not only dependent on the rpm and the milling time but also on the presence of the coupling agent. In this work we illustrate that the grinding bowl has an influence on the milling results as well. Compared to previous studies where a WC/Co hard metal grinding bowl was used it turned out that the overall phase transition is lower and there is less surface modification by using a  $\text{ZrO}_2$  ceramic grinding bowl. Another difference is the contamination caused by the abrasion of the grinding bowl. These impurities are lower when a  $\text{ZrO}_2$  grinding bowl is used.

## Experimental section

### Materials

Titanium(IV)-oxide powder anatase (99.8%) and phenylphosphonic acid (98%) were purchased from Sigma Aldrich (Steinheim, Germany). All chemicals have been used without further purification.

### Instruments and characterization

FT-IR measurements were performed under ambient air (40 scans at a resolution of  $4\text{ cm}^{-1}$ ) in attenuated total reflectance (ATR) mode on a Bruker Vertex 70 spectrometer. X-ray powder diffraction was carried out on two different diffractometers a Panalytical X'Pert and a Bruker D8 Advance-system, Bragg-Brentano geometry and  $\text{CuK}\alpha$  radiation were used in both cases. The quantitative analysis was carried out by the Rietveld-method using the program TOPAS<sup>15</sup> and crystallographic data for the modifications of titania (anatase,<sup>16</sup> rutile,<sup>17</sup> high pressure  $\text{TiO}_2$ ).<sup>18</sup> The same program package was used for the determination of the

crystallite sizes applying the Pawley-method. X-ray fluorescence spectroscopy measurements were performed on an Eagle EDAX and EDAX II instrument. Thermogravimetric analysis (TGA) was carried out on a Netzsch Iris TG 209. The sample was placed in an alumina crucible which was then heated from room temperature to  $700\text{ }^\circ\text{C}$  under nitrogen atmosphere followed by heating to  $800\text{ }^\circ\text{C}$  under oxygen atmosphere with a rate of  $20\text{ K min}^{-1}$ . The mass loss during the thermal analysis was used to calculate the amount of coupling agent on the surface of the titania particles. Here one has to consider that the residue is not only titania because the phosphonate groups are oxidized to phosphate which remains on the surface of the particles. Eqn (1) gives the molar amount of coupling agent per gram particles.

$$c_{\text{CA}} = \frac{\Delta m \cdot 10}{M_{\Delta m}} \quad (1)$$

$c_{\text{CA}}$ : molar concentration of coupling agent per gram [ $\text{mmol g}^{-1}$ ]

$\Delta m$ : mass loss during thermal analysis [%]

$M_{\Delta m}$ : molar mass of the molecule which leaves during thermal analysis [ $\text{g mol}^{-1}$ ]

Elemental analysis was carried out on a Leco CHN-900 analyzer. The amount of coupling agent on the surface of the titania particles was calculated by using the percentage of carbon from elemental analysis. The molar amount of coupling agent per gram of particles can be calculated by using eqn (2).

$$c_{\text{CA}} = \frac{m_{\text{C}} \cdot 10}{M_{\text{C}} \cdot N_{\text{C}}} \quad (2)$$

$c_{\text{CA}}$ : molar concentration of coupling agent per gram [ $\text{mmol g}^{-1}$ ]

$m_{\text{C}}$ : mass of carbon from elemental analysis [%]

$M_{\text{C}}$ : molar mass of carbon [ $\text{g mol}^{-1}$ ]

$N_{\text{C}}$ : number of carbon atoms per coupling agent

Solid state NMR spectroscopy was carried out on a Bruker Avance DPX 300 instrument equipped with a 4 mm broad band cross-polarization Magic Angle Spinning probe head operating at  $75.40\text{ MHz}$  for  $^{13}\text{C}$  and  $121.39\text{ MHz}$  for  $^{31}\text{P}$ . The spinning rate was  $3976\text{ Hz}$  for  $^{13}\text{C}$  spectra and  $2040\text{ Hz}$  for  $^{31}\text{P}$  spectra. Scanning electron microscopy (SEM) images were recorded on a JEOL SEM-7000 microscope. The SEM samples were prepared by placing some grains on a specimen stub with attached carbon adhesive foil followed by deposition of a gold layer. Dynamic light scattering (DLS) measurements were carried out on an ALV/CGS-3 compact goniometer system with an ALV/LSE-5003 multiple  $\tau$  correlator at a wavelength of  $632.8\text{ nm}$  (He-Ne Laser) and at a  $90^\circ$  goniometer angle. The particle radius was then determined by the analysis of the correlation-function *via* the  $g_2(t)$  method followed by a logarithmic number-weighting (n.w.) of the distribution function.

### Synthesis

The following experiments were performed in a high energy planetary ball mill Retsch PM 100. The material of the grinding bowl was a  $\text{ZrO}_2$ -ceramic. We used a 50 mL grinding bowl and 200 corresponding milling balls with a diameter of 5 mm. Systematic studies on the effect of the milling time and the

rpm on the result of the milling process were carried out. The milling time was varied between 12 h and 48 h and the rpm had values of 200 rpm, 250 rpm and 300 rpm.

In each case 4 g of titania (anatase) and 1 g of the respective coupling agent (phenylphosphonic acid) were placed in the grinding bowl and milled at specific parameters.

After the milling process the product was washed with ethanol (three times) and distilled water (three times). Finally, the functionalized particles were separated by centrifugation (13 000 rpm) and dried at 100 °C.

## Acknowledgements

We thank Dr Robert Haberkorn (Saarland University) for the assistance with the analysis of the X-ray powder patterns and Susanne Harling (Saarland University) for the elemental analysis. Furthermore, we thank Dr Michael Puchberger (Vienna University of Technology) for the solid state NMR spectroscopy and Prof. Dr Hartmann (University of Erlangen) for the ESR measurements.

## Notes and references

- 1 G. Kaupp, *CrystEngComm*, 2006, **8**, 794–804.
- 2 S. L. James, *et al.*, *Chem. Soc. Rev.*, 2012, **41**, 413–447.
- 3 C. Ney, H. Kohlmann and G. Kickelbick, *Int. J. Hydrogen Energy*, 2011, **36**, 9086–9090.
- 4 G. Kaupp, *CrystEngComm*, 2011, **13**, 3108–3121.
- 5 D. Braga and F. Grepioni, *Angew. Chem.*, 2004, **116**, 4092–4102.
- 6 A. F. Fuentes and L. Takacs, *J. Mater. Sci.*, 2013, **48**, 598–611.
- 7 K. C. Leung, *et al.*, *Chem. Soc. Rev.*, 2012, **41**, 1911–1928.
- 8 S. Hameed, P. Predeep and M. R. Baiju, *Rev. Adv. Mater. Sci.*, 2012, **26**, 30–42.
- 9 W. Chen, Y. Qiu and S. Yang, *Phys. Chem. Chem. Phys.*, 2012, **14**, 10872–10881.
- 10 A. J. Mieszawska, W. J. M. Mulder, Z. A. Fayad and D. P. Cormode, *Mol. Pharmaceutics*, 2013, **10**, 831–847.
- 11 A. Fischer, C. Ney and G. Kickelbick, *Eur. J. Inorg. Chem.*, 2013, 5701–5707.
- 12 G. Guerrero, P. H. Mutin and A. Vioux, *Chem. Mater.*, 2001, **13**, 4367–4373.
- 13 F. Brodard-Severac, G. Guerrero, J. Maquet, P. Florian, C. Gervais and P. H. Mutin, *Chem. Mater.*, 2008, **20**, 5191–5196.
- 14 L. Xiong, J. Li, B. Yang and Y. Yu, *J. Nanomater.*, 2012, **2012**, 13.
- 15 *Topas V4.2; General profile and structure analysis software for powder diffraction data, User Manual*, Bruker AXS, Karlsruhe, Germany, 2008.
- 16 D. W. Kim, N. Enomoto, Z. Nakagawa and K. Kawamura, *J. Am. Ceram. Soc.*, 1996, **4**, 1095–1099.
- 17 R. J. Hill and C. Madsen, *Z. Kristallogr.*, 1991, **196**, 73–92.
- 18 S. K. Fulatov, N. A. Bendeliani, B. Albert, J. Kopf, T. I. Dyuzheva and L. M. Lityagina, *Dokl. Phys.*, 2007, **52**(4), 195–199.

### 3.1.3 LONG ALKYL CHAIN ORGANOPHOSPHORUS COUPLING AGENTS FOR *IN SITU* SURFACE FUNCTIONALIZATION BY REACTIVE MILLING

The previous studies reveal that reactive milling is a promising technique for the synthesis of inorganic particles with *in situ* surface functionalization. Titania has been successfully modified with phenylphosphonic acid applying this top-down approach. Now an interesting question was whether this process is suitable for the surface functionalization with long alkyl chain organophosphorus surface-modifying agents.

This is particularly interesting due to the fact that in contrast to phenylphosphonic acid a functionalization with long alkyl chain organophosphorus coupling agents using conventional synthetic strategies is not possible without the use of an organic solvent. To clarify this question experiments using dodecylphosphonic acid as surface-modifying agent were performed. Again titania was used as inorganic pigment due to its various crystallographic phases.

These experiments were performed using a high-energy planetary ball mill and the zirconia grinding sphere material as it lead to lower impurities which has been demonstrated in the previous studies. Systematic studies on the influence of the milling time and milling speed were performed. The obtained samples were characterized with respect to the stability of the surface-modifying agent (NMR), their phase composition (XRD), surface coverage (FT-IR, TGA, CHN), particle size and morphology (SEM) as well as impurities due to abrasion of the grinding sphere material (XRF).

The results show that the dodecylphosphonic acid is not degraded during the milling process. A surface-modification has taken place and a surface coverage of up to 0.8 mmol phosphonate per gram particle was obtained. The amount of surface coverage increases with increasing milling time and milling speed. In analogy to the previous studies with phenylphosphonic acid as surface-modifier a tribochemical phase transition from anatase to rutile and high-pressure titania occurs during the milling process. Just as in the previous studies the amount of phase transition is dependent on the energy input to the system and increases with this parameter. Even the impurity concentrations due to abrasion of the grinding bowl were negligible low equal to the findings in the previous studies.

The experiments demonstrate successfully that the approach of surface functionalization using a high-energy ball milling process is suitable for dodecylphosphonic acid as surface-modifying agent as well. Consequently, an interesting question was whether this approach is assignable on other long alkyl chain organophosphorus surface-modifying species. In order to clarify this question octadecylphosphonic acid was used as surface-modifying agent. The results show that also octadecylphosphonic acid can be applied to this approach. For this case a degree of surface coverage of 0.6 mmol phosphonate per gram particle was obtained.

The mentioned studies reveal that the approach of *in situ* surface functionalization using a planetary ball mill is extendable on a wide range of coupling agents. The supporting information (see chapter 7.3) belonging to this publication contains tables summarizing the phase composition of all samples and IR spectra as well as XRD pattern of all samples are shown. Furthermore, the liquid- and solid-state NMR spectra as well as the ESR spectra are presented.

The results of these studies are to be published in a further paper. The publication has been submitted to *Inorganics* but is not published yet:

A. Betke, G. Kickelbick, Long alkyl chain organophosphorus coupling agents for *in situ* surface functionalization by reactive milling, *Inorganics*, **2014**, *submitted*.

The publication was written by Annika Betke and all experiments and characterizations presented were performed by her. Guido Kickelbick has contributed suggestions for improvements and is mentioned as corresponding author as he is the working group leader and Ph.D. supervisor.

*Type of the Paper (Article, Review, Communication, etc.)*

## Long alkyl chain organophosphorus coupling agents for *in situ* surface functionalization by reactive milling

Annika Betke, Guido Kickelbick\*

Inorganic Chemistry, Saarland University, Am Markt Zeile 3, 66125 Saarbrücken, Germany;  
E-Mail: guido.kickelbick@uni-saarland.de

\* Guido Kickelbick; E-Mail: guido.kickelbick@uni-saarland.de;  
Tel.: +49-(0)681-302 70651; Fax: +49-(0)681-302 70652.

*Received: / Accepted: / Published:*

---

**Abstract:** The great innovation of the synthesis approach which is presented in this paper is the achievement of a surface modification with long alkyl chain organophosphorus coupling agents without the need of a solvent. As a result, this technique is environmentally as well as ecologically friendly. In addition, it is a great benefit to realize two goals in one step: size reduction and simultaneously surface functionalization. A top-down approach for the synthesis of metal oxide particles with *in situ* surface functionalization is used to modify titania with long alkyl chain organophosphorus coupling agents. A high energy planetary ball mill was used to perform reactive milling using titania as inorganic pigment and long alkyl chain organophosphorus coupling agents like dodecyl and octadecyl phosphonic acid. The final products were characterized by IR, NMR and X-ray fluorescence spectroscopy, thermal and elemental analysis as well as by X-ray powder diffraction and scanning electron microscopy. The process entailed a tribochemical phase transformation from the starting material anatase to a high-pressure modification of titania and the thermodynamically more stable rutile depending on the process parameters. Furthermore, the particles show sizes between 100 nm to 300 nm and a degree of surface coverage up to 0.8 mmol phosphonate per gram.

**Keywords:** reactive milling, titania particles, long alkyl chain organophosphorus coupling agents, tribochemical phase transition

---

## 1. Introduction

Surface modified particles are important building blocks for various applications in optics [1], electronics [2], materials science [3] and in the biomedical field [4]. For this reason there is increasing interest in economic synthetic strategies. In this context, there has been significant interest in mechanochemical approaches [5, 6]. Reactive milling turned out to be a promising technique because it is a solvent-free and environmentally friendly alternative to conventional synthetic strategies [7, 8]. Reactive milling has proven its suitability for the synthesis of various materials, for example calcium hydride by reactive milling of calcium and phenylphosphonic acid (PPA) under an inert atmosphere [9] or  $ZrTiO_4$  [10] to name only two examples out of many others. Recently we investigated the suitability of reactive milling for the preparation of surface functionalized titania nanoparticles. We were able to show that an *in situ* surface functionalization using PPA as coupling agent is possible and that the organophosphorus surface functionalization can stabilize crystallographic high-pressure phases [11, 12]. Often the surface functionalization of particles with organic coupling agents involves the use of organic solvents, our technique allows a solvent free ecologically more friendly approach. In case of PPA the surface functionalization of titania can also be obtained in water as solvents [13]. This is not the case for long alkyl chain phosphonic acids. Here, definitely an organic solvent is necessary for the complete dissolution of the respective coupling agent [14, 15]. This was the reason for us to expand our previous studies to this type of surface modifier. Dodecylphosphonic acid (DDPA) was used to perform a systematic study on the behavior at different process parameters. Afterwards octadecylphosphonic acid (ODPA) was used to demonstrate that the approach is assignable on other long alkyl chain organophosphorus species.

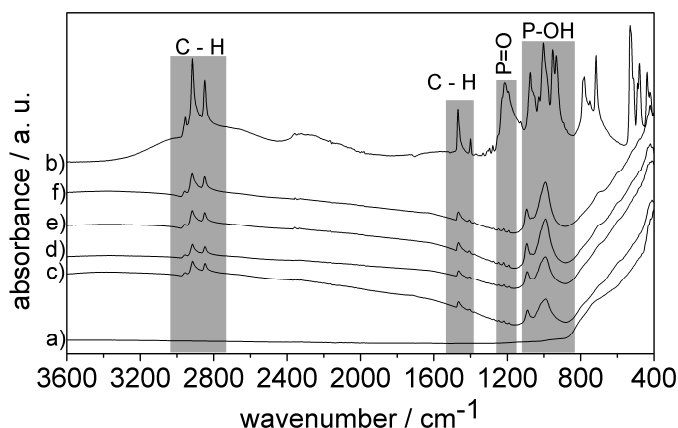
## 2. Results and Discussion

Reactive milling was carried out using titania as inorganic pigment and long alkyl chain organophosphorus coupling agents. The experiments were performed in a high energy planetary ball mill using a  $ZrO_2$ -ceramic grinding bowl and varying the reaction conditions such as milling time and rotational speed (revolutions per minute, rpm). Titania has several crystallographic phases that can be converted into each other depending on the energy input into the system. Consequently, the ratio between the different crystallographic phases is an indicator for the energy applied to the samples. After the milling process the obtained material was thoroughly washed and dried. The washing solution was analyzed to demonstrate that the coupling agent is not degraded due to the high energy impact during the milling process.  $^1H$ ,  $^{13}C$  and  $^{31}P$  NMR spectra confirm that DDPA was the only species present in the washing solution (see ESI Figure S5-S10).

The final products were analyzed applying various techniques. A systematic study on the influence of different process parameters was performed for the DDPA functionalized particles. FTIR analyses show that the milling process results in a bonding between the coupling agent and the titania phase. The starting material reveals no absorption in the typical regions for organic molecules. In contrast, the samples after the milling process display bands that are characteristic for C-H vibrations ( $2900\text{ cm}^{-1}$  and  $1450\text{ cm}^{-1}$ ) as well as P-O oscillations ( $1000\text{ cm}^{-1}$ ) (Figure 1). The broad band at approximately

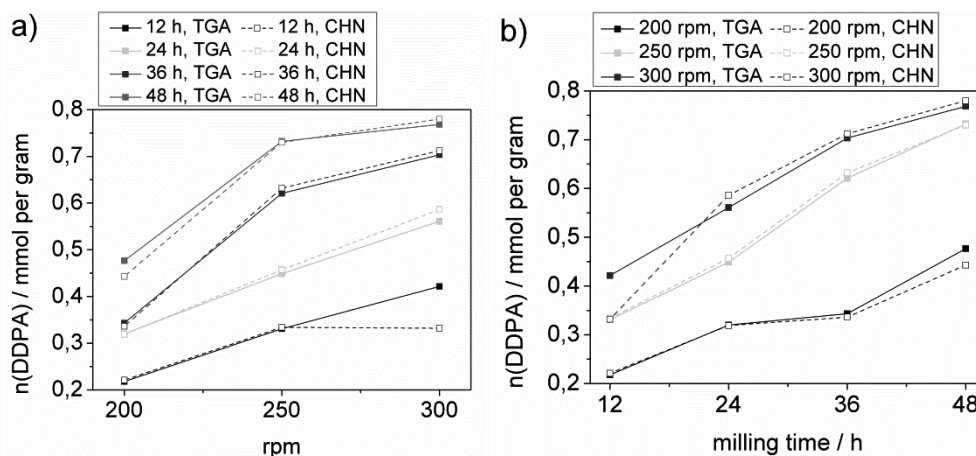
$1000\text{ cm}^{-1}$  is characteristic for surface bonded phosphonates; the width of this band is due to the different bonding types (e. g. bi- and tridentate) of the phosphonates on the titania surface [16].

**Figure 1.** FTIR-spectra: a) starting material titania, b) coupling agent dodecylphosphonic acid and samples after the milling process: c) 300 rpm / 12 h, d) 300 rpm / 24 h, e) 300 rpm / 36 h, f) 300 rpm / 48 h; surface modification has taken place after the milling process, which is indicated by the characteristic bands for the C-H oscillation ( $1450\text{ cm}^{-1}$  and  $2900\text{ cm}^{-1}$ ) and the wide band at  $1000\text{ cm}^{-1}$  (P-O region).



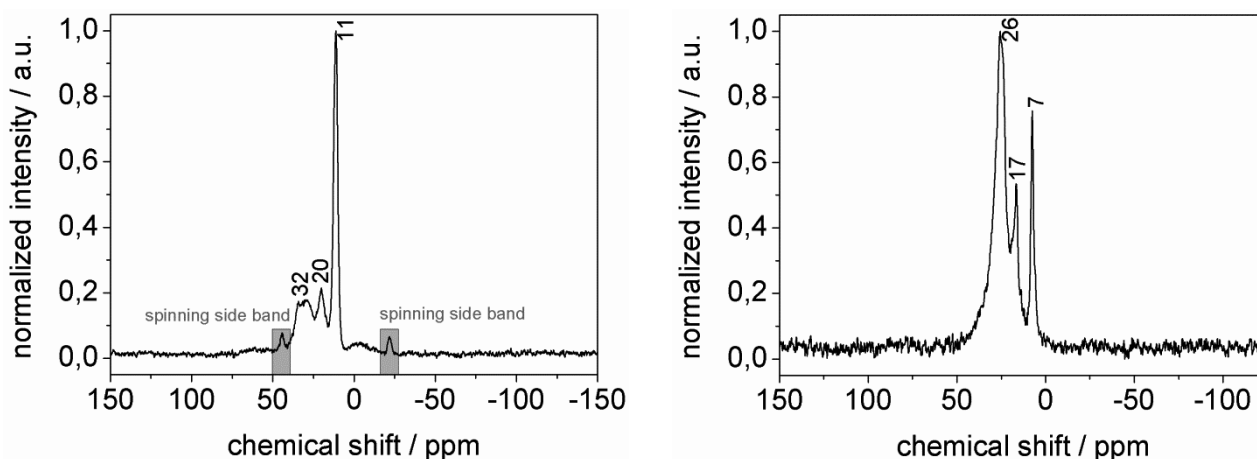
To determine the amount of surface coverage thermal gravimetric (TGA) and elemental (CHN) analyses were performed and the results were correlated with the process parameters rotational speed and milling time (Figure 2). It turned out that the degree of surface coverage increases with increasing milling time as well as increasing milling speed. This correlation can have two reasons. On the one hand a better binding of the organic groups to the titania surface can have its origin in the increased energy input. On the other hand the surface area of the particles is increased which could lead to a higher portion of coupling agent bound to the surface. The results show that the correlation between the surface coverage and the milling time or speed is almost linear. CHN and TGA results show similar development, the slight discrepancies are due to measuring inaccuracies of both methods.

**Figure 2.** Surface modification in dependence of a) the rpm or b) the milling time, results calculated from TGA analyses (straight line) and from CHN analyses (dashed line).

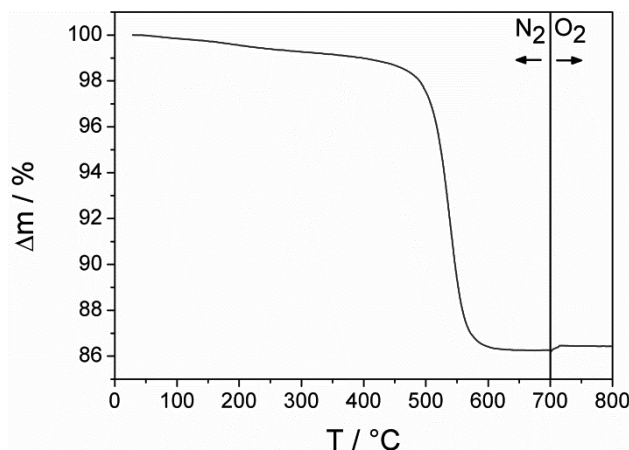


The binding modes of the DDPA to the titania surface were studied by the use of solid-state NMR spectroscopy. The results reveal that DDPA was bonded to the titania surface. Pure DDPA yields in a solid-state  $^{31}\text{P}$  NMR signal at  $\delta = 31.9$  ppm [17], whereas the samples after the milling process show a series of partially broad signals in the range of  $\delta = 10 - 35$  ppm. Furthermore, a sharp peak is observed at  $\delta = 11$  ppm (Figure 3 and ESI Figure S11-S14). This is in good agreement with the variety of possible binding modes of the phosphonate to the metal oxide surface. In literature, for tridentate coordination modes sharp peaks with chemical shifts of around 20 ppm to lower fields with respect to the free phosphonic acid are reported [18]. For bi- and monodentate binding modes the downfield shift is less pronounced and the corresponding peaks are significantly broader [19]. Consequently, the peaks in the range of 10 to 35 ppm correspond to the bi- and monodentate bonded phosphonates and the sharp signal at around 11 ppm can be assigned to the tridentate coordinated species for the samples obtained by reactive milling of titania with DDPA. Theoretically, the signal for tridentate phosphonate species at around 11 ppm could be attributed to layered bulk titanium alkylphosphonates [19]. However, these species show a significantly increased decomposition temperature ( $\sim 750$  °C) compared to alkyl phosphonate modified titania nanoparticles ( $\sim 550$  °C) represented by an additional exothermic step in TG measurements. The TG measurements of the samples obtained by reactive milling of titania with DDPA clearly show only one decomposition step for the degradation of phosphonate species at around 550 °C (Figure 4). Therefore, the presence of layered titanium phosphonate compounds can be excluded. The solid-state  $^{13}\text{C}$  NMR spectra of all samples show signals in the alkyl chain region between  $\delta = 5 - 30$  ppm which reveals that the alkyl chain is still present after the milling process (Figure 3 and ESI Figure S11-S14).

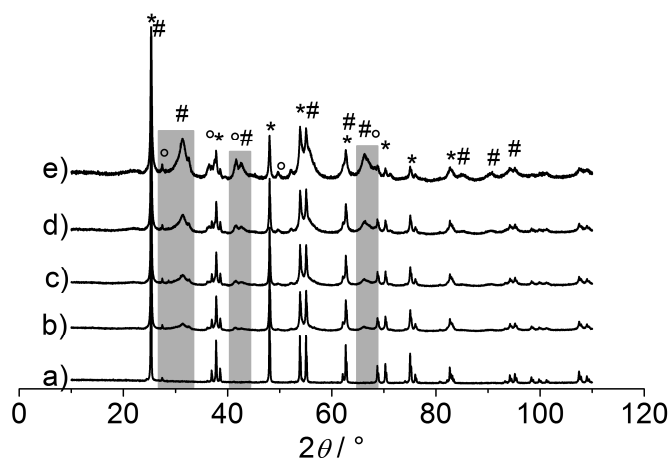
**Figure 3.** CP-MAS  $^{31}\text{P}$  (left) and  $^{13}\text{C}$  (right) spectra of titania milled with dodecylphosphonic acid at 200 rpm for 48 h.





**Figure 4.** TGA of a sample obtained by reactive milling of titania with DDPA.

X-ray powder diffraction was used to study the phase composition of the final products. The results show that a tribochemical phase transition from the starting material anatase to the thermodynamic more stable rutile as well as a high-pressure modification of titania occurs. It turned out that the degree of the phase transition is dependent on the process parameters. The reflections belonging to the rutile and the high-pressure phase ( $2\theta = 27^\circ$  or  $31^\circ$ ,  $42^\circ$  and  $66^\circ$ , respectively) become more intensive when the milling time or the rotational speed are enhanced (Figure 5). The difference between the rutile and the high-pressure modification present itself in the orientation of the vertex-connected  $\text{TiO}_6$ -octahedra along the  $c$ -axis. In case of rutile they form straight lines and in case of high-pressure titania they build zigzag chains.

**Figure 5.** XRD patterns of a) the starting material anatase (\*) and some samples after milling with dodecylphosphonic acid: b) 300 rpm / 12 h, c) 300 rpm / 24 h, d) 300 rpm / 36 h, e) 300 rpm / 48 h. The selection indicates the main differences in the reflections: The presence of high-pressure  $\text{TiO}_2$  (#) ( $2\theta = 31^\circ$ ,  $42^\circ$  and  $66^\circ$ ) and rutile (°) ( $2\theta = 27^\circ$ ) is indicated by additional reflections.

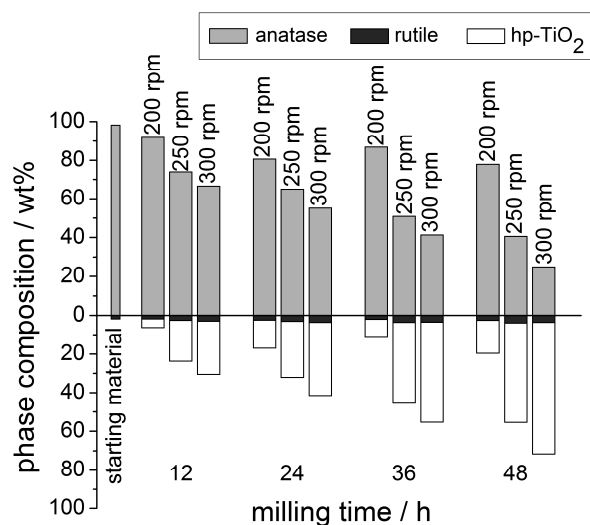
Additional to the qualitatively visible change in the reflection intensity a quantitative Rietveld phase analysis was performed. The development of the background gives no evidence for the presence of an amorphous phase. Nevertheless the presence of such a phase cannot be excluded but if it should be

present its proportion is estimated to be less than 5%. The summarized results are presented in Figure 6 and some results are listed in Table 1. The Rietveld analysis confirms that the fraction of rutile and high-pressure TiO<sub>2</sub> increases with longer milling time and higher milling speed.

**Table 1.** Titania milled with dodecylphosphonic acid, phase composition of some selected samples

Process parameter	Anatase / wt%	Rutile / wt%	hp-TiO <sub>2</sub> / wt%
0 h / 0 rpm	98.2 ± 0.1	1.8 ± 0.1	0
12 h / 200 rpm	91.9 ± 0.2	1.8 ± 0.1	6.3 ± 0.2
48 h / 200 rpm	77.8 ± 0.3	2.6 ± 0.1	19.6 ± 0.3
12 h / 300 rpm	66.5 ± 0.2	2.9 ± 0.2	30.6 ± 0.2
48 h / 300 rpm	24.9 ± 0.2	3.5 ± 0.2	71.6 ± 0.2

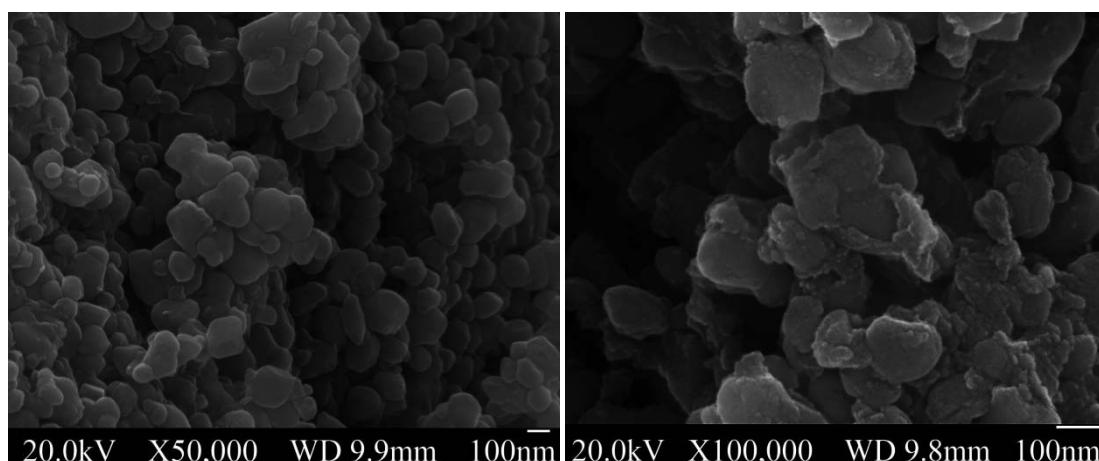
**Figure 6.** Titania milled with dodecylphosphonic acid: Phase composition of the samples after the milling process determined by X-ray powder diffraction and Rietveld analysis. Phase composition occurs from the starting material anatase to rutile and high-pressure (hp) TiO<sub>2</sub>.



Besides the surface functionalization and phase transition further important characteristics of the samples are the crystallite as well as the particle size. The crystallite sizes were derived from XRD pattern applying the Pawley method. The starting material was granular crystalline anatase which exhibits crystallite sizes above 300 nm. The high-pressure TiO<sub>2</sub> formed during the milling process has crystallite sizes around 6 nm but the residual anatase phase remains in the granular crystalline dimension. Compared to the starting material there is only a reduction of about 100 nm. For the rutile phase no reliable refinement of crystallite size could be performed due to the low percentage of this phase in the mixture. These results show that the milling time and the rotational speed primarily have influence on the phase transition but not on the particle size. Regardless of how the process parameters were selected the resulting high-pressure TiO<sub>2</sub> is nano crystalline and the residual anatase remains

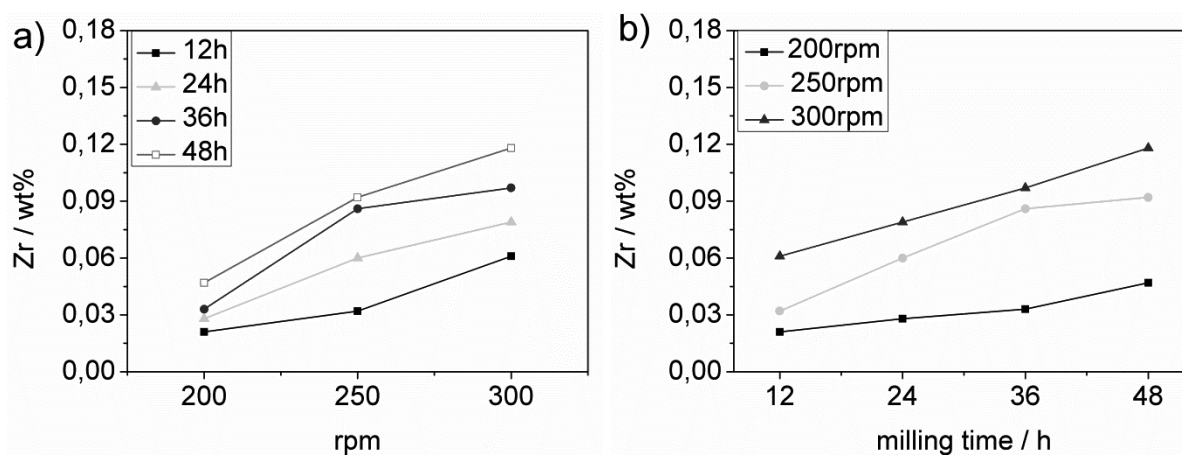
granular crystalline. Furthermore, the morphology of the obtained samples was analyzed applying SEM measurements (Figure 7). The SEM images display that the particles are not uniformly shaped and agglomerated with particle sizes in a range of 100 nm to 300 nm. It is visible that the particle size decreases with increasing milling time and rotational speed.

**Figure 7.** SEM images of two selected samples: titania milled with dodecylphosphonic acid at 200 rpm for 12 h (left) and at 300 rpm for 48 h (right). The size of the particles decreases with increasing energy input, but both samples are agglomerated and not uniformly shaped.



Due to abrasion of the grinding bowl a contamination of the samples cannot be avoided but it is expected to be insignificantly small. X-ray fluorescence spectroscopy was used to analyze these impurities (Figure 8). The results confirm that the contamination of the samples due to abrasion of the grinding bowl is negligible. The contamination increases with increasing milling time and rotational speed.

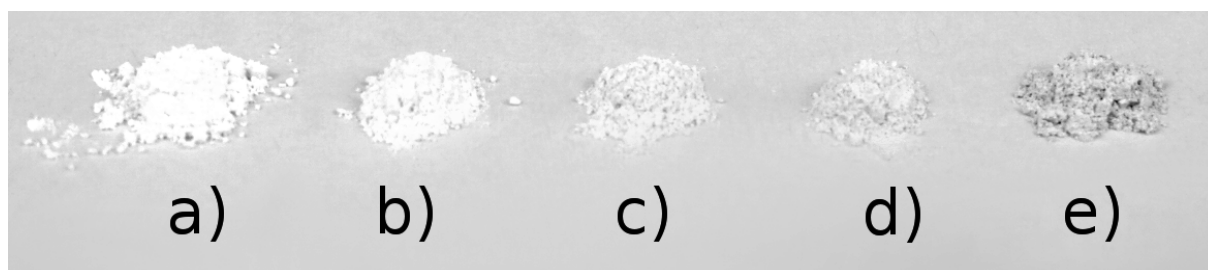
**Figure 8.** Impurities introduced by the grinding bowl according to (a) rotational speed (rpm) or (b) milling time determined by X-ray fluorescence spectroscopy, titania milled with dodecylphosphonic acid.



The samples after the milling process show a grey discoloration which becomes more intensive with increasing milling time and speed (Figure 9). Based on the fact that starting materials,  $\text{TiO}_2$  and

DDPA, as well as the grinding bowl material are white this discoloration must have another origin than the impurities due to the abrasion of the grinding bowl. Electron paramagnetic resonance was applied to clarify the reason for the mentioned discoloration (see ESI S15). The results indicate the presence of  $\text{Ti}^{3+}$  ions which are known to entail a darkening of the material [20]. An explanation for the appearance of a subvalent Ti species is the fact that the DDPA acts not only as a coupling but also as a reducing agent under the harsh conditions present during the milling process. Most likely, the organic moiety is oxidized to phenolic/chinoide species or splitted off from the coupling agent molecule, respectively. However, as the concentration of  $\text{Ti}^{3+}$  is low, the amount of possible oxidation products of DDPA in the washing solution is clearly below the detection limit of NMR spectroscopy. Therefore an identification of these side products was not successful.

**Figure 9.** Images of some selected samples: a)  $\text{TiO}_2$  b) 200 rpm / 12 h c) 200 rpm / 48 h d) 300 rpm / 12 h e) 300 rpm / 48 h The grey discoloration increases with increasing energy input.



After the successful studies on DDPA as long alkyl chain phosphonate coupling agent, again ODPa was used to demonstrate that this approach is assignable on other long alkyl chain organophosphorus species. The sample was prepared in the same way using those process parameters which end up in the highest surface functionalization (300 rpm and 48 h). FTIR analysis showed that a surface functionalization has taken place in case of using ODPa as well (Figure 10). The degree of surface functionalization was determined to be 0.6 mmol/g by the use of TGA as well as CHN analysis. The binding modes of the ODPa on the titania surface were studied using solid state  $^{31}\text{P}$  NMR spectroscopy (Figure 11). Similar to the results of the studies with DDPA the spectrum show a series of partially broad signals in the range of  $\delta = 10 - 30$  ppm and a sharp peak at  $\delta = 6$  ppm. Pure ODPa shows a solid-state  $^{31}\text{P}$  NMR signal at  $\delta = 30$  ppm [21]. The  $^{31}\text{P}$  NMR is in good agreement with the variety of possible binding modes of the phosphonate to the metal oxide surface (tridentate coordination modes shift around 20 ppm to lower fields with respect to the free phosphonic acid, for bi- and monodentate binding modes a downfield shift of 5 – 15 ppm compared to the free acid is reported) [18]. Consequently, the peaks in the range of 10 to 30 ppm correspond to the bi- and monodentate bonded phosphonates and the sharp signal at around 6 ppm can be assigned to the tridentate coordinated species. These shifts confirm the covalent bonding of the ODPa on the titania surface and demonstrate the different binding modes. Analogous to DDPA functionalized titania the presence of layered alkyl phosphonates can be excluded by TG measurements of the with ODPa functionalized sample (Figure 12).

**Figure 10.** FTIR-spectra of the starting material, the coupling agent OPDA and the sample after the milling process.

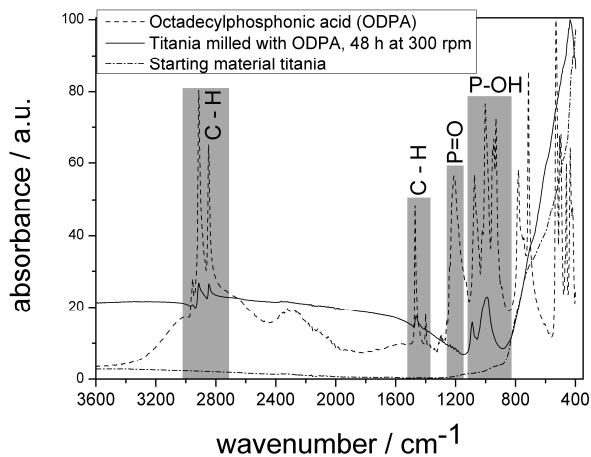


**Figure 11.** CP-MAS  $^{31}\text{P}$  NMR spectrum of titania milled with octadecylphosphonic acid.

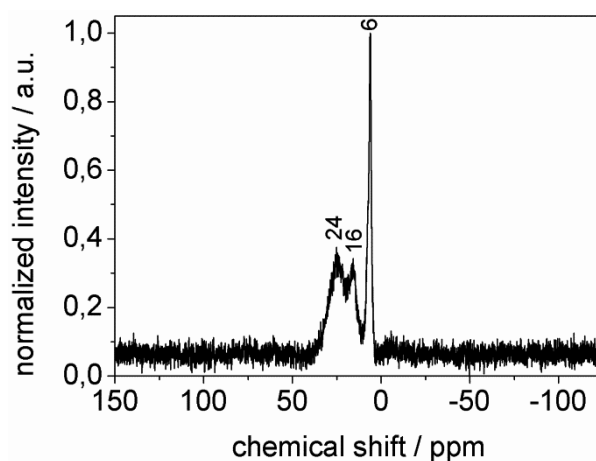
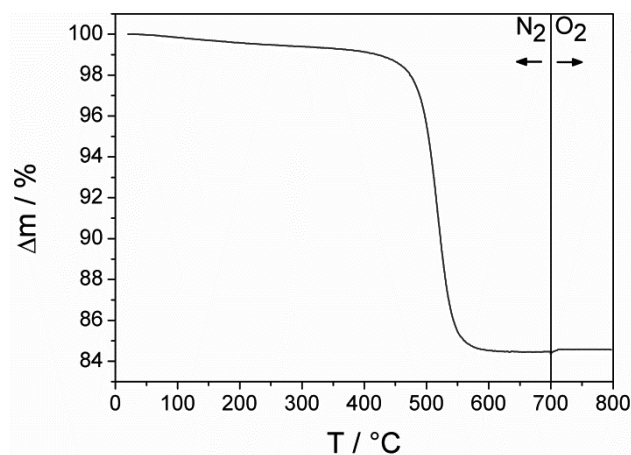
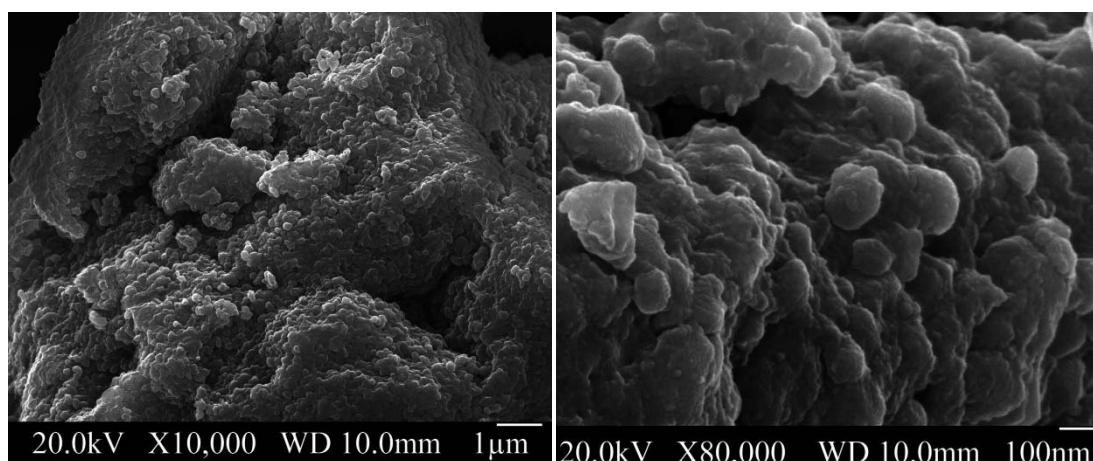


**Figure 12.** TGA of the sample obtained by reactive milling of titania with ODPA.



The sample with ODPAs as coupling agent was analyzed using X-ray diffraction as well to determine the phase composition or rather to describe the tribochemical phase transformation. The sample was composed of  $29.1\pm 0.2\%$  anatase,  $2.1\pm 0.2\%$  rutile and  $68.8\pm 0.3\%$  high-pressure  $\text{TiO}_2$ . Comparing these results with the findings of DDPA as coupling agent it emphasizes that in case of DDPA a slightly higher degree of functionalization can be reached. In contrast, the degree of the tribochemical phase transformation is almost similar. Just as in case of DDPA the particles functionalized with ODPAs are not uniformly shaped and agglomerated which was determined by using SEM techniques (Figure 13).

**Figure 13.** SEM image of titania functionalized with ODPAs



### 3. Experimental Section

#### Materials

Titanium(IV)-oxide powder anatase (99.8%) was purchased from Sigma Aldrich (Steinheim, Germany) and has been used without further purification. Dodecylphosphonic and octadecylphosphonic acid were synthesized in the working group.

#### Instruments and Characterization

FTIR measurements were performed under ambient air (40 scans at a resolution of  $4\text{ cm}^{-1}$ ) in attenuated total reflectance (ATR) mode on a Bruker Vertex 70 spectrometer. X-ray powder diffraction was carried out on two different diffractometers a Panalytical X'Pert and a Bruker D8 Advance-system, Bragg-Brentano geometry and  $\text{CuK}\alpha$  radiation was used in both cases. The quantitative analysis was carried out by the Rietveld-method using the program TOPAS [22] and crystallographic data for the modifications of titania (anatase [23], rutile [24], high-pressure  $\text{TiO}_2$  [25]). The same program package was used for the determination of the crystallite sizes applying the Pawley-method. X-ray fluorescence spectroscopy measurements were performed on an Eagle EDAX II instrument. Thermogravimetric analysis (TGA) was carried out on a Netzsch Iris TG 209. The sample was placed in an alumina crucible which was then heated from room temperature to  $700\text{ }^\circ\text{C}$  under nitrogen atmosphere followed by heating to  $800\text{ }^\circ\text{C}$  under oxygen atmosphere with a rate of  $20\text{ K min}^{-1}$ . The mass loss during the thermal analysis was used to calculate the amount of coupling agent on the surface of the titania particles. Here one has to consider that the residue is not only titania

because the phosphonate groups are oxidized to phosphate which remains on the surface of the particles. Equation 1 gives the molar amount of coupling agent per gram particles.

$$c_{CA} = \frac{\Delta m \cdot 10}{M_{\Delta m}} \quad (1)$$

$c_{CA}$ : molar concentration of coupling agent per gram [mmol g<sup>-1</sup>]

$\Delta m$ : mass loss during thermal analysis [%]

$M_{\Delta m}$ : molar mass of the molecule which leave during thermal analysis [g mol<sup>-1</sup>]

Elemental analysis was carried out on a Leco CHN-900 analyzer. The amount of coupling agent on the surface of the titania particles was calculated by using the percentage of carbon from elemental analysis. The molar amount of coupling agent per gram of particles can be calculated by using Equation 2.

$$c_{CA} = \frac{m_C \cdot 10}{M_C \cdot N_C} \quad (2)$$

$c_{CA}$ : molar concentration of coupling agent per gram [mmol g<sup>-1</sup>]

$m_C$ : mass of carbon from elemental analysis [%]

$M_C$ : molar mass of carbon [g mol<sup>-1</sup>]

$N_C$ : number of carbon atoms per coupling agent

Liquid state NMR spectra were recorded on a Bruker Avance 300 spectrometer operating at 300.13 MHz for <sup>1</sup>H, 75.47 MHz for <sup>13</sup>C and at 121.49 MHz for <sup>31</sup>P. Solid state NMR spectroscopy was carried out on a Bruker Avance DPX 300 instrument equipped with a 4 mm broad band cross-polarization Magic Angle Spinning probe head operating at 75.40 MHz for <sup>13</sup>C and 121.39 MHz for <sup>31</sup>P or on a Bruker DSX Avance NMR spectrometer (125.78 MHz for <sup>13</sup>C and 202.48 MHz for <sup>31</sup>P). Scanning electron microscopy (SEM) images were recorded on a JEOL SEM-7000 microscope. The SEM samples were prepared by placing some grains on a specimen stub with attached carbon adhesive foil followed by deposition of a gold layer.

### Synthesis

The experiments were performed in a high energy planetary ball mill Retsch PM 100. The material of the grinding bowl was a ZrO<sub>2</sub>-ceramic. We used a 50 mL grinding bowl and 200 corresponding milling balls with a diameter of 5 mm. Systematic studies on the effect of the milling time and the rpm on the result of the milling process were carried out. The milling time was varied between 12 h and 48 h and the rpm had values of 200 rpm, 250 rpm and 300 rpm.

In each case 4 g of titania (anatase) and 1 g of the respective coupling agent (dodecylphosphonic and octadecylphosphonic acid) were placed in the grinding bowl and milled at specific parameters.

After the milling process the product was washed with ethanol and water. Finally, the functionalized particles were separated by centrifugation (13000 rpm) and dried at 100°C.

## 4. Conclusions

Reactive milling can be used for the synthesis of metal oxide particles with *in situ* surface functionalization. It was shown that this technique can be successfully conducted using long alkyl

chain organophosphorus coupling agents. DDPA was used to conduct systematic studies on the influence of the process parameters milling time and rotational speed. The results reveal that increasing milling time as well as increasing rotational speed results in an increasing phase transition of the starting material anatase to rutile and high-pressure titania. Furthermore, an increase of the mentioned process parameters results in an increase of surface functionalization. Afterwards ODPa was used to successfully demonstrate that the approach is assignable on other long alkyl chain organophosphorus species.

### Acknowledgments

The authors thank Susanne Harling (Saarland University) for the elemental analysis and Matthias Gasthauer (Saarland University) for the synthesis of the coupling agents. Furthermore, we thank Dr. Michael Puchberger (Vienna University of Technology) and Dirk Schaffner (University of Kaiserslautern) for the solid state NMR spectroscopy and Prof. Dr. Hartmann (University of Erlangen) for the ESR measurements.

### Conflicts of Interest

The authors declare no conflict of interest.

### References and Notes

1. Hameed, S.; Predeep, P.; Baiju, M.R. Polymer Light Emitting Diodes – A Review on Materials and Techniques. *Rev. Adv. Mater. Sci.* **2010**, *26*, 30-42.
2. Chen, W.; Qiu, Y.; Yang, S. Branched ZnO nanostructures as building blocks of photoelectrodes for efficient solar energy conversion. *Phys. Chem. Chem. Phys.* **2012**, *14*, 10872-10881.
3. Leung, K.C.-F.; Xuan, S.; Zhu, X.; Wang, D.; Chak, C.-P.; Lee, S.-F.; Ho, W.K.-W.; Chung, B.C.-T. Gold and iron oxide hybrid nanocomposite materials. *Chem. Soc. Rev.* **2012**, *41*, 1911-1928.
4. Mieszawska, A.J.; Mulder, W. J. M.; Fayad, Z. A.; Cormode, D. P. Multifunctional Gold Nanoparticles for Diagnosis and Therapy of Disease. *Mol. Pharmaceutics* **2013**, *10*, 831-847.
5. Fernández-Bertran, J.F. Mechanochemistry: an overview. *Pure Appl. Chem.* **1999**, *71*, 581-586.
6. Garay, A.L.; Pichon, A.; James, S.L. Solvent-free synthesis of metal complexes. *Chem. Soc. Rev.* **2007**, *36*, 846-855.
7. Kaupp, G. Waste-free large-scale synthesis without auxiliaries for sustainable production omitting purifying workup. *CrystEngComm.* **2006**, *8*, 794-804.
8. James, S.L.; Adams, C.J.; Bolm, C.; Braga, D.; Collier, P.; Friscic, T.; Grepioni, F.; Harris, K.D.M.; Hyett, G.; Jones, W.; et al. Mechanochemistry: opportunities for new and cleaner synthesis. *Chem. Soc. Rev.* **2012**, *41*, 413-447.
9. Ney, C.; Kohlmann, H.; Kickelbick, G. Metal hydride synthesis through reactive milling of metals with solid acids in a planetary ball mill. *Int. J. Hydrogen Energy* **2011**, *36*, 9086-9090.
10. Fuentes, A.F.; Takacs, L. Preparation of multicomponent oxides by mechanochemical methods. *J. Mater. Sci.* **2013**, *48*, 598-611.



11. Fischer, A.; Ney, C.; Kickelbick, G. Synthesis of Surface-Functionalized Titania Particles with Organophosphorus Coupling Agents by Reactive Milling. *Eur. J. Inorg. Chem.* **2013**, *33*, 5701-5707.
12. Betke, A.; Kickelbick, G. Important reaction parameters in the synthesis of phenylphosphonic acid functionalized titania particles by reactive milling. *New J. Chem.* **2014**, *38*, 1264-1270.
13. Guerrero, G.; Mutin, P.H.; Vioux, A. Anchoring of Phosphonate and Phosphinate Coupling Molecules on Titania Particles. *Chem. Mater.* **2001**, *13*, 4367-4373.
14. Convertino, A.; Leo, G.; Tamborra, M.; Sciancalepore, C.; Striccoli, M.; Curri, M.L.; Agostiano, A. TiO<sub>2</sub> colloidal nanocrystals functionalization on PMMA: A tailoring of optical properties and chemical adsorption. *Sens. Actuators B* **2007**, *B126*, 138-143.
15. Cozzoli, P.D.; Kornowski, A.; Weller, H. Low-Temperature Synthesis of Soluble and Processable Organic-Capped Anatase TiO<sub>2</sub> Nanorods. *J. Am. Chem. Soc.* **2003**, *125*, 14539-14548.
16. El Malti, W.; Laurencin, D.; Guerrero, G.; Smith, M.E.; Mutin, P.H. Surface modification of calcium carbonate with phosphonic acids. *J. Mater. Chem.* **2012**, *22*, 1212-1218.
17. Brodard-Severac, F.; Guerrero, G.; Maquet, J.; Florian, P.; Gervais, C.; Mutin, P.H. High-Field <sup>17</sup>O MAS NMR Investigation of Phosphonic Acid Monolayers on Titania. *Chem. Mater.* **2008**, *20*, 5191-5196.
18. Pica, M.; Donnadio, A.; Troni, E.; Capitani, D.; Casciola, M. Looking for New Hybrid Polymer Fillers: Synthesis of Nanosized  $\alpha$ -Type Zr(IV) Organophosphonates through an Unconventional Topotactic Anion Exchange Reaction. *Inorg. Chem.*, **2013**, *52*, 7680-7687.
19. Souma, H.; Chiba, R.; Hayashi, S. Solid-State NMR Study of Titanium Dioxide Nanoparticles Surface-Modified by Alkylphosphonic Acids. *Bull. Chem. Soc. Jpn.*, **2011**, *84*, *11*, 1267-1275.
20. Xiong, L.-B.; Li, J.-L.; Yang, B.; Yu, Y. Ti<sup>3+</sup> in the Surface of Titanium Dioxide: Generation, Properties and Photocatalytic Application. *J. Nanomater.* **2012**, *2012*, 13 pages.
21. Tienes, B.M.; Perkins, R.J.; Shoemaker, R.K.; Dukovic, G. Layered Phosphonates in Colloidal Synthesis of Anisotropic ZnO Nanocrystals. *Chem. Mater.*, **2013**, *25*, 4321-4329.
22. *Topas V4.2; General profile and structure analysis software for powder diffraction data, User Manual*, Bruker AXS, Karlsruhe, Germany, **2008**.
23. Kim, D.-W.; Enomoto, N.; Nakagawa, Z.; Kawamura, K. Molecular Dynamic Simulation in Titanium Dioxide Polymorphs: Rutile, Brookite, and Anatase. *J. Am. Ceram. Soc.* **1996**, *4*, 1095-1099.
24. Hill, R.J.; Madsen, C. Rietveld analysis using para-focusing and Debye-Scherrer geometry data collected with a Bragg-Brentano diffractometer. *Z. Kristallogr.* **1991**, *196*, 73-92.
25. Fulatov, S.K.; Bendeliani, N.A.; Albert, B.; Kopf, J.; Dyuzheva, T.; Lityagina, L.M. Crystalline structure of the TiO<sub>2</sub> II high-pressure phase at 293, 223, and 133 K according to single-crystal x-ray diffraction data. *Doklady Physics* **2007**, *52*, *4*, 195-199.

### 3.2 MICROJET REACTOR PROCESS

The synthesis of nanoparticles is of great interest for a wide field of applications. For this reason, there is constant effort regarding to improvements to the conventional synthetic strategies. In order to eliminate differences in nanoparticle properties from batch to batch it would be a great benefit to perform the synthesis continuously.

Some continuous techniques are known but they all require an improvement regarding to the mixing time which should be as fast as possible. The microjet reactor process fulfills fast mixing and it allows performing a continuous synthesis process. The precursor solutions are transported to the microjet reactor by the use of two pumps. The reaction solutions are forced with high-pressure through a narrow cone in a reaction chamber. The reaction takes place in a confined reaction environment which is given by the microjet reactor geometry. The reaction chamber is constantly flushed with a gas flow. Consequently, the formed nuclei are directly transported from the reaction chamber to a tubing where the particle growth occurs.

The microjet reactor process has shown to be a promising technique for the synthesis of inorganic nanoparticles already. In this work the suitability of the microjet reactor process for the synthesis of oxide inorganic nanoparticles was investigated systematically. In order to demonstrate the wide field of application zinc oxide (ZnO), magnetite ( $\text{Fe}_3\text{O}_4$ ) as well as brushite ( $\text{CaHPO}_4 \cdot 2\text{H}_2\text{O}$ ) were synthesized using the microjet reactor process.

Systematic studies on the influence of the flow rate as well as the process temperature were conducted. An interesting question was whether the particle size is controllable by means of these parameters. The obtained particles were characterized with respect to their phase composition as well as crystallite and particle size and morphology.

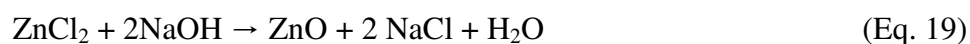
Zinc oxide, magnetite and brushite were used as they are in particular interesting for optoelectronics, clinical and biomedical applications.

The results of the described studies have been presented in a further publication.

### 3.2.1 BOTTOM-UP, WET CHEMICAL TECHNIQUE FOR THE CONTINUOUS SYNTHESIS OF INORGANIC NANOPARTICLES

In this publication the microjet reactor process is presented. It is a bottom-up wet chemical technique for the continuous synthesis of inorganic nanoparticles. The technique fulfils fast mixing of the precursor solutions which is crucial for nanoparticle synthesis. The microjet reactor process has been used for the synthesis of nanoparticles already. This paper deals with the investigation of the suitability of the microjet reactor process for the production of oxide inorganic nanoparticles. Systematically studies on the influence of the flow rate and the process temperature were conducted in order to investigate whether the particle size is controllable by the means of these process parameters. In order to demonstrate the wide application field this technique was systematically investigated for the synthesis of three types of inorganic nanoparticles, i.e. zinc oxide (ZnO), magnetite (Fe<sub>3</sub>O<sub>4</sub>), and brushite (CaHPO<sub>4</sub>·2H<sub>2</sub>O).

The synthesis of zinc oxide was conducted based on zinc chloride and sodium hydroxide:



The synthesis of magnetite was performed using ferrous and ferric chloride as well as ammonia as starting materials:



As the synthesis was performed under air where Fe<sup>2+</sup> ions tend to oxidize and form Fe<sup>3+</sup> ions divergent to the stoichiometric reaction equation ferrous chloride was applied in excess.

Brushite was synthesized applying calcium nitrate and di-ammonium hydrogen phosphate as starting materials:



The pH of the precursor solutions was adjusted to 5 in order to obtain calcium phosphate in the brushite phase.

The obtained particles were characterized using various techniques. X-ray fluorescence spectroscopy was applied to analyze the phase composition of the samples. The results reveal that pure zinc oxide with crystallite sizes between 17 - 22 nm was obtained. In case of magnetite there was a slight amount of a side product which was identified to be maghemite. The magnetite phase show crystallite sizes around 10 nm. Pure brushite with crystallite sizes in the range of 200 - 300 nm was obtained. Dynamic light scattering and scanning electron microscopy were used to determine the particle size and morphology of the obtained particles. Zinc oxide was obtained with particle sizes between 44 - 102 nm. The magnetite particles show sized in the range of 46 - 132 nm. It turned out that the particle size is controllable by means of the process parameters flow rate and process temperature. With increasing temperature as well as increasing pressure the particles reveal smaller particle sizes and better size distribution. While zinc oxide and magnetite were spherical shaped brushite was obtained as small plates with edge lengths between 100 - 500 nm. FT-IR spectroscopy and thermo gravimetric analyses were used to identify side products but in each case no side product was detectable.

The performed studies demonstrate that the microjet reactor process is a promising method for the continuous synthesis of inorganic nanoparticles. The benefit against conventional synthetic strategies is that the synthesis can be performed continually with good particle size control.

These results have been published in *Inorganics*:

A. Betke, G. Kickelbick, Bottom-Up, Wet Chemical Technique for the Continuous Synthesis of Inorganic Nanoparticles, *Inorganics*, **2014**, 2, 1-15.

The publication was written by Annika Betke and all experiments and characterizations presented were performed by her. Guido Kickelbick has contributed suggestions for improvements and is mentioned as corresponding author as he is the working group leader and Ph.D. supervisor.

Article

## Bottom-Up, Wet Chemical Technique for the Continuous Synthesis of Inorganic Nanoparticles

Annika Betke and Guido Kickelbick \*

Inorganic Chemistry, Saarland University, Am Markt Zeile 3, 66125 Saarbrücken, Germany;  
E-Mail: annika.betke@uni-saarland.de

\* Author to whom correspondence should be addressed; E-Mail: guido.kickelbick@uni-saarland.de;  
Tel.: +49-0-681-302 (ext. 70651); Fax: +49-0-681-302 (ext. 70652).

Received: 20 December 2013; in revised form: 14 January 2014 / Accepted: 16 January 2014 /

Published: 27 January 2014

---

**Abstract:** Continuous wet chemical approaches for the production of inorganic nanoparticles are important for large scale production of nanoparticles. Here we describe a bottom-up, wet chemical method applying a microjet reactor. This technique allows the separation between nucleation and growth in a continuous reactor environment. Zinc oxide (ZnO), magnetite (Fe<sub>3</sub>O<sub>4</sub>), as well as brushite (CaHPO<sub>4</sub>·2H<sub>2</sub>O), particles with a small particle size distribution can be obtained continuously by using the rapid mixing of two precursor solutions and the fast removal of the nuclei from the reaction environment. The final particles were characterized by FT-IR, TGA, DLS, XRD and SEM techniques. Systematic studies on the influence of the different process parameters, such as flow rate and process temperature, show that the particle size can be influenced. Zinc oxide was obtained with particle sizes between 44 nm and 102 nm. The obtained magnetite particles have particle sizes in the range of 46 nm to 132 nm. Brushite behaves differently; the obtained particles were shaped like small plates with edge lengths between 100 nm and 500 nm.

**Keywords:** continuous synthesis; precipitation; inorganic nanoparticles; microjet reactor

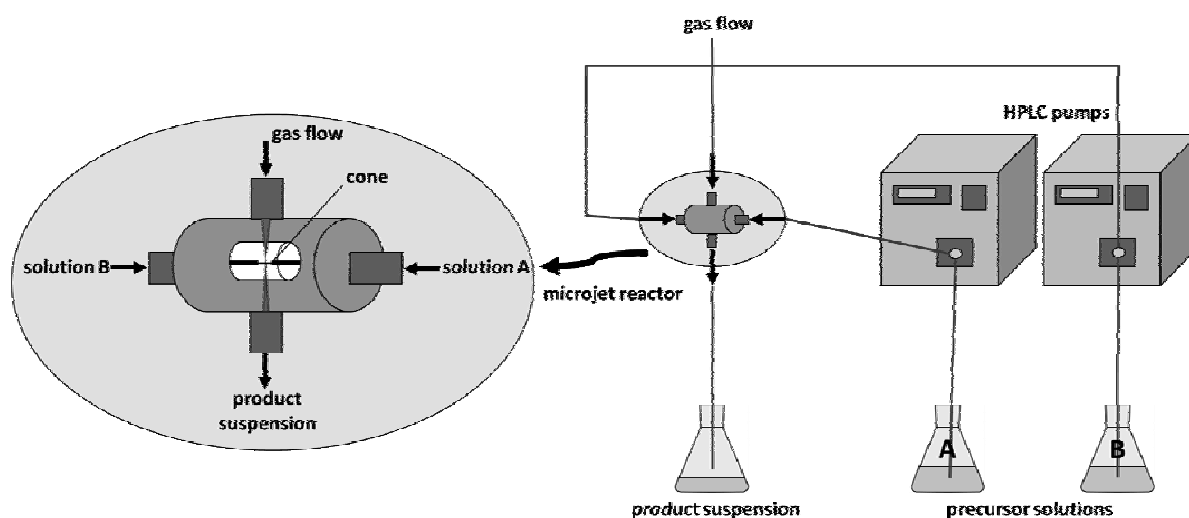
---

### 1. Introduction

Nanoparticles have been identified as major compounds for many applications in the last decades. They are used in many different fields such as medicine, optics, electronics or catalysis [1]. For this reason, there is a lot of interest in facile synthetic routes for nanoparticles with controllable size and

narrow size distribution. There are many different possibilities for the production of particles but due to its simplicity, low cost, and easy application in industrial production, stirred tank batch reactor processes are still the most employed wet chemical systems [2,3]. However, this method has often limitations for the preparation of nanoparticles on an industrial scale, because of long mixing times and thus uncontrolled nucleation and growth. To obtain nanoparticles with particle sizes smaller than 100 nm very short mixing times are required. Although there are methods which can be employed on a laboratory scale to obtain rapid mixing, their scale up is quite difficult [4,5]. In addition, it would be of great benefit if the synthesis could be performed continuously, because this would eliminate differences in nanoparticle properties from batch to batch [6–8]. There are continuous techniques, such as mixing starting material solutions on a macroscopic scale (e.g., tee shaped connectors) or microreactors [9]. These techniques have been used already for the synthesis of anatase-TiO<sub>2</sub>, gold, and cobalt nanoparticles as well as tricalcium phosphate ceramics [10–13]. In general, all the above-mentioned techniques require an improvement with respect to the mixing time. There are several studies, which indicate that the effect of mixing has an important influence on the particle size distribution. Experimental, as well as theoretical, precipitation experiments using a tee-mixer and barium sulfate as exemplary material show that the particles becomes smaller with increasing mixing intensity [14,15]. In further studies, it was found that confined impinging jet reactors are more efficient than tee-mixers. Using such a reactor type, it is possible to generate polymer nanoparticles which have potential application in biomedicine; for example for controlled drug delivery [16,17]. Biocompatible nanomaterial for biomedicine and pharmaceutical applications can also be produced by using a novel continuous industrial reactor, called NETmix. This reactor is a network of interconnected chambers and channels creating zones of complete mixing and segregation. This technique is used already for the synthesis of hydroxyapatite nanoparticles with extremely high purity and crystallinity [18]. Fast mixing is also fulfilled when a microjet reactor (Figure 1) is used. The excellent improvement is that the reagent solutions are forced with high pressure through a narrow cone in a reaction chamber that is constantly flushed with a gas flow. As a result, the obtained product is removed directly from the reaction chamber so that clogging is avoided.

**Figure 1.** Schematic set-up of the microjet reactor.



This technique can be used to perform different precipitation reactions continuously. Two pumps are used to transport the solutions containing the starting materials as dissolved substances to the microjet reactor. The collision takes place in a confined reaction environment, which is given by the format of the microjet reactor. Due to the fluid dynamics in the microjet reactor, there is a very short mixing time. Consequently, there is a maximum number of nuclei in an absolute homogeneous environment. In addition the nucleation rate is increased compared to the nucleus growth [19,20]. Directly after the nuclei are formed, they are transported from the reaction room to a tubing where the particle growth occurs. The length of this tubing up to the collection vessel influences the particle growth. The method has the advantage of being able to prepare nanoparticles even from a system with very low solubility products, e.g. barium sulfate [21]. However, it is also able to produce metal oxides, such as titania [22]. One great advantage is that the particles are obtained in a suspension, which could be used for a direct application, e.g. in spray coating or inkjet printing.

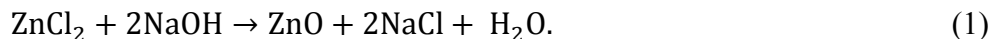
In this study, we investigated the microjet reactor technique for the synthesis of three types of inorganic nanoparticles, *i.e.*, zinc oxide (ZnO), magnetite (Fe<sub>3</sub>O<sub>4</sub>), and brushite (CaHPO<sub>4</sub>·2H<sub>2</sub>O). These particles are not only interesting for academic reasons, but also have applications in optoelectronics and clinical, as well as biomedical devices [23–25]. The goal was to define the possibilities and limitations of this technique with regard to the different process parameters, such as flow rate and temperature, on the result of the precipitation reaction. Here, we do not focus on the importance of the time between nuclei formation and collection of the products, which also influences the size of the particles as this will be investigated in a further study.

## 2. Results and Discussion

The synthesis of inorganic nanoparticles was carried out using a microjet reactor system. In order to reveal the wide application field of the microjet reactor we performed the synthesis of three different species: zinc oxide (ZnO), magnetite (Fe<sub>3</sub>O<sub>4</sub>), as well as brushite (CaHPO<sub>4</sub>·2H<sub>2</sub>O). All of these three systems show a low solubility under the applied reaction conditions. Two isocratic preparative HPLC pumps were used to transport the solutions containing the starting materials as dissolved substances. In the microjet-reactor, these two solutions clash and the precipitation reaction takes place. The precipitate was directly removed from the reactor by the use of a nitrogen gas flow. This process was performed with various flow rates of the precursor solutions (150 mL/min, 200 mL/min and 250 mL/min) and at different temperatures (25 °C, 50 °C and 75 °C). The reproducibility of the method was investigated by performing all experiments several times. The obtained material was thoroughly washed with water and the resulting compound was characterized applying FT-IR-spectroscopy, XRD, TGA and DLS analysis, as well as SEM. The final products were analyzed with respect to changes in the composition, the particle size and morphology depending on the process parameters.

### 2.1. Zinc Oxide

The synthesis of zinc oxide was performed by using aqueous solutions of zinc chloride and sodium hydroxide as starting materials (Equation 1) for the solution A and B, respectively.



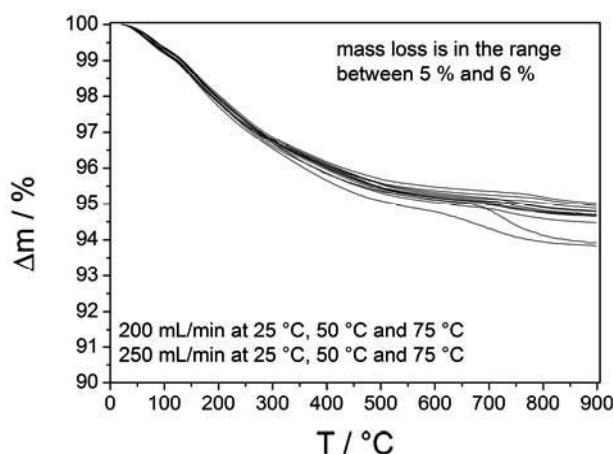
Under conventional precipitation conditions in an open vessel, the same starting materials deliver disc-like ZnO submicrometer structures with diameters between 300 nm and 500 nm [26].

Smaller particles could be obtained applying controlled double-jet-precipitation, which produces primary particles with diameters between 20–30 nm that tend to agglomerate in ellipsoidal particles with sizes of a few hundred nanometers [5].

The particles that were obtained by using the microjet reactor were characterized using various techniques. FT-IR-analysis of the prepared materials showed no specific signals with exception of OH and CO bands of adsorbed CO<sub>2</sub> and H<sub>2</sub>O as well as a strong ZnO band around 400 cm<sup>-1</sup>.

Thermogravimetric analysis (Figure 2) was performed to determine the amount of adsorbed CO<sub>2</sub> and H<sub>2</sub>O. The results show that the samples contain between 5% and 6% adsorbed species. The development of the mass loss looks similar for all samples.

**Figure 2.** Thermogravimetric analysis of the final products. The samples show a mass loss of between 5 and 6%.



X-ray powder diffraction was applied to study the phase composition and crystallite size of the obtained material in dependence on the different synthesis parameters. The XRD pattern show that in each case pure zinc oxide is generated (Figure 3). The crystallite sizes decrease with increasing temperature and increasing flow rate (Table 1).

A further important parameter is the particle size including the size distribution, which is given by the standard deviation of the particle size. These parameters were determined using dynamic light scattering (Figure 4). The samples were dispersed in ethanol by the exposition to ultrasound for 5 min. The results show that the particles are easily dispersible and their size depends on the process parameters. The particle size decreases with increasing temperature and increasing flow rate, in addition the particle size distribution becomes smaller (Table 2).



**Figure 3.** X-ray powder pattern of the obtained particles. The results show that pure zinc oxide was obtained.

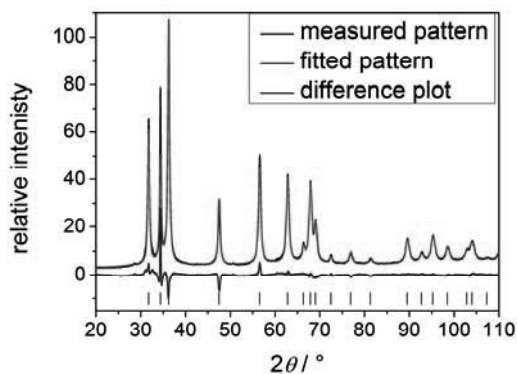


**Table 1.** Crystallite size in dependence on the process parameters.

Process parameters	Crystallite size
200 mL/min/25 °C	22.2 ± 0.5
200 mL/min/50 °C	20.4 ± 0.7
200 mL/min/75 °C	16.3 ± 0.3
250 mL/min/25 °C	22.7 ± 0.5
250 mL/min/50 °C	21.3 ± 0.4
250 mL/min/75 °C	16.9 ± 0.3

**Figure 4.** Particle sizes of the obtained zinc oxide particles determined by dynamic light scattering.

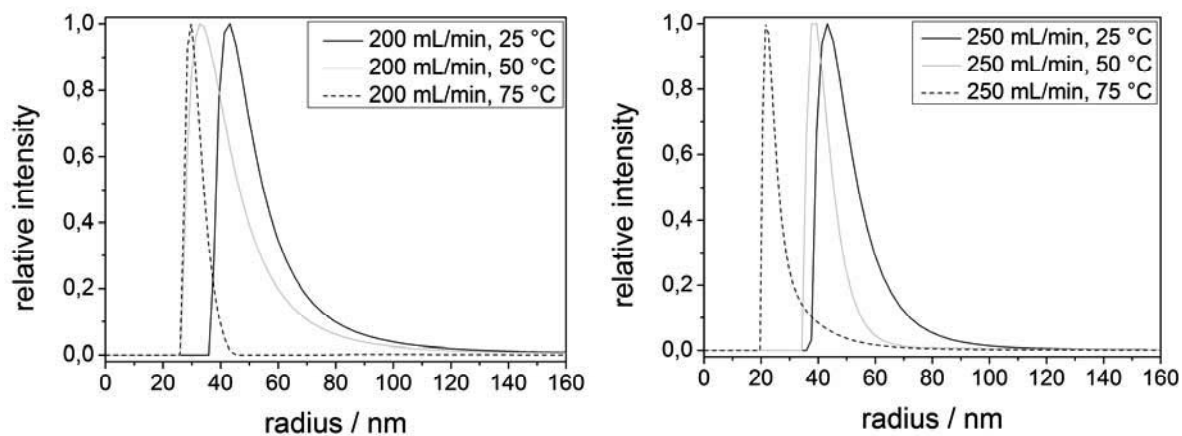


**Table 2.** Particle size determined using dynamic light scattering.

Process parameters	Radius/nm
200 mL/min/25 °C	51 ± 7
200 mL/min/50 °C	41 ± 8
200 mL/min/75 °C	27 ± 3
250 mL/min/25 °C	43 ± 6
250 mL/min/50 °C	36 ± 4
250 mL/min/75 °C	22 ± 2

The particle morphology was investigated by means of scanning electron microscopy (Figures 5 and 6). The images confirm that the particles are in the nanometer size range. However, SEM analysis does not show the pronounced differences in the particles sizes that were observed in the DLS measurements for the parameter variations. Generally, it can be observed in SEM that the particles are all sphere-shaped and the size distribution becomes more uniform with increasing temperature.

**Figure 5.** SEM images of zinc oxide synthesized with a flow rate of 200 mL/min at 25 °C (left) and at 75 °C (right).

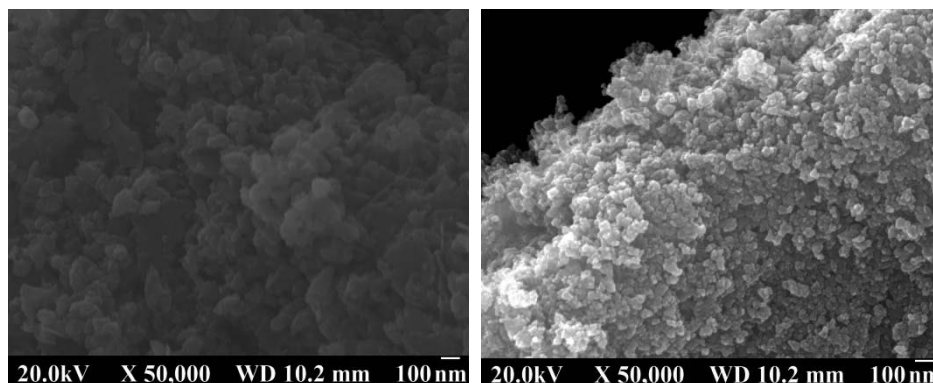
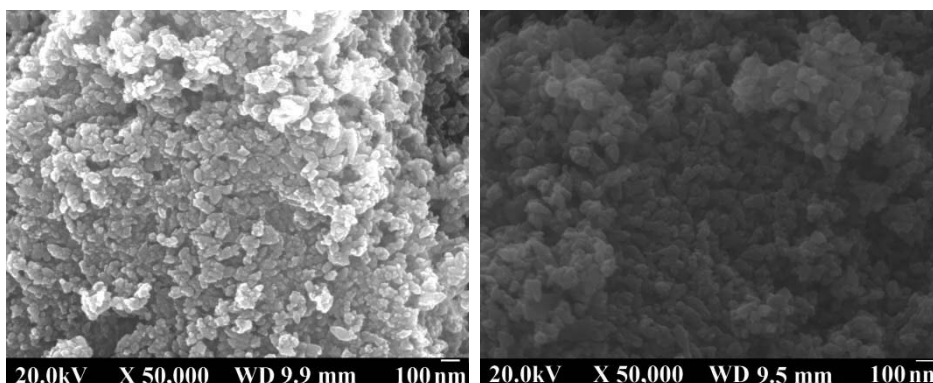
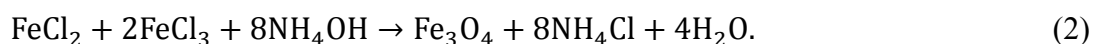


**Figure 6.** SEM images of zinc oxide synthesized at 50 °C with a flow rate of 200 mL/min (left) and with a flow rate of 250 mL/min (right).



## 2.2. Magnetite

Systematic studies with respect to the synthesis of magnetite nanoparticles using a microjet reactor were performed with an aqueous solution of ferric and ferrous chloride as solution A and an ammonia solution B (Equation 2).

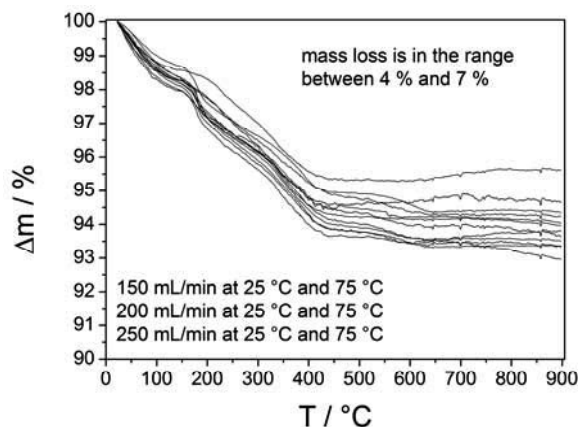


Ferrous chloride must be applied in excess because the synthesis was performed under air. Consequently, the  $\text{Fe}^{2+}$  ions tend to oxidize and form  $\text{Fe}^{3+}$  ions [27]. Magnetite nanoparticles were already obtained applying conventional synthetic routes using the same starting materials [28].

FT-IR analysis of the particles that were obtained in the microjet reactor does not show specific bands for the products with exception of the Fe-O band around  $500 \text{ cm}^{-1}$ .

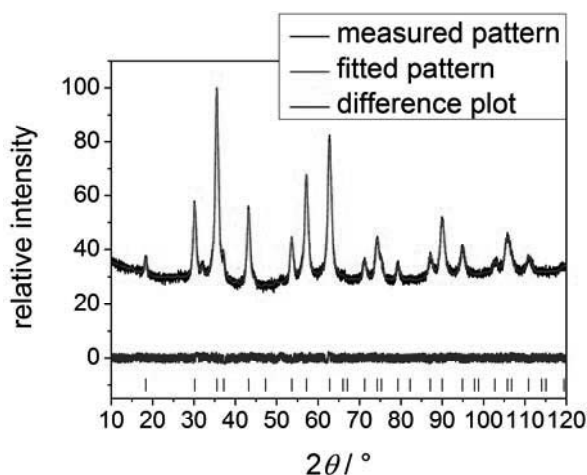
Thermo gravimetric analysis (Figure 7) was performed to determine if the samples contain any adsorbed species like water. The particles show a mass loss between 4 and 7%, which can be explained by adsorbed water or the production of water by condensation of free hydroxyl groups.

**Figure 7.** Thermo gravimetric analysis of the final products. The samples show a mass loss of between 4 and 7%.



The phase composition and crystallite size of the obtained particles were determined by X-ray powder diffraction (Figure 8). The results show that magnetite with crystallite sizes around 10 nm were obtained in the microjet reactor. There are a few very weak reflections which cannot be correlated to magnetite. Consequently, there is a small fraction of an impurity phase. The reflection at approximately  $2\theta = 32^\circ$  suggest this phase to be maghemite.

**Figure 8.** XRD pattern of the obtained particles. The results show that magnetite was obtained.



The particle size of the attained material was determined by using dynamic light scattering (Figure 9). The results reveal that particles between 46 nm and 112 nm were obtained. Just as in case of the ZnO particles the particle sizes including the size distribution decrease with increasing process temperature and flow rate (Table 3).

Previous studies applying rapid mixing techniques showed much smaller nanoparticle sizes around 7 nm [4]. The difference between the technique presented here and previous studies is the altered time

for growth of the particles, which depends in our setup on the length of the tubing between microjet-reactor and collecting vessel. We are currently investigating these parameters in an additional study.

**Figure 9.** Particle size of the synthesized magnetite determined by dynamic light scattering.

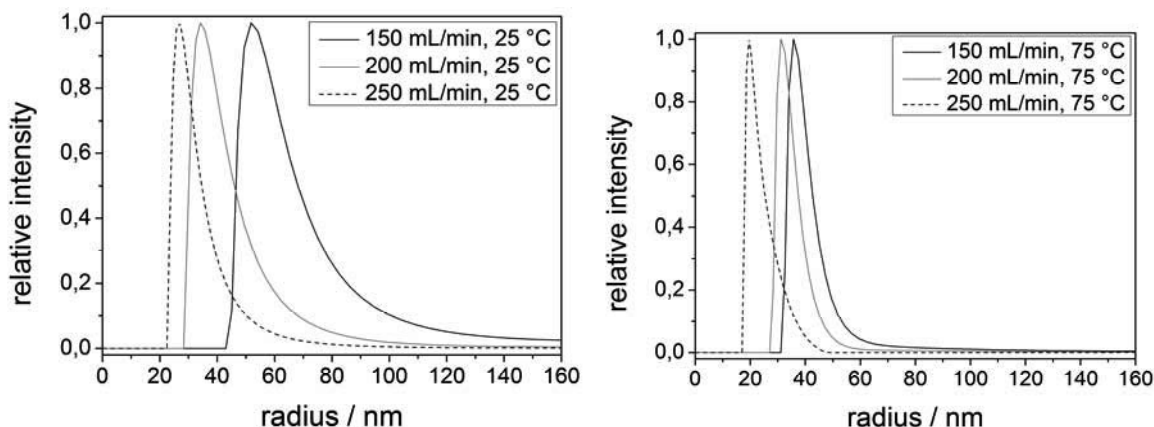
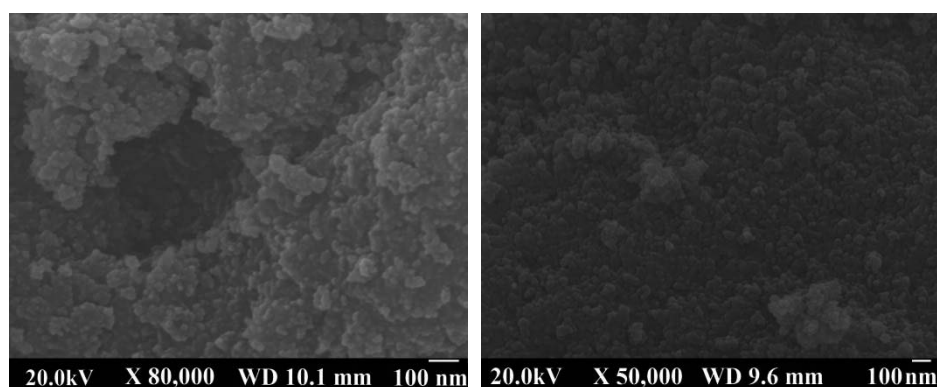


**Table 3.** Particle size determined using dynamic light scattering.

Process parameters	Radius/nm
150 mL/min/25 °C	66 ± 9
200 mL/min/25 °C	42 ± 7
250 mL/min/25 °C	32 ± 5
150 mL/min/75 °C	41 ± 4
200 mL/min/75 °C	35 ± 4
250 mL/min/75 °C	23 ± 3

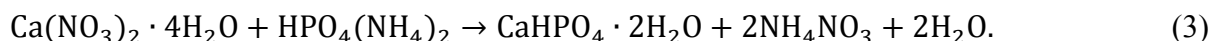
SEM was applied to determine the morphology of the obtained magnetite particles (Figure 10). The results show that the particles are sphere-shaped and become smaller with increasing flow rate and temperature.

**Figure 10.** SEM images of the obtained magnetite particles synthesized at 25 °C with a flow rate of 150 mL/min (**left**) and at 75 °C with a flow rate of 250 mL/min (**right**).



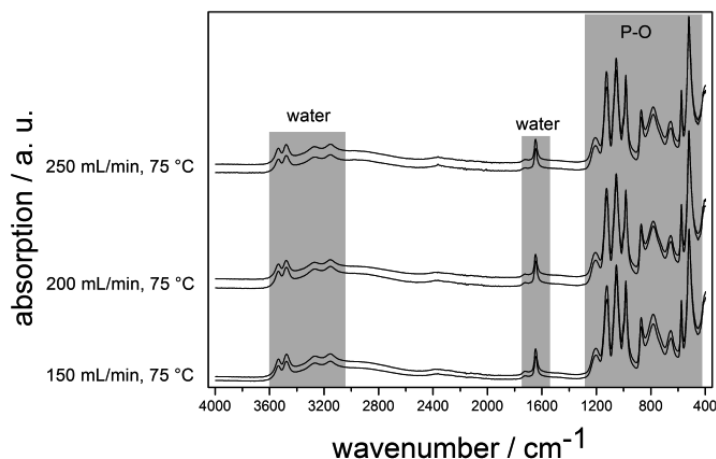
### 2.3. Calcium Hydrogen Phosphate/Brushite

As a third system the synthesis of calcium hydrogen phosphate particles using the microjet-reactor was investigated. An aqueous solution of calcium nitrate (solution A) and di-ammonium hydrogen phosphate (solution B) were mixed in the microjet reactor (Equation 3). The pH of both solutions was adjusted to 5 in order to obtain the calcium hydrogen phosphate in the brushite phase.



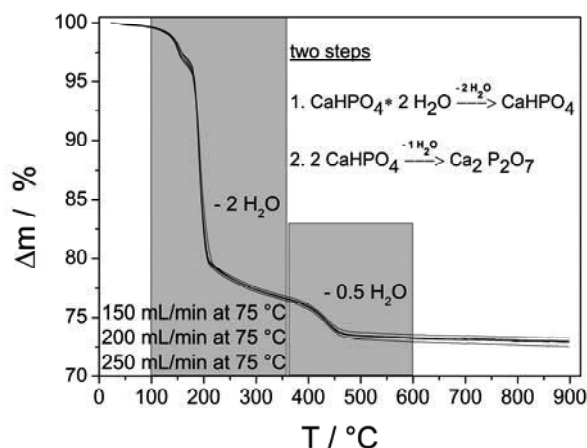
Using the same starting materials, but applying a conventional batch reactor synthesis route, plate-like brushite particles in the micrometer range were obtained [29]. Employing the microjet reactor for this reaction it turned out that the precipitation reaction does not proceed at 25 °C. The material obtained using 75 °C as process temperature was analyzed with respect to composition and morphology. FT-IR analyses (Figure 11) of the obtained materials show that the synthesis of calcium hydrogen phosphate was successful at 75 °C. The spectra show absorption bands between 1200  $\text{cm}^{-1}$  and 400  $\text{cm}^{-1}$  which is the typical P-O region and indicates P-O vibrations as well as vibrations of a  $\text{HPO}_4$  group. In addition, absorption bands relating to water are visible. At 1650  $\text{cm}^{-1}$  there is the typical absorption band for the  $\text{H}_2\text{O}$  bending. Furthermore, between 3550  $\text{cm}^{-1}$  and 3000  $\text{cm}^{-1}$ , the absorption bands relating to the OH stretching of water are visible. This agrees well with FT-IR data of calcium hydrogen phosphate reported in the literature [30,31].

**Figure 11.** FT-IR spectra of the obtained materials. Absorption bands in the P-O region are observable as well as absorption bands relating to water. For each condition two spectra were shown in order to illustrate the reproducibility.



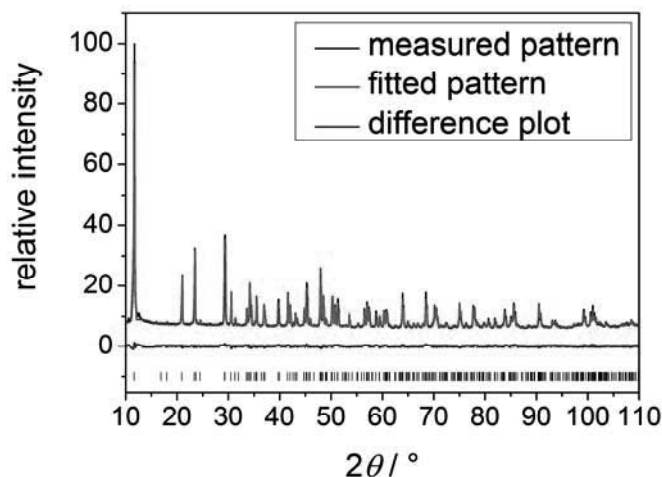
Thermo gravimetric analysis was performed to analyze the thermal decomposition of the obtained material (Figure 12). The results show that the decomposition takes place in two steps, which confirms that calcium hydrogen phosphate was obtained in the brushite phase. The first decomposition step proceeds between 100 °C and 350 °C degree and is relating to the loss of two molecules of crystal water. Consequently  $\text{CaHPO}_4$  is formed. The second decomposition step takes place between 350 °C and 600 °C and is relating to the loss of 0.5 water molecules per  $\text{Ca}^{2+}$  ion and the formation of  $\text{Ca}_2\text{P}_2\text{O}_7$ . This is the typical pattern for decomposition of brushite.

**Figure 12.** Thermal decomposition of the obtained material. The decomposition takes place in two steps, which is typical for the thermal decomposition of calcium hydrogen phosphate in the brushite phase.



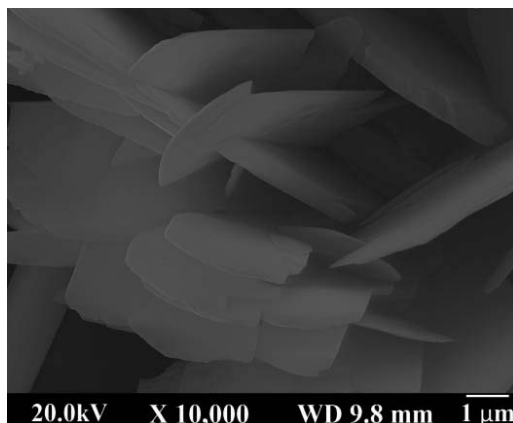
The results of the X-ray powder diffraction measurements (Figure 13) confirm that pure brushite was obtained. The particles show a high anisotropy in their crystallite sizes. An average crystallite size could be determined which is in the range of 200 to 300 nm depending on the reaction conditions.

**Figure 13.** X-ray powder pattern. Pure calcium hydrogen phosphate in the brushite phase was obtained.



SEM was applied to analyze the morphology of the obtained material (Figure 14). The results show that the particles are shaped like small plates based on the layered structure of brushite. The layers grow faster in two directions so that plates are formed. The edge lengths of these plates were determined to be between 100 nm and 500 nm.

**Figure 14.** SEM image of the obtained material. Brushite synthesized at 75 °C with a flow rate of 250 mL/min.



All three examples showed that the continuous production of nanoparticles, in case of ZnO and Fe<sub>3</sub>O<sub>4</sub>, or submicron sized plates in case of brushite is possible with the wet chemical microjet reaction technique. All samples showed that flow rates as well as temperatures have an important influence on the size and size-distribution of the particles. In the microjet environment the nuclei are formed and the particle growth most likely occurs in the tube between the reactor and the collecting vessel. We did not investigate the effect of this distance on the particle growth yet. This will be the focus of a further study.

### 3. Experimental Section

#### 3.1. Materials

Zinc chloride, sodium hydroxide and ferric chloride were purchased from Grüssing GmbH (Filsum, Germany). Calcium nitrate and di-ammonium hydrogen phosphate were purchased from Fluka (Buchs, Switzerland). Ferrous chloride was purchased from Alfa Aesar (Karlsruhe, Germany). Ammonia was purchased from VWR (Fontenay-sous-Bois, France). All chemicals were used without further purification.

#### 3.2. Instruments and Characterization

FT-IR measurements were performed under ambient air (40 scans at a resolution of 4 cm<sup>-1</sup>) in attenuated total reflectance (ATR) mode on a Bruker Vertex 70 spectrometer. X-ray powder diffraction was carried out on two different diffractometers a Panalytical X'Pert and a Bruker D8 Advance-system, Bragg-Brentano geometry and CuK $\alpha$  radiation was used in both cases. The quantitative analysis was carried out by the Rietveld-method using the program TOPAS [32] and crystallographic data for the different species (zinc oxide [33], magnetite [34] and brushite [35]). Thermogravimetric analysis (TGA) was carried out on a Netzsch Iris TG 209. The sample was placed in an alumina crucible which was then heated from room temperature to 900 °C under nitrogen atmosphere with a rate of 20 K min<sup>-1</sup>.

Scanning electron microscopy (SEM) images were recorded on a JEOL SEM-7000 microscope. The SEM samples were prepared by placing some grains on a specimen stub with attached carbon adhesive foil followed by deposition of a gold layer. Dynamic light scattering (DLS) measurements were carried out on an ALV/CGS-3 compact goniometer system with an ALV/LSE-5003 multiple  $\tau$

correlator at a wavelength of 632.8 nm (He-Ne Laser) and at a 90° goniometer angle. The particle radius was then determined by the analysis of the correlation-function via the  $g_2(t)$  method followed by a logarithmic number-weighting (n.w.) of the distribution function.

### 3.3. Synthesis

The following experiments were performed in a microjet reactor construction. Two LaPrep P110 preparative HPLC pumps (VWR) are responsible for the transport of the solutions containing the starting materials as dissolved substances. The reaction takes place in a microjet reactor (Synthesechemie, Heusweiler, Germany and MJR PharmJet, Homburg, Germany) with a cone diameter of 300 micrometers. The precipitate was directly removed from the reactor by the use of a nitrogen gas flow. The length of the tube between the microjet reactor and the collecting vessel was 150 cm. Zinc oxide was synthesized using a 1 M aqueous zinc chloride and a 2 M aqueous sodium hydroxide solution as starting materials. Magnetite was obtained using a 0.4 M aqueous ammonia solution and an aqueous solution containing 0.0625 M ferric and ferrous chloride respectively. Brushite was synthesized by using 0.2 M aqueous solution of calcium nitrate and a 0.1 M aqueous solution of di-ammonium hydrogen phosphate, the pH of both solutions was adjusted to 5 using acetic acid or ammonia. The synthesis of each species was performed using different process parameters. The temperature was varied between 25 °C and 75 °C, the flow rate was varied between 150 mL/min and 250 mL/min.

## 4. Conclusions

The microjet-reactor technique is a promising method for the continuous synthesis of inorganic nanoparticles. Systematic studies on the effect of the process parameters, such as flow rate and process temperature, show that the particle size is controllable by means of these parameters. Our aim was the continuous synthesis of inorganic nanoparticles with controllable particle size. In our work we successfully demonstrated that it is possible to obtain pure zinc oxide nanoparticles using the microjet-reactor system. The prepared particles are uniformly shaped with a particle size of between 44 nm and 102 nm depending on the reaction conditions. The same could be shown for the synthesis of magnetite nanoparticles that were obtained with particle sizes between 46 nm and 132 nm. In both cases, the size distributions were quite small and decreased with increasing reaction temperature. Furthermore, we demonstrated the synthesis of calcium hydrogen phosphate (brushite) by using the microjet-reactor. In this case brushite as a layered structure formed small plates.

## Conflicts of Interest

The authors declare no conflict of interest.



## References

1. Kango, S.; Kalia, S.; Celli, A.; Njuguna, J.; Habibi, Y.; Kumar, R. Surface modification of inorganic nanoparticles for development of organic-inorganic nanocomposites - A review. *Prog. Polym. Sci.* **2013**, *38*, 1232–1261.
2. Castro, F.; Kuhn, S.; Jensen, K.; Ferreira, A.; Rocha, F.; Vicente, A.; Teixeira, J.A. Process intensification and optimization for hydroxyapatite nanoparticles production. *Chem. Eng. Sci.* **2013**, *100*, 352–359.
3. Ying, Y.; Chen, G.; Zhao, Y.; Li, S.; Yuan, Q. A high throughput methodology for continuous preparation of monodispersed nanocrystals in microfluidic reactors. *Chem. Eng. J.* **2008**, *135*, 209–215.
4. Ström, V.; Olsson, R.T.; Rao, K.V. Real-time monitoring of the evolution of the magnetism during precipitation of superparamagnetic nanoparticles for bioscience application. *J. Mater. Chem.* **2010**, *20*, 4168–4175.
5. Van den Rul, H.; Mondelaers, D.; van Bael, M.K.; Mullens, J. Water-based wet chemical synthesis of (doped) ZnO nanostructures. *J. Sol-Gel Sci. Tech.* **2006**, *39*, 41–47.
6. Jones, A.; Rigopoulos, S.; Zauner, R. Crystallisation and precipitation engineering. *Comput. Chem. Eng.* **2005**, *29*, 1159–1166.
7. Chen, J.; Zheng, C.; Chen, G. Interaction of macro- and micromixing on particle size distribution in reactive precipitation. *Chem. Eng. Sci.* **1996**, *51*, 1957–1966.
8. Mersmann, A. Crystallization and precipitation. *Chem. Eng. Process.* **1999**, *38*, 345–353.
9. Luo, G.; Du, L.; Wang, Y.; Lu, Y.; Xu, J. Controllable preparation of particles with microfluidics. *Particuology* **2011**, *9*, 545–558.
10. Chen, G.; Luo, G.; Yang, X.; Sun, Y.; Wang, J. Anatase-TiO<sub>2</sub> nano-particle preparation with a micro-mixing technique and its photocatalytic performance. *Mater. Sci. Eng. A* **2004**, *380*, 320–325.
11. Wagner, J.; Kirner, T.; Mayer, G.; Albert, J.; Köhler, J.M. Generation of metal nanoparticles in a microchannel reactor. *Chem. Eng. J.* **2004**, *101*, 251–260.
12. Zinoveva, S.; De Silva, R.; Louis, R.D.; Datta, P.; Kumar, C.S.S.R.; Goettert, J.; Hormes, J. The wet chemical synthesis of Co nanoparticles in a microreactor system: A time-resolved investigation by X-ray absorption spectroscopy. *Nucl. Instrum. Methods Phys. Res. Sect. A* **2007**, *582*, 239–241.
13. Du, L.; Wang, Y.J.; Lu, Y.C.; Luo, G.S. Preparation of highly purified  $\beta$ -tricalcium phosphate ceramics with a microdispersion process. *Chem. Eng. J.* **2013**, *221*, 55–61.
14. Schwarzer, H.C.; Schwertfirm, F.; Manhart, M.; Schmid, H.J.; Peukert, W. Predictive simulation of nanoparticle precipitation based on the population balance equation. *Chem. Eng. Sci.* **2006**, *61*, 167–181.
15. Schwarzer, H.C.; Peukert, W. Experimental Investigation into the Influence of Mixing on Nanoparticles Precipitation. *Chem. Eng. Technol.* **2002**, *25*, 6, 657–661.
16. Lince, F.; Marchisio, D.L.; Barresi, A.A. A comparative study for nanoparticle production with passive mixers via solvent-displacement: Use of CFD models for optimization and design. *Chem. Eng. Process.* **2011**, *50*, 356–368.

17. Lince, F.; Marchisio, D.L.; Barresi, A.A. Smart mixers and reactors for the production of pharmaceutical nanoparticles: Proof of concept. *Chem. Eng. Res. Des.* **2009**, *87*, 543–549.
18. Silva, V.M.T.M.; Quadros, P.A.; Laranjeira, P.E.M.S.C.; Dias, M.M.; Lopes, J.C.B. A novel Continuous Industrial Process for Producing Hydroxyapatite Nanoparticles. *J. Dispersion Sci. Technol.* **2008**, *29*, 542–547.
19. Penth, B. (K)ein Fall für die Fällung. *Chem. Tech.* **2004**, *3*, 18–20.
20. Penth, B. Kontinuierliche Produktion in Mikroreaktoren. German Patent DE 102006004350 A1, August 2006.
21. Rüfer, A.; Räuchle, K.; Krahl, F.; Reschetilowski, W. Kontinuierliche Darstellung von Bariumsulfat-Nanopartikeln im MicroJet-Reaktor. *Chem. Ing. Tech.* **2009**, *81*, 1949–1954.
22. Dittert, B.; Gavrilovic, A.; Schwarz, S.; Angerer, P.; Steiner, H.; Schöftner, R. Phase content controlled TiO<sub>2</sub> nanoparticles using the MicroJetReactor technology. *J. Eur. Ceram. Soc.* **2011**, *31*, 2475–2480.
23. Djutisic, A.B.; Ng, A.M.C.; Chen, X.Y. ZnO nanostructures for optoelectronics: Material properties and device applications. *Prog. Quantum Electron.* **2010**, *34*, 191–259.
24. Sugawara, A.; Asaoka, K.; Ding, S.J. Calcium phosphate-based cements: Clinical needs and recent progress. *J. Mater. Chem. B* **2013**, *1*, 1081–1089.
25. Vékás, L.; Tombácz, E.; Turcu, R.; Morjan, I.; Avdeev, M.V.; Krasia-Christoforou, T.; Socoliuc, V. Synthesis of Magnetite Nanoparticles and Magnetic Fluids for Biomedical Applications. Nanomedicine-Basic and Clinical Applications in Diagnostics and Therapy. *Else Kröner-Fresenius Symp. Basel Karger* **2011**, *2*, 35–52.
26. Samanta, P.K.; Mishra, S. Wet chemical growth and optical property of ZnO nanodiscs. *Optik* **2013**, *124*, 2871–2873.
27. RuizMoreno, R.G.; Martínez, A.I.; Falcony, C.; Castro-Rodriguez, R.; Bartolo-Pérez, P.; Castro-Román, M. One pot synthesis of water compatible and monodisperse magnetite nanoparticles. *Mater. Lett.* **2013**, *92*, 181–183.
28. Fang, M.; Ström, V.; Olsson, R.T.; Belova, L.; Rao, K.V. Particle size and magnetic properties dependence on growth temperature for rapid mixed co-precipitated magnetite nanoparticles. *Nanotechnology* **2012**, *23*, 145601.
29. Arifuzzaman, S.M.; Rohani, S. Experimental study of brushite precipitation. *J. Cryst. Growth* **2004**, *267*, 624–634.
30. Petrov, I.; Soptrajanov, B.; Fuson, N.; Lawson, J.R. Infra-red investigation of dicalcium phosphates. *Spectrochim. Acta* **1967**, *23A*, 2637–2646.
31. Trpkovska, M.; Soptrajanov, B.; Malkov, P. FTIR reinvestigation of the spectra of synthetic brushite and its partially deuterated analogues. *J. Mol. Struct.* **1999**, *480–481*, 661–666.
32. *Topas*, V4.2; General profile and structure analysis software for powder diffraction data, User Manual; Bruker AXS: Karlsruhe, Germany, 2008.
33. Khan, A.A. X-ray determination of thermal expansion of zinc oxide. *Acta Cryst. A* **1968**, *24*, 403.
34. Okudera, H.; Kihara, K.; Matsumoto, T. Temperature Dependence of Structure Parameters in Natural Magnetite: Single Crystal X-ray Studies from 126 to 773 K. *Acta Cryst. B* **1996**, *52*, 450–457.

35. Beevers, C.A. The Crystal Structure of Dicalcium Phosphate Dihydrate,  $\text{CaHPO}_4 \cdot 2\text{H}_2\text{O}$ . *Acta Cryst.* **1958**, *11*, 273–277.

© 2014 by the authors; licensee MDPI, Basel, Switzerland. This article is an open access article distributed under the terms and conditions of the Creative Commons Attribution license (<http://creativecommons.org/licenses/by/3.0/>).

#### 4. SUMMARY

Two new synthetic strategies for the synthesis of inorganic nanoparticles were investigated. On the one hand there is reactive milling as a *top-down* approach and on the other hand there is the microjet reactor process as a *bottom-up* approach. It was shown that both approaches are promising methods for the synthesis of inorganic nanoparticles. Each has some benefits compared to conventional synthetic strategies but there are also some disadvantages.

Reactive milling has been successfully used for the synthesis of particles with *in situ* surface functionalization. The benefit compared to conventional synthetic strategies is that it is solvent free and therefore environmentally friendly and more economic.

Titania surfaces have been modified with suitable coupling agents and the influence of various process parameters has been investigated. For the first experiments a WC/Co-hard metal grinding bowl and corresponding milling balls were used. Titania was used as inorganic pigment and phenylphosphonic acid as surface-modifying agent. By varying the milling time and the rotational speed the influence of these process parameters was investigated.

The obtained products were characterized by various techniques with respect to changes in the sample composition, particle size and surface-modification. TG-IR and NMR studies verified that a surface-modification has taken place and that the surface-modifying agent was not degraded during the milling process. CHN as well as TGA analysis showed that the degree of surface coverage increased with increasing milling time and rotational speed, thus with increasing energy input. A surface coverage of up to 1.4 mmol phosphonate per gram particle could be obtained.

To reach such a high amount of surface-modification the milling process was conducted for 48 h with 300 rpm. In comparison, milling only for 12 h with 300 rpm lead to a surface coverage of 1.1 mmol phosphonate per gram particle. Using a rotational speed of 200 rpm and a milling time of 12 h resulted in a surface coverage of 0.7 mmol phosphonate per gram particle. Thus, increasing milling time as well as increasing rotation speed lead to an increase of the amount of surface coverage.

X-ray powder diffraction studies revealed that the milling process was accompanied by a tribochemical phase transition from the starting material anatase to rutile and a high-pressure modification of titania. This phase transition depended on the specific process parameters and increased with increasing energy input. Furthermore, it turned out that more rutile is generated if titania was milled without the coupling agent. Consequently, the presence of a surface-modifying molecule seemed to stabilize the high-pressure phase.

Independently of the milling parameters the high-pressure phase revealed crystallite sizes of 5-6 nm. The starting material anatase was applied in granular crystalline dimensions with crystallite sizes above 300 nm. Due to the milling process there was a decrease of the crystallite size but with crystallite sizes of around 100 nm it remained granular crystalline.

The particle size and morphology was determined by SEM and DLS studies. The SEM images showed that the final particles were agglomerated and not uniformly shaped. Depending on the selected parameters sizes of 100 nm to 300 nm could be observed. This agreed well with the findings of the DLS studies. Here the samples exhibited two distinct particle size fractions. There existed particles with sizes of approximately 120 nm as well as particles with sizes of around 400 nm. Both methods revealed that the particle size decreases with increasing milling time and rotational speed.

The two fractions of different particle sizes were in good agreement with the results of the XRD analysis which revealed that the samples consist of various crystallographic phases with different crystallite sizes.

X-ray fluorescence spectroscopy was used to investigate potential contamination due to abrasion of the grinding bowl. The results showed that the level of contamination increased with increasing milling time and rotational speed. In addition, it turned out that the impurities were significantly higher if titania was milled without any additive. Milling titania with phenylphosphonic acid for 12 h at 200 rpm a contamination of 0.046 wt-% tungsten was found. An extension of the milling time to 48 h leads to a contamination of 0.196 wt-% tungsten. Impurities of 0.071 wt-% tungsten were found for the case that the milling speed was increased to 300 rpm applying a milling time of 12 h. A milling process at 300 rpm for 48 h resulted in a contamination of 0.277 wt-% tungsten. Using the

same process parameters but milling titania without any additive lead to a contamination of 0.957 wt-%.

However, in each case the contamination was negligible low. Nevertheless, the samples after the milling process showed a grey discoloration which became more intensive with increased energy input. Electron paramagnetic resonance was applied to clarify the origin of these discolorations. The results showed that the samples of titania milled with phenylphosphonic acid contain  $\text{Ti}^{3+}$  species which most likely lead to the darkening of the sample. In case of those samples which were milled without any additive no signal associated with  $\text{Ti}^{3+}$  was detectable. Consequently, the discoloration of these samples has its origin in the contamination with abrasion of the grinding bowl.

The results received so far demonstrate that reactive milling is a suitable top-down approach for the preparation of nanoparticles with *in situ* surface functionalization. The great benefit of this method is that it is solvent free and therefore environmentally friendly.

The studies were expanded to investigate the influence of the grinding bowl and grinding sphere material which is supposed to have crucial influence on the energy impact in the milling process. Again titania was used as inorganic pigment and phenylphosphonic acid as coupling agent but this time a  $\text{ZrO}_2$ -ceramic grinding bowl with corresponding milling balls instead of the WC/Co-hard metal implements were used. Systemic studies on the influence of the milling time and the rotational speed showed that the basic behavior of the samples is equal to the behavior in the WC/Co-hard metal grinding bowl.

Various experiments showed that a surface functionalization took place and that the coupling agent was not degraded during the milling process. Furthermore, the degree of surface coverage as well as the level of phase transformation from anatase to rutile and high-pressure  $\text{TiO}_2$  increased with enhanced energy input.

Milling titania with phenylphosphonic acid in the  $\text{ZrO}_2$ -ceramic grinding bowl for 12 h at 200 rpm resulted in a degree of surface coverage of 0.6 mmol phosphonate per gram particle. Applying enhanced energy input (48 h at 300 rpm) lead to a significantly higher amount of surface-modification of 1.2 mmol phosphonate per gram particle. Regarding to the phase transformation it was found that after milling 12 h at 200 rpm the sample consisted still of 70 wt-% anatase. After

milling for 48 h at 300 rpm there remained just 18 wt-% anatase and the main phase was represented by the high-pressure modification.

The differences appeared in the overall energy input which was lower in the case that a ZrO<sub>2</sub>-ceramic grinding bowl was used. The reason for this is the lower density of the ZrO<sub>2</sub>-ceramic. As a result, the overall surface coverage as well as the amount of phase transition decreased when a ZrO<sub>2</sub>-ceramic grinding bowl instead of the WC/Co-hard metal grinding bowl was used.

On the average it was possible to achieve a surface-modification with the WC/Co grinding bowl increased by approximately 0.2 mmol phosphonate per gram particle compared to the ZrO<sub>2</sub> grinding equipment.

The difference in the degree of surface transition can be demonstrated by means of the amount of remaining anatase phase. In case of those parameters which lead to the highest energy input for the WC/Co grinding bowl only 8 wt-% anatase are left in the sample after the milling process. In contrast, when a ZrO<sub>2</sub> grinding bowl was used, the equivalent sample contains 18 wt-% anatase.

The contamination of the samples due to abrasion of the grinding bowl was analyzed by applying X-ray fluorescence spectroscopy. As expected there was more contamination with increasing milling time and rotational speed. Compared to the results obtained using the WC/Co grinding bowl the amount of impurities was smaller. In the case of the WC/Co grinding bowl impurities of 0.05 wt-% (12 h at 200 rpm) up to 0.28 wt-% (48 h at 300 rpm) tungsten were found. Milling in the ZrO<sub>2</sub> grinding bowl resulted in impurities between only 0.03 wt-% (12 h at 200 rpm) and 0.15 wt-% (48 h at 300 rpm) Zr. In case of milling titania with the coupling agent a slight discoloration of the samples could be observed. In analogy to the findings of the WC/Co grinding bowl they had their origin in the presence of Ti<sup>3+</sup> species which were generated during the milling process.

By using reactive milling for the generation of particles with *in situ* surface functionalization a solvent free and therefore environmentally friendly approach has been investigated. Using conventional synthetic strategies in case of phenylphosphonic acid the surface functionalization of titania could also be obtained in water as solvent. This is not the case for long alkyl chain phosphonic acids. Here, definitely an organic solvent is necessary for the complete dissolution of the respective coupling agent. For this reason the previous studies were expanded to this type of surface-modifier. Because the ZrO<sub>2</sub>-ceramic grinding

bowl lead to lower impurity concentrations the following experiments were conducted with this type of grinding bowl and grinding sphere material. Again, titania was used as inorganic pigment and dodecylphosphonic acid as well as octadecylphosphonic acid were used as coupling agents. Systematic studies on the behavior at different process parameters were performed using dodecylphosphonic acid as coupling agent.

The obtained products were characterized using various techniques. The results revealed that a surface functionalization by reactive milling was possible with long alkyl chain organophosphorus coupling agents as well. There was no evidence of a degradation of the coupling agent due to the strong forces which act in the ball mill. In analogy to the previous studies the process entailed a tribochemical phase transition from the starting material anatase to rutile and high-pressure TiO<sub>2</sub>. Also the amount of this phase transition as well as the degree of surface coverage increased with enhanced energy input. The final particles showed sizes between 100 nm and 300 nm and a degree of surface coverage up to 0.8 mmol phosphonate per gram particle could be reached.

After these promising studies on dodecylphosphonic acid as long alkyl chain phosphonate surface-modifier, octadecylphosphonic acid was used to successfully demonstrate that this approach is assignable on other long alkyl chain organophosphorus species. Using octadecylphosphonic acid as surface-modifying agent and performing the milling process for 48 h at 300 rpm a degree of surface coverage 0.6 mmol phosphonate per gram particle could be reached.

The second approach which has been investigated in the context of this thesis is the microjet reactor process. This technique is a bottom-up, wet-chemical method and has the benefit that it can be performed continuously. Two pumps were used to transport the precursor solutions to the microjet reactor. The reaction took place in a confined reaction environment which is given by the microjet reactor geometry. Using an inert gas flow the formed nuclei were directly transported from the reaction chamber to a tubing where the particle growth occurred. Systematic studies on the influence of different process parameters such as flow rate and process temperature were conducted with a view to the possibilities and limitations of this process.

In order to reveal the wide field of application of the microjet reactor technique syntheses of three different species have been performed. The approach was



successfully used for the production of zinc oxide (ZnO), magnetite ( $\text{Fe}_3\text{O}_4$ ) as well as brushite ( $\text{CaHPO}_4 \cdot 2\text{H}_2\text{O}$ ). In each case appropriate precursor solutions were used and the obtained products were characterized with various techniques with respect to the sample composition and the particle size.

Zinc oxide was obtained using a 1 M aqueous zinc chloride and a 2 M aqueous sodium hydroxide solution as starting materials. X-ray powder diffraction showed that pure zinc oxide can be obtained independent of the flow rate and the process temperature. However, the crystallite sizes became smaller with increased process temperature as well as enhanced flow rate. In addition, the particle sizes were determined by dynamic light scattering. Here, the same effect was observable. The obtained particles showed sized between 44 nm and 102 nm depending on the process parameters. The higher the process temperature and the flow rate the smaller were the obtained particles. Furthermore, the size distribution becomes more uniform with increased process temperature and flow rate. The particle morphology was investigated by means of scanning electron microscopy. It could be observed that the particles are uniform and sphere-shaped.

Magnetite was obtained using a 0.4 M aqueous ammonia solution and an aqueous solution containing 0.0625 M ferric and ferrous chloride respectively. Ferrous chloride must be applied in excess because the synthesis was performed under air where  $\text{Fe}^{2+}$  ions tend to oxidize and form  $\text{Fe}^{3+}$  ions. The obtained particles were analyzed by X-ray powder diffraction. The results reveal that all samples mostly consisted of magnetite with crystallite sizes around 10 nm, but there was a small fraction of an impurity phase which is suggested to be maghemite. The particle sizes ranged between 46 nm and 132 nm depending on the process parameters. The particle sizes as well as the size distribution became smaller with increased process temperature and enhanced flow rate. Scanning electron microscopical images revealed that the particles are uniform and sphere-shaped.

Brushite was synthesized using 0.2 M aqueous solution of calcium nitrate and 0.1 M aqueous solution of di-ammonium hydrogen phosphate, the pH of both solutions was adjusted to 5. FT-IR and TGA measurements indicated that pure brushite has been obtained. These results were confirmed by the X-ray powder analysis. The particles showed a high anisotropy in their crystallite sizes. The average crystallite size was determined to be in the range of 200 nm to 300 nm depending on the reaction conditions. Scanning electron microscopy revealed that

the particles were shaped like small plates. The edge lengths of these plates were determined to be between 100 nm and 500 nm.

The microjet reactor technique was demonstrated to be a promising method for the continuous synthesis of inorganic nanoparticles. The particle size was controllable by means of the process temperature as well as the flow rate.

The following illustrations give a summarized overview on the benefits and drawbacks of both new synthetic strategies which have been investigated in the context of this work.

	<b>benefit</b>	<b>drawback</b>
<b>Reactive milling</b>	<ul style="list-style-type: none"> <li>➤ Solvent free</li> <li>➤ Good raw material and energy balance</li> <li>➤ Simple handling</li> <li>➤ Two goals in one step: size reduction with <i>in situ</i> surface functionalization</li> </ul>	<ul style="list-style-type: none"> <li>➤ Limited control over the particle size</li> <li>➤ Broad particle size distribution</li> <li>➤ Impurity of the sample due to abrasion of the grinding bowl</li> </ul>
<b>Microjet reactor process</b>	<ul style="list-style-type: none"> <li>➤ Controllable particle size</li> <li>➤ Uniform particle size distribution</li> <li>➤ Simple handling and good efficiency</li> <li>➤ Good reproducibility</li> <li>➤ Reduced solvent use compared to batch syntheses</li> <li>➤ Easy transfer from laboratory to larger scale</li> </ul>	<ul style="list-style-type: none"> <li>➤ Solvent based</li> <li>➤ Potentially second step necessary (calcination)</li> </ul>

## 5. OUTLOOK

In line with this work two new promising synthetic strategies for the production of inorganic nanoparticles have been investigated: reactive milling with *in situ* surface functionalization and the microjet reactor process.

Reactive milling has been shown to be suitable for the preparation of nanoparticles with *in situ* surface functionalization. Titania has been successfully modified with various organophosphorus coupling agents. Regarding to further studies it would be interesting whether this process is assignable on other inorganic pigments and/or other coupling agents. In addition, an interesting aspect would be the direct incorporation of the obtained functionalized particles in an organic matrix like a polymer during the milling process.

The microjet reactor process has been shown to be a beneficial continuous approach for the synthesis of inorganic nanoparticles. Regarding to further studies there are various process parameters whose influence has not been sufficient investigated yet. Till now it has been shown that the reaction temperature and the flow rate have an influence on the obtained particles. The particle size could be controlled by means of these parameters. Now it would be interesting if the tubing length between the microjet reactor and the collecting vessel has an influence as well. Some experiments have been conducted with respect to the influence of this parameter but the results were not without any doubt. Consequently, further studies are necessary. Another parameter that has to be investigated is the influence of the concentration of the starting material solutions. Referring to this, some experiments have been performed as well. But even here, further investigations are necessary to be able to give clear results. Furthermore, it would be interesting to verify the use of this approach for the synthesis of a couple of other species.

The production of zinc oxide, magnetite and brushite has been performed successfully already. In order to avoid unrequested side products and impurities in case of zinc oxide the use of other starting materials than  $ZnCl_2$  and  $NaOH$  would be interesting. Here, organic species would be of interest with the aim to remove side products and impurities in a trailed calcination step.

## 6. LITERATURE

- [1] A. J. Mieszawska, Mulder, Willem J. M., Z. A. Fayad, D. P. Cormode, *Mol. Pharmaceutics* **2013**, *10*, 831.
- [2] S. Hameed, Predeep. P., M. R. Baiju, *Rev. Adv. Mater. Sci.* **2010**, *26*, 30.
- [3] W. Chen, Y. Qiu, S. Yang, *Phys. Chem. Chem. Phys.* **2012**, *14*, 10872.
- [4] K. C.-F. Leung et al., *Chem. Soc. Rev.* **2012**, *41*, 1911.
- [5] S. Suresh, *Nanosci. Nanotechnol.* **2013**, *3*, 62.
- [6] D. Astruc, F. Lu, J. R. Aranzaes, *Angew. Chem.* **2005**, *117*, 8062.
- [7] D. F. Shriver, P. W. Atkins, C. H. Langford, *Anorganische Chemie: Ein weiterführendes Lehrbuch*, VCH Verlagsgesellschaft, Weinheim **1992**.
- [8] P. W. Atkins, *Physikalische Chemie*, 4th ed., WILEY-VCH, Weinheim **2006**.
- [9] L. D. Winkler, J. F. Arceo, W. C. Hughes, B. A. DeGraff, and B. H. Augustine, *J. Chem. Educ.* **2005**, *82*, 1700.
- [10] A. P. Alivisatos, *Science* **1996**, *271*, 933.
- [11] C. Lin, w. Lin, *J. Food Drug Anal.* **2011**, *19*, 1.
- [12] P. Singh, A. Nanda, *Int. J. Cosmet. Sci.* **2014**, *36*, 273.
- [13] J.-W. Shiu et al., *J. Mater. Chem. A* **2014**, *2*, 8749.
- [14] A. Tomar, G. Garg, *Global J. Pharmacol.* **2013**, *7*, 34.
- [15] N. Lee, T. Hyeon, *Chem. Soc. Rev.* **2012**, *41*, 2575.
- [16] Y. Zhang, N. Kohler, M. Zhang, *Biomaterials* **2002**, *23*, 1553.
- [17] A. D. Padhye, G. D. Mavale, *Pop. Plast. Packag.* **2013**, 28.
- [18] S. Kango et al., *Prog. Polym. Sci.* **2013**, *38*, 1232.
- [19] D. Tristantini, Salmat, R. Mustikasari, Widuri, *Int. J. Eng. Technol.* **2011**, *11*, 73.
- [20] C. Bréchnignac, P. Houdy, M. Lahmani, *Nanomaterials and Nanotechnology*, Springer, Berlin, Heidelberg, New York **2006**.
- [21] S. Donthu, T. Sun, V. Dravid, *Adv. Mater.* **2007**, *19*, 125.
- [22] D. P. Sanders, *Chem. Rev.* **2010**, *110*, 321.
- [23] A. F. Fuentes, L. Takacs, *J. Mater. Sci.* **2013**, *48*, 598.
- [24] M. Barberio, P. Barone, F. Xu, A. Bonanno, *J. Chem. Chem. Eng.* **2013**, *7*, 1142.
- [25] V. K. LaMer, R. H. Dinegar, *J. Am. Chem. Soc.* **1950**, *72*, 4847.

- [26] C. C. Yec, H. C. Zeng, *J. Mater. Chem. A* **2014**, *2*, 4843.
- [27] W. Ostwald, *Z. Phys. Chem.* **1900**, *34*, 495.
- [28] W. Stöber, A. Fink, E. Bohn, *J. Colloid Interface Sci.* **1968**, *26*, 62.
- [29] Y. Zhu, L. Zhang, C. Gao, L. Cao, *J. Mater. Sci.* **2000**, *35*, 4049.
- [30] B. Baruwati, D. K. Kumar, S. V. Manorama, *Sens. Actuators, B* **2006**, *119*, 676.
- [31] R. Mueller, L. Mädler, S. E. Pratsinis, *Chem. Eng. Sci.* **2003**, *58*, 1969.
- [32] T. Karhunen et al., *ISRN Nanotechnology* **2011**, *2011*, 1.
- [33] J. Park et al., *Angew. Chem. Int. Ed.* **2007**, *46*, 4630.
- [34] P. T. Chung et al., *Mater. Chem. Phys.* **2012**, *136*, 868.
- [35] G. Guerrero, P. H. Mutin, A. Vioux, *Chem. Mater.* **2001**, *13*, 4367.
- [36] A. Convertino et al., *Sens. Actuators, B* **2007**, *126*, 138.
- [37] P. D. Cozzoli, A. Kornowski, H. Weller, *J. Am. Chem. Soc.* **2003**, *125*, 14539.
- [38] M.-A. Neouze, U. Schubert, *Monatsh Chem* **2008**, *139*, 183.
- [39] S. Marcinko, A. Y. Fadeev, *Langmuir* **2004**, *20*, 2270.
- [40] F. Brodard-Severac et al., *Chem. Mater.* **2008**, *20*, 5191.
- [41] A. K. Bhattacharya, G. Thyagarajan, *Chem. Rev.* **81**, *1981*, 415.
- [42] C. E. McKenna, J. Schmidhuser, *J. Chem. Soc., Chem. Commun.* **1979**, 739.
- [43] C. J. Brinker, G. W. Scherer, *Sol-Gel-Science - The Physics and Chemistry of Sol-Gel Processing*, Elsevier Academic Press Inc., San Diego **1990**.
- [44] A. Ulman, *Chem. Rev.* **1996**, *96*, 1533.
- [45] C. Yee et al., *Langmuir* **1999**, *15*, 7111.
- [46] M. Szekeres et al., *J. Mater. Chem.* **2002**, *12*, 3268.
- [47] E. Ramirez et al., *J. Organomet. Chem.* **2004**, *689*, 4601.
- [48] M. Raza, A. Bachinger, N. Zahn, G. Kickelbick, *Materials* **2014**, *7*, 2890.
- [49] C. Suryanarayana, *Prog. Mater. Sci.* **2001**, *46*, 1.
- [50] J. F. Fernández-Bertran, *Pure Appl. Chem.* **1999**, *71*, 581.
- [51] A. L. Garay, A. Pichon, S. L. James, *Chem. Soc. Rev.* **2007**, *36*, 846.
- [52] G. Kaupp, *CrystEngComm* **2006**, *8*, 794.
- [53] S. L. James et al., *Chem. Soc. Rev.* **2011**, *41*, 413.
- [54] A. Gajovic et al., *J. Am. Ceram. Soc. (Journal of the American Ceramic Society)* **2006**, *89*, 2196.
- [55] Da Silva, Klebson L. et al., *J. Phys. Chem. C* **2011**, *115*, 7209.

- [56] G. Kaupp, *CrystEngComm* **2011**, *13*, 3108.
- [57] T. Alonso, M. P. Dallimore, P. G. McCormick, *Scr. Metall. Mater.* **1993**, *29*, 55.
- [58] G. Kaupp, *CrystEngComm* **2009**, *11*, 388.
- [59] M. Urano, S. Wada, H. Suzuki, *Chem. Commun.* **2003**, 1202.
- [60] C. Ney, H. Kohlmann, G. Kickelbick, *Int. J. Hydrogen Energy* **2011**, *36*, 9086.
- [61] M. Salari, S. M. Mousavi khoie, P. Marashi, M. Rezaee, *J. Alloys Compd.* **2009**, *469*, 386.
- [62] P. Billik et al., *J. Phys. Chem. Solids* **2007**, *68*, 1112.
- [63] R. Ren, Z. Yang, L. L. Shaw, *J. Mater. Sci.* **2000**, *35*, 6015.
- [64] S. Begin-Colin, T. Giroto, G. Le Caer, A. Mocellin, *J. Solid State Chem.* **2000**, *149*, 41.
- [65] S. Indris, D. Bork, P. Heitjans, *J. Mater. Synth. Process.* **2000**, *8*, 245.
- [66] T. Oztas, J. Park, A. Ozturk, *Adv. Mater. Res.* **2013**, *650*, 44.
- [67] M. Senna et al., *J. Solid State Chem.* **2012**, *187*, 51.
- [68] Y. Ying et al., *Chem. Eng. J.* **2008**, *135*, 209.
- [69] H.-C. Schwarzer et al., *Chem. Eng. Sci.* **2006**, *61*, 167.
- [70] H.-C. Schwarzer, W. Peukert, *Chem. Eng. Technol.* **2002**, *25*, 657.
- [71] J. Stavek, *Chem. Mater.* **1992**, *4*, 545.
- [72] Oliveira, Ana Paula A., J.-F. Hochepped, F. Grillon, M.-H. Berger, *Chem. Mater.* **2003**, *15*, 3202.
- [73] I. Hirasawa, T. Mikami, A. Katayama, T. Sakuma, *Chem. Eng. Technol.* **2006**, *29*, 212.
- [74] H.-C. Schwarzer, W. Peukert, *Chem. Eng. Technol.* **2002**, *25*, 657.
- [75] H.-C. Schwarzer, W. Peukert, *Chem. Eng. Commun.* **2004**, *191*, 580.
- [76] M. Engler, N. Kockmann, T. Kiefer, P. Woias, *Chem. Eng. J.* **2004**, *101*, 315.
- [77] B. Palanisamy, B. Paul, *Chem. Eng. Sci.* **2012**, *78*, 46.
- [78] L. Wei, M. Hervé, P. Edouard, *J. Cryst. Growth* **2012**, *342*, 21.
- [79] S.-A. Hong et al., *J. Supercrit. Fluids* **2013**, *73*, 70.
- [80] A. Gedanken, *Ultrason. Sonochem.* **2004**, *11*, 47.
- [81] J. Zhu et al., *J. Solid State Chem.* **2000**, *153*, 342.
- [82] Y. Mastai et al., *J. Am. Chem. Soc.* **1999**, *121*, 10047.
- [83] H.-I. Li et al., *J. Solid State Chem.* **2003**, *172*, 102.

- [84] H.-I. Li et al., *J. Mater. Chem.* **2002**, *12*, 3723.
- [85] S. I. Nikitenko et al., *J. Mater. Chem.* **2002**, *12*, 1450.
- [86] S. Ramesh et al., *J. Am. Ceram. Soc. (Journal of the American Ceramic Society)* **2000**, *83*, 89.
- [87] V. G. Pol, O. Palchik, A. Gedanken, I. Felner, *J. Phys. Chem. B* **2002**, *106*, 9737.
- [88] E. Ohayon, A. Gedanken, *Ultrason. Sonochem.* **2010**, *17*, 173.
- [89] B. Pohl, R. Jamshidi, G. Brenner, U. A. Peuker, *Chem. Ing. Tech.* **2012**, *84*, 70.
- [90] F. Dang et al., *Chem. Eng. J.* **2011**, *170*, 333.
- [91] G. Luo et al., *Particuology* **2011**, *9*, 545.
- [92] B. Penth, *German Patent DE 102006004350 A1*, 2006.
- [93] A. Betke, G. Kickelbick, *Inorganics* **2014**, *2*, 1.
- [94] B. Penth, *Chem. Tech.* **2004**, *3*, 18.
- [95] A. Rüfer, K. Räuchle, F. Krahl, W. Reschetilowski, *Chem. Ing. Tech.* **2009**, *81*, 1949.
- [96] B. Dittert et al., *J. Eur. Ceram. Soc.* **2011**, *31*, 2475.
- [97] P. K. Samanta, S. Mishra, *Optik* **2013**, *124*, 2871.
- [98] H. Yin, P. S. Casey, *Mater. Lett.* **2014**, *121*, 8.
- [99] A. S. Lanje et al., *Adv. Powder Technol.* **2013**, *24*, 331.
- [100] H. Rul, D. Mondelaers, M. K. Bael, J. Mullens, *J. Sol-Gel Sci. Technol. (Journal of Sol-Gel Science and Technology)* **2006**, *39*, 41.
- [101] H. W. Kang, J. Leem, S. Y. Yoon, H. J. Sung, *Nanoscale* **2014**, *6*, 2840.
- [102] K. Sue, K. Murata, K. Kimura, K. Arai, *Green Chem.* **2003**, *5*, 659.
- [103] R. G. RuizMoreno et al., *Mater. Lett.* **2013**, *92*, 181.
- [104] M. Fang et al., *Nanotechnology* **2012**, *23*, 145601.
- [105] S.-D. Seo et al., *J. Am. Ceram. Soc. (Journal of the American Ceramic Society)* **2014**, *97*, 1413.
- [106] B. Veriansyah, J.-D. Kim, B. K. Min, J. Kim, *Mater. Lett.* **2010**, *64*, 2197.
- [107] B. Mostaghaci, B. Loretz, R. Haberkorn, G. Kickelbick, *Chem. Mater.* **2013**, *25*, 3667.
- [108] S. Arifuzzaman, S. Rohani, *J. Cryst. Growth* **2004**, *267*, 624.
- [109] S. Singh, V. Singh, S. Aggarwal, U. K. Mandal, *Chem. Pap.* **2010**, *64*, 491.

[110] J. P. Maity et al., *Int. J. Mol. Sci.* **2011**, *12*, 3821.



## **7. SUPPORTING INFORMATION**

The results of this work have been published. Supporting information belonging to the publications presented in this work are provided in this chapter.

### **7.1 SYNTHESIS OF SURFACE-FUNCTIONALIZED TITANIA PARTICLES WITH ORGANOPHOSPHORUS COUPLING AGENTS BY REACTIVE MILLING**

Supporting information belonging to the following publication:

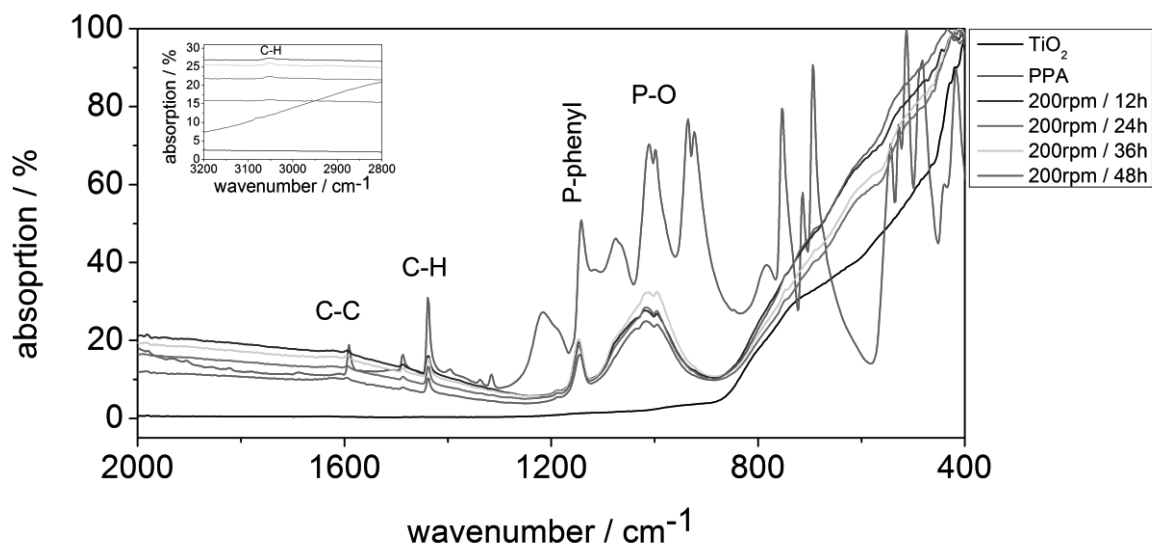
A. Fischer, C. Ney, G. Kickelbick, Synthesis of Surface-Functionalized Titania Particles with Organophosphorus Coupling Agents by Reactive Milling, *Eur. J. Inorg. Chem.*, **2013**, *33*, 5701-5707.

**SUPPORTING INFORMATION**

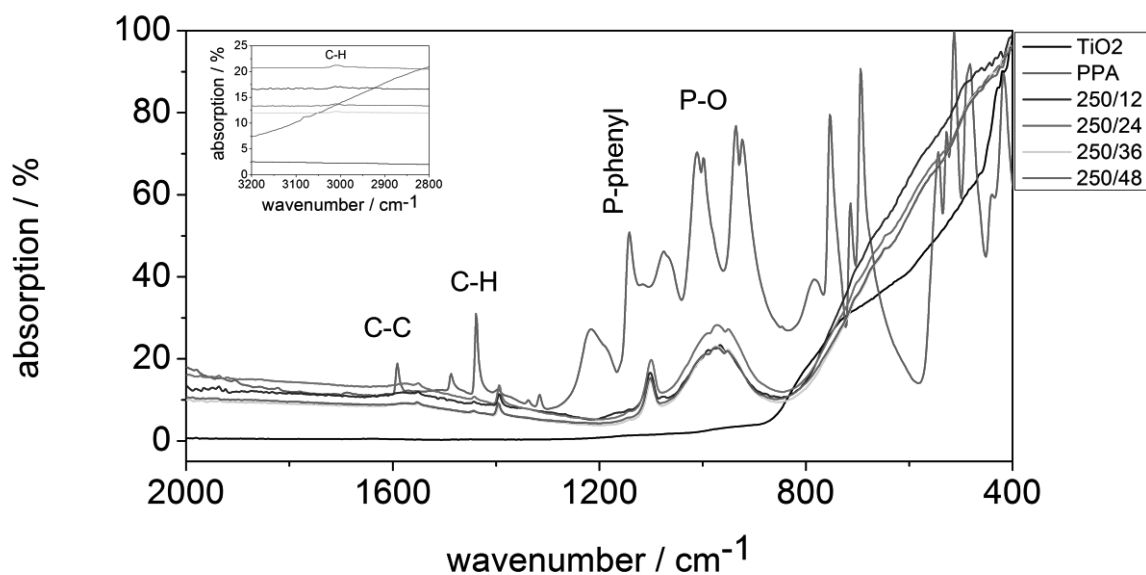
**DOI:** 10.1002/ejic.201300589

**Title:** Synthesis of Surface-Functionalized Titania Particles with Organophosphorus Coupling Agents by Reactive Milling

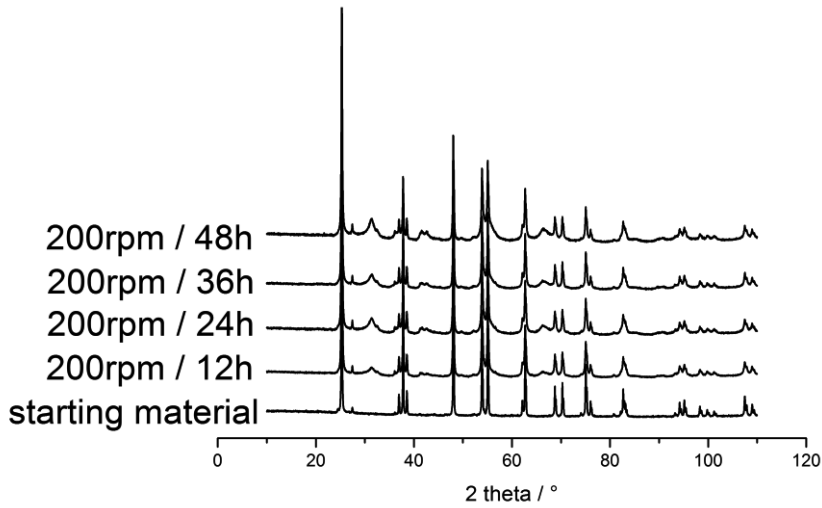
**Author(s):** Annika Fischer, Christoph Ney, Guido Kickelbick\*



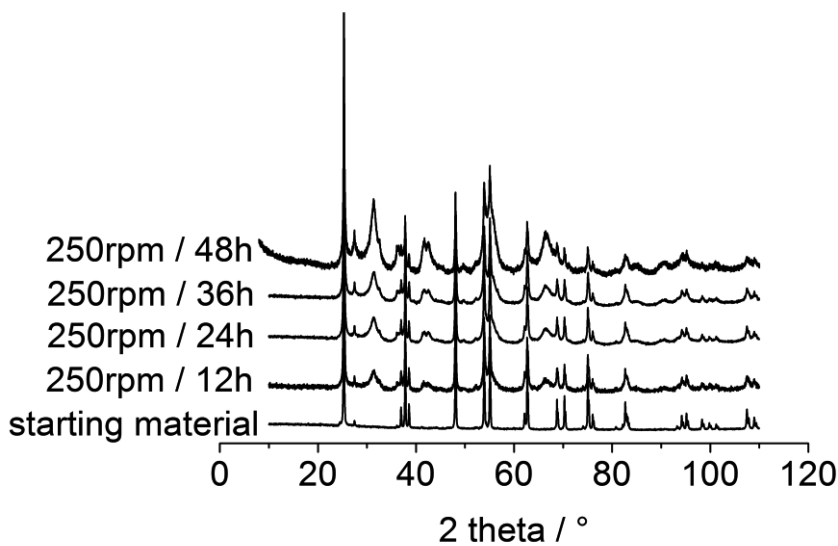
**S 1:** FTIR-spectra: starting material titania, coupling agent phenylphosphonic acid and samples after the milling process: 200 rpm / 12 h, 200 rpm / 24 h, 200 rpm / 36 h, 200 rpm / 48 h; surface modification has taken place after the milling process, which is indicated by the characteristic bands for aromatic C-C oscillation ( $1600\text{ cm}^{-1}$ ), the C-H oscillation ( $1440\text{ cm}^{-1}$ ), P-phenyl vibrations ( $1150\text{ cm}^{-1}$ ), the wide band at  $1000\text{ cm}^{-1}$  (P-O region) and the aromatic C-H oscillation at  $3050\text{ cm}^{-1}$ .



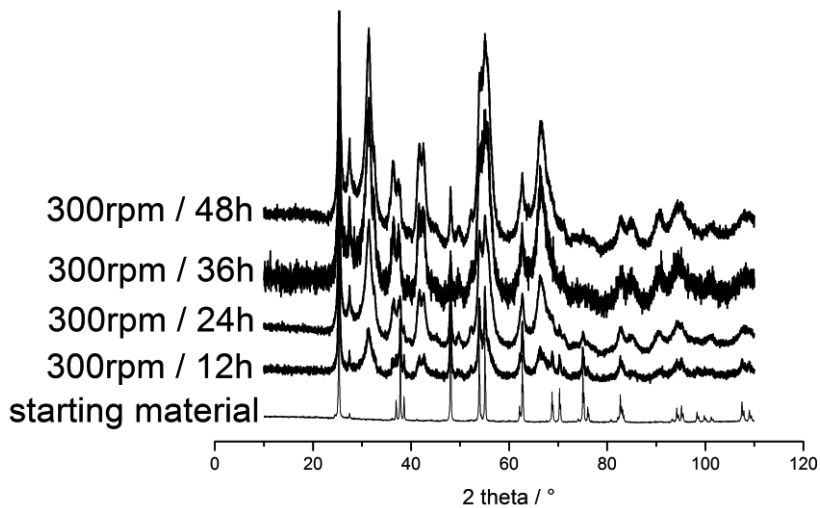
**S 2:** FTIR-spectra: starting material titania, coupling agent phenylphosphonic acid and samples after the milling process: 250 rpm / 12 h, 250 rpm / 24 h, 250 rpm / 36 h, 250 rpm / 48 h; surface modification has taken place after the milling process, which is indicated by the characteristic bands for aromatic C-C oscillation ( $1600\text{ cm}^{-1}$ ), the C-H oscillation ( $1440\text{ cm}^{-1}$ ), P-phenyl vibrations ( $1150\text{ cm}^{-1}$ ), the wide band at  $1000\text{ cm}^{-1}$  (P-O region) and the aromatic C-H oscillation at  $3050\text{ cm}^{-1}$ .



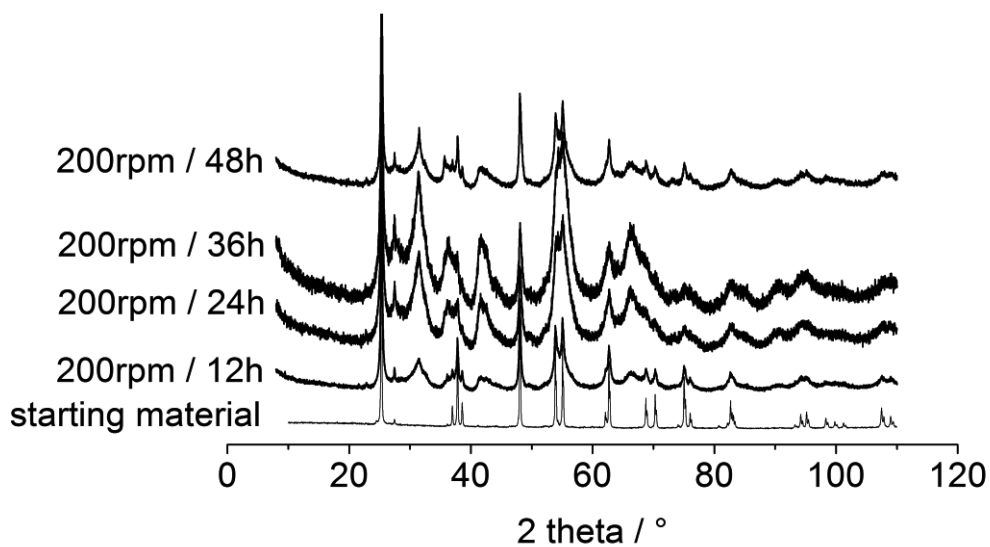
**S 3:** XRD patterns of the starting material anatase and the samples after milling with phenylphosphonic acid at 200 rpm with different durations. After the milling the presence of high pressure  $\text{TiO}_2$  ( $2\theta = 31^\circ$ ,  $42^\circ$  and  $66^\circ$ ) and rutile ( $2\theta = 27^\circ$ ) is indicated by additional reflections.



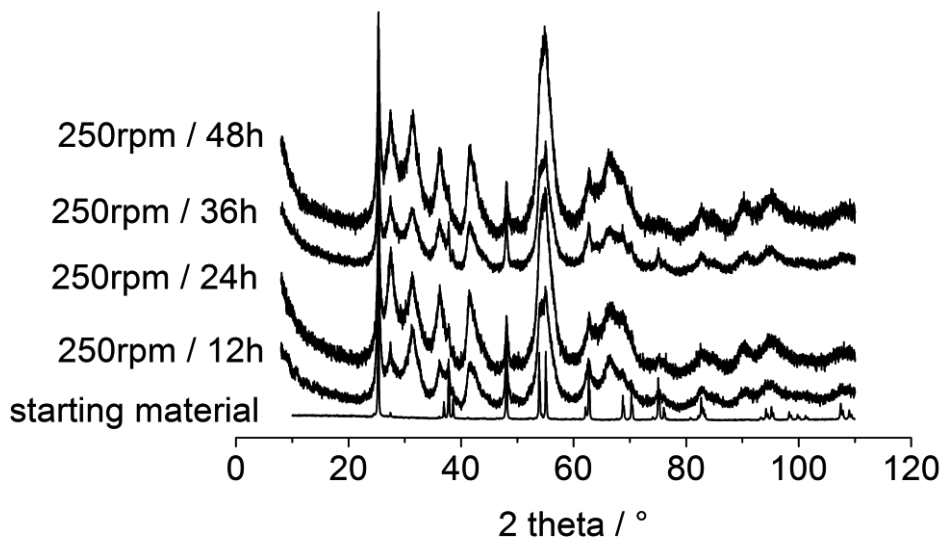
**S 4:** XRD patterns of the starting material anatase and the samples after milling with phenylphosphonic acid at 250 rpm with different durations. After the milling the presence of high pressure  $\text{TiO}_2$  ( $2\theta = 31^\circ$ ,  $42^\circ$  and  $66^\circ$ ) and rutile ( $2\theta = 27^\circ$ ) is indicated by additional reflections.



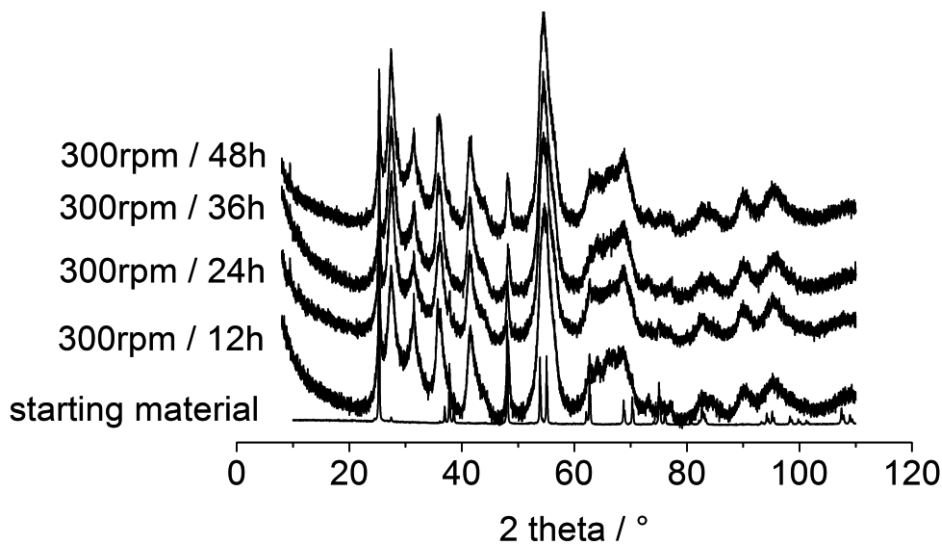
**S 5:** XRD patterns of the starting material anatase and the samples after milling with phenylphosphonic acid at 300 rpm with different durations. After the milling the presence of high pressure  $\text{TiO}_2$  ( $2\theta = 31^\circ$ ,  $42^\circ$  and  $66^\circ$ ) and rutile ( $2\theta = 27^\circ$ ) is indicated by additional reflections.



**S 6:** XRD patterns of the starting material anatase and the samples after milling at 200 rpm with different durations. After the milling the presence of high pressure  $\text{TiO}_2$  ( $2\theta = 31^\circ$ ,  $42^\circ$  and  $66^\circ$ ) and rutile ( $2\theta = 27^\circ$ ) is indicated by additional reflections.



**S 7:** XRD patterns of the starting material anatase and the samples after milling at 250 rpm with different durations. After the milling the presence of high pressure TiO<sub>2</sub> ( $2\theta = 31^\circ$ ,  $42^\circ$  and  $66^\circ$ ) and rutile ( $2\theta = 27^\circ$ ) is indicated by additional reflections.



**S 8:** XRD patterns of the starting material anatase and the samples after milling at 300 rpm with different durations. After the milling the presence of high pressure TiO<sub>2</sub> ( $2\theta = 31^\circ$ ,  $42^\circ$  and  $66^\circ$ ) and rutile ( $2\theta = 27^\circ$ ) is indicated by additional reflections.

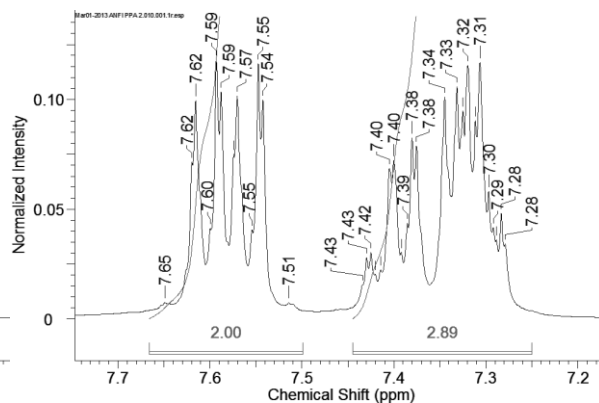
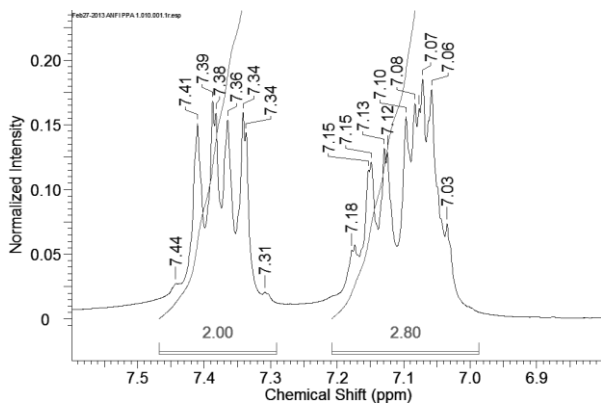
**Table S1: Composition of titania milled with phenylphosphonic acid as coupling agent at specific process parameters**

Process parameters	anatase / wt%	rutile / wt%	high pressure / wt%
starting material	98.2 ± 0.1	1.8 ± 0.1	0
200 rpm / 12 h	73.0 ± 0.2	2.5 ± 0.1	24.5 ± 0.2
200 rpm / 24 h	59.5 ± 0.2	3.3 ± 0.1	37.2 ± 0.2
200 rpm / 36 h	60.9 ± 0.2	3.9 ± 0.1	35.2 ± 0.2
200 rpm / 48 h	49.3 ± 0.2	4.4 ± 0.1	46.3 ± 0.2
250 rpm / 12 h	53.5 ± 0.3	3.8 ± 0.2	42.7 ± 0.3
250 rpm / 24 h	43.5 ± 0.2	4.5 ± 0.1	52.0 ± 0.2
250 rpm / 36 h	38.7 ± 0.2	4.8 ± 0.1	56.5 ± 0.2
250 rpm / 48 h	18.6 ± 0.2	12.7 ± 0.3	68.7 ± 0.3
300 rpm / 12 h	32.6 ± 0.3	4.1 ± 0.2	63.3 ± 0.3
300 rpm / 24 h	15.7 ± 0.2	5.6 ± 0.2	78.7 ± 0.2
300 rpm / 36 h	8.3 ± 0.2	5.8 ± 0.2	85.9 ± 0.3
300 rpm / 48 h	7.6 ± 0.1	7.0 ± 0.2	85.4 ± 0.2

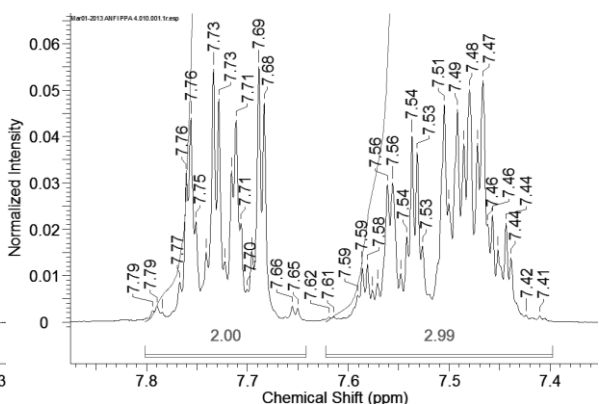
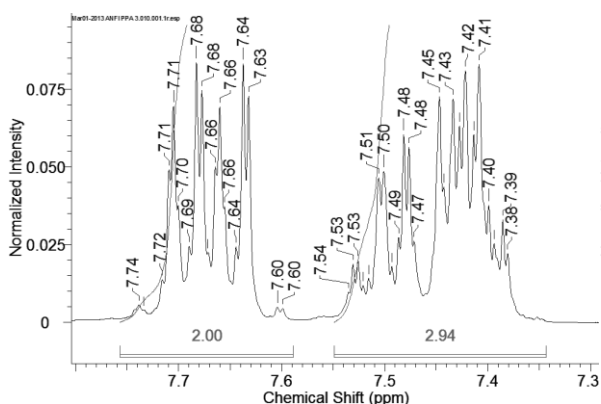
**Table S2: Composition of titania milled without any coupling agent at specific process parameters**

Process parameters	anatase / wt%	rutile / wt%	high pressure / wt%
starting material	98.2 ± 0.1	1.8 ± 0.1	--
200 rpm / 12 h	39.8 ± 0.3	5.1 ± 0.2	55.1 ± 0.4
200 rpm / 24 h	15.0 ± 0.2	15.7 ± 0.4	69.3 ± 0.4
200 rpm / 36 h	10.3 ± 0.2	19.1 ± 0.4	70.6 ± 0.5
200 rpm / 48 h	31.3 ± 0.3	13.3 ± 0.4	55.4 ± 0.5
250 rpm / 12 h	12.6 ± 0.2	20.9 ± 0.4	66.5 ± 0.4
250 rpm / 24 h	6.4 ± 0.1	38.6 ± 0.5	55.0 ± 0.6
250 rpm / 36 h	11.2 ± 0.2	32.3 ± 0.5	56.5 ± 0.5
250 rpm / 48 h	5.6 ± 0.1	34.8 ± 0.5	59.6 ± 0.5
300 rpm / 12 h	6.1 ± 0.1	44.2 ± 0.6	49.7 ± 0.7
300 rpm / 24 h	5.8 ± 0.1	43.6 ± 0.6	50.6 ± 0.6
300 rpm / 36 h	1.8 ± 0.1	46.6 ± 0.7	51.6 ± 0.7
300 rpm / 48 h	4.2 ± 0.1	52.3 ± 0.6	43.5 ± 0.7

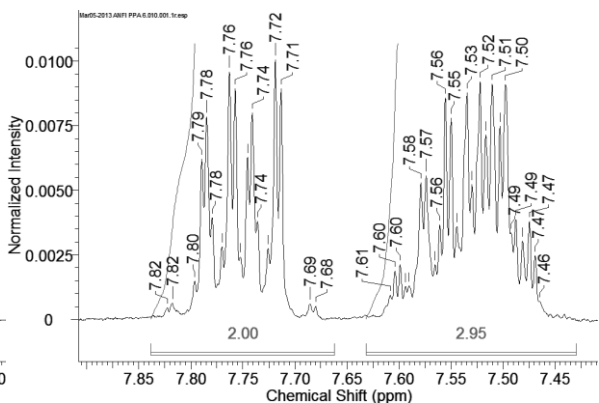
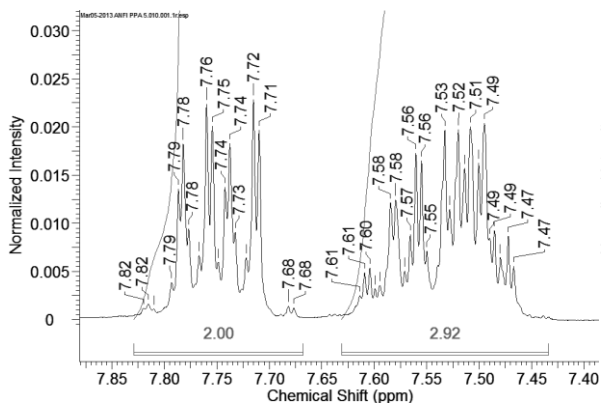
The washing solution of the sample which was exposed to the strongest conditions was analyzed to clarify whether changes occurred at the phenylphosphonic acid due to the milling process. It turned out that the NMR spectra depend on the concentration of the phenylphosphonic acid. For this reason a serial dilution was prepared and analyzed by NMR spectroscopy. The concentration decreases from sample PPA\_1 to PPA\_6. At the end the washing solution was analyzed (Figure S9 – S20). <sup>1</sup>H-, <sup>13</sup>C- and <sup>31</sup>P-NMR spectra show the phenyl phosphonic acid being the only species present in the washing solution, no side or decomposition products were detected. Therefore it can be assumed that the coupling agent is not degraded during the milling process.



**S 9:** PPA\_1:  $^1\text{H-NMR}$  (300 MHz,  $\text{D}_2\text{O}$ ,  $25^\circ\text{C}$ ):  $\delta = 7.44 - 7.31$  (m, 2 H),  $7.18 - 7.03$  (m, 3 H) ppm (left) and PPA\_2:  $^1\text{H-NMR}$  (300 MHz,  $\text{D}_2\text{O}$ ,  $25^\circ\text{C}$ ):  $\delta = 7.65 - 7.51$  (m, 2 H),  $7.43 - 7.28$  (m, 3 H) ppm (right).

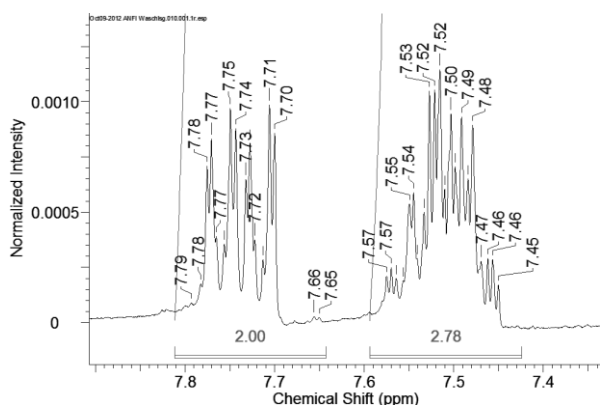


**S 10:** PPA\_3:  $^1\text{H-NMR}$  (300 MHz,  $\text{D}_2\text{O}$ ,  $25^\circ\text{C}$ ):  $\delta = 7.74 - 7.60$  (m, 2 H),  $7.54 - 7.39$  (m, 3 H) ppm (left) and PPA\_4:  $^1\text{H-NMR}$  (300 MHz,  $\text{D}_2\text{O}$ ,  $25^\circ\text{C}$ ):  $\delta = 7.79 - 7.65$  (m, 2 H),  $7.62 - 7.41$  (m, 3 H) ppm (right)

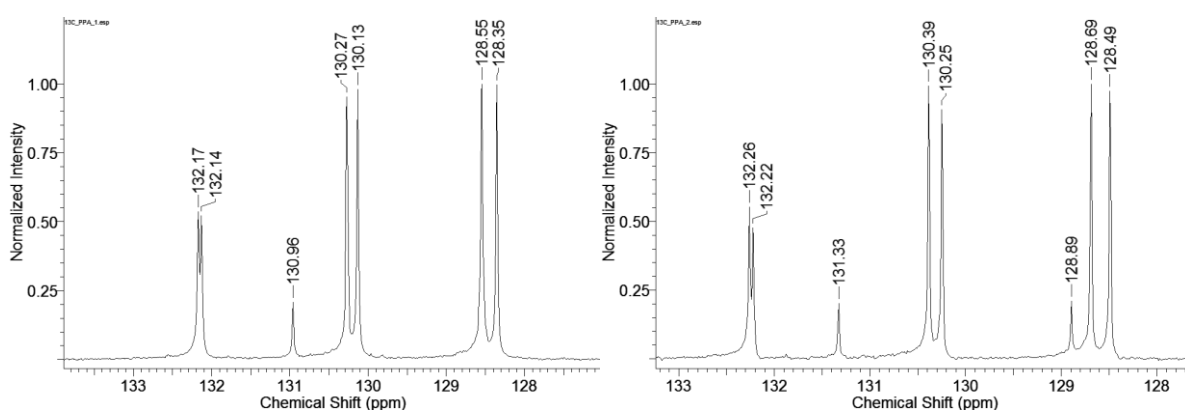


**S 11:** PPA\_5:  $^1\text{H-NMR}$  (300 MHz,  $\text{D}_2\text{O}$ ,  $25^\circ\text{C}$ ):  $\delta = 7.82 - 7.68$  (m, 2 H),  $7.61 - 7.47$  (m, 3 H) ppm (left) and PPA\_6:  $^1\text{H-NMR}$  (300 MHz,  $\text{D}_2\text{O}$ ,  $25^\circ\text{C}$ ):  $\delta = 7.82 - 7.68$  (m, 2 H),  $7.61 - 7.46$  (m, 3 H) ppm (right)

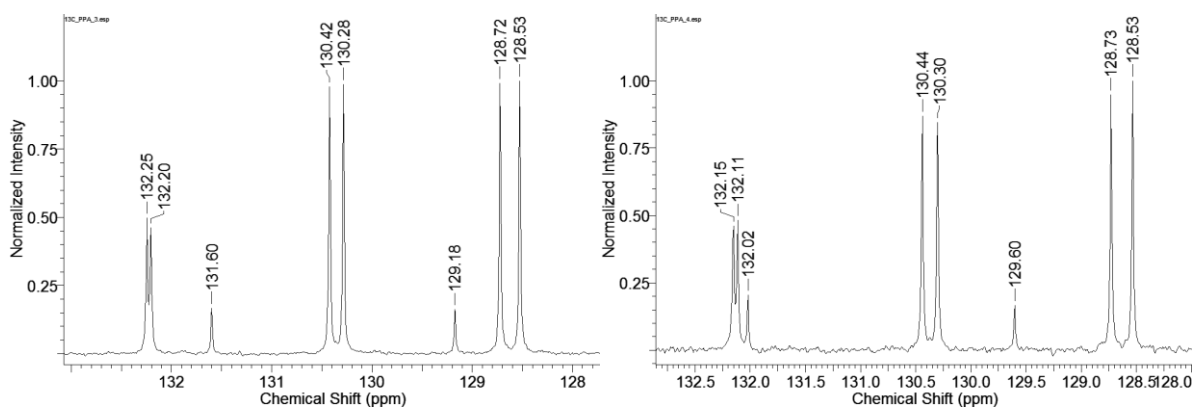




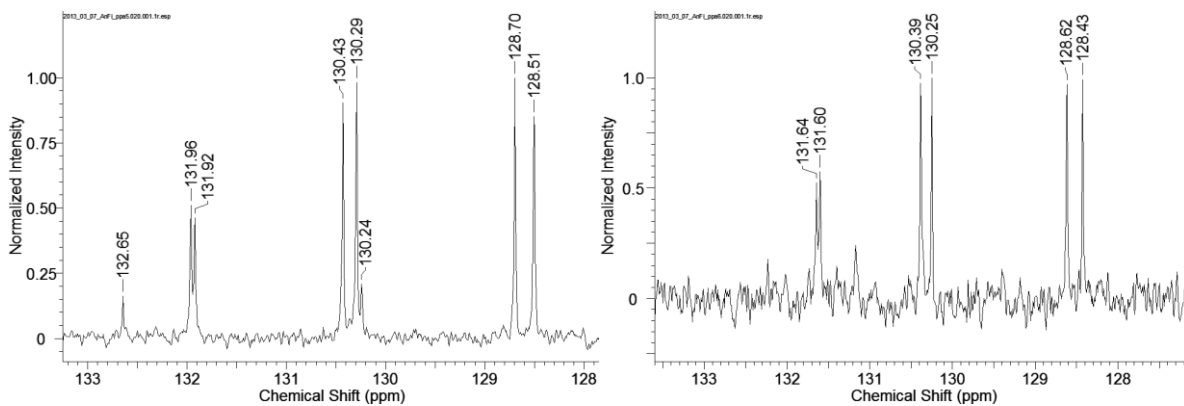
**S 12:** Washing solution:  $^1\text{H-NMR}$  (300 MHz,  $\text{D}_2\text{O}$ ,  $25^\circ\text{C}$ ):  $\delta = 7.79 - 7.65$  (m, 2 H),  $7.57 - 7.45$  (m, 3 H) ppm



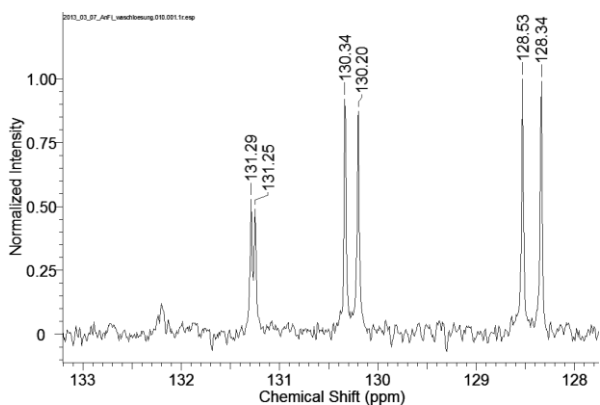
**S 13:** PPA\_1:  $^{13}\text{C NMR}$  (75 MHz,  $\text{D}_2\text{O}$ ,  $25^\circ\text{C}$ ):  $\delta = 132.16$  (d,  $^4\text{J} = 2.75$  Hz, 1 C),  $130.96$  (d,  $^1\text{J} = ?$  Hz (second peak is overlain by the doublet at 128 ppm), 1 C),  $130.20$  (d,  $^3\text{J} = 10.45$  Hz, 2 C),  $128.45$  (d,  $^2\text{J} = 14.86$  Hz, 2 C) ppm (left) and PPA\_2:  $^{13}\text{C NMR}$  (75 MHz,  $\text{D}_2\text{O}$ ,  $25^\circ\text{C}$ ):  $\delta = 132.24$  (d,  $^4\text{J} = 2.75$  Hz, 1 C),  $130.32$  (d,  $^3\text{J} = 10.45$  Hz, 2 C),  $130.11$  (d,  $^1\text{J} = 183.77$  Hz, 1 C),  $128.59$  (d,  $^2\text{J} = 14.85$  Hz, 2 C) ppm (right)



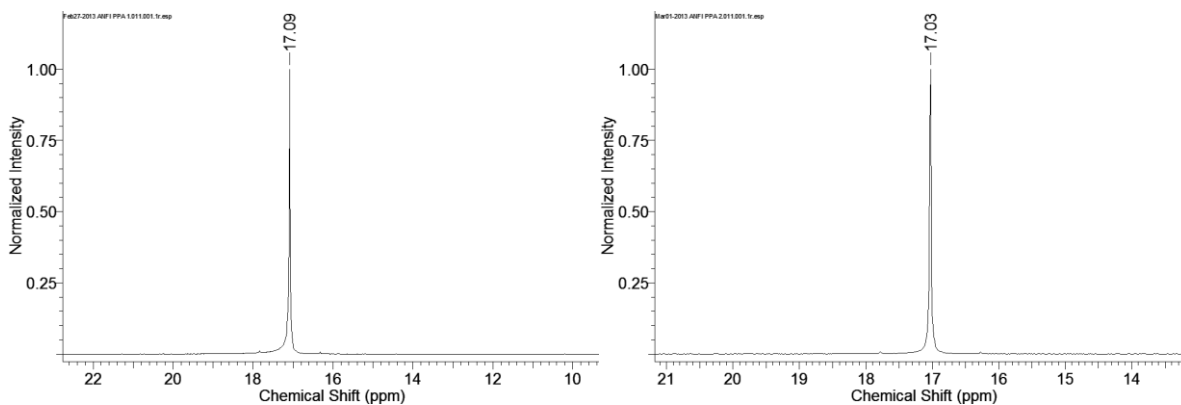
**S 14:** PPA\_3:  $^{13}\text{C NMR}$  (75 MHz,  $\text{D}_2\text{O}$ ,  $25^\circ\text{C}$ ):  $\delta = 132.23$  (d,  $^4\text{J} = 3.30$  Hz, 1 C),  $130.35$  (d,  $^3\text{J} = 10.45$  Hz, 2 C),  $130.39$  (d,  $^1\text{J} = 182.67$  Hz, 1 C),  $128.63$  (d,  $^2\text{J} = 14.85$  Hz, 2 C) ppm (left) and PPA\_4:  $^{13}\text{C NMR}$  (75 MHz,  $\text{D}_2\text{O}$ ,  $25^\circ\text{C}$ ):  $\delta = 132.13$  (d,  $^4\text{J} = 2.75$  Hz, 1 C),  $130.81$  (d,  $^1\text{J} = 182.67$  Hz, 1 C),  $130.37$  (d,  $^3\text{J} = 10.45$  Hz, 2 C),  $128.63$  (d,  $^2\text{J} = 14.85$  Hz, 2 C) ppm (right)



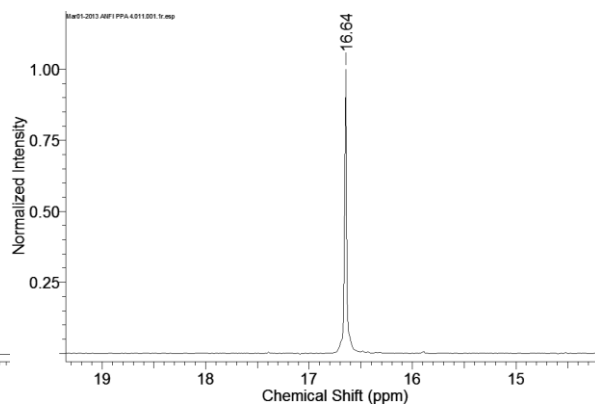
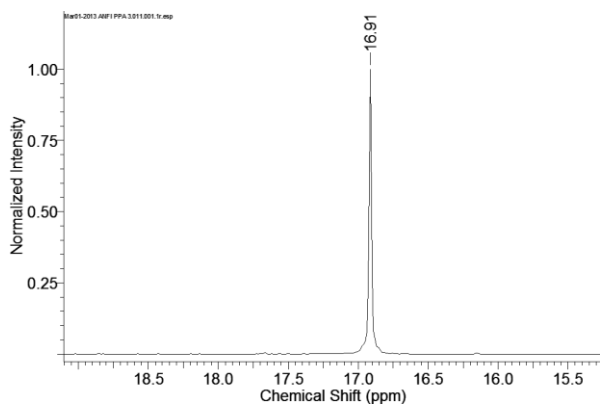
**S 15:** PPA\_5:  $^{13}\text{C}$  NMR (75 MHz,  $\text{D}_2\text{O}$ ,  $25^\circ\text{C}$ ):  $\delta = 131.94$  (d,  $^4J = 3.30$  Hz, 1 C),  $131.45$  (d,  $^1J = 181.56$  Hz, 1 C),  $130.36$  (d,  $^3J = 10.45$  Hz, 2 C),  $128.61$  (d,  $^2J = 14.31$  Hz, 2 C) ppm (left) and PPA\_6:  $^{13}\text{C}$  NMR (75 MHz,  $\text{D}_2\text{O}$ ,  $25^\circ\text{C}$ ):  $\delta = 131.62$  (d,  $^4J = 2.75$  Hz, 1 C),  $130.32$  (d,  $^3J = 10.45$  Hz, 2 C),  $128.53$  (d,  $^2J = 14.30$  Hz, 2 C) ppm, the doublet for the last carbon atom disappears in the background due to the poor concentration (right)



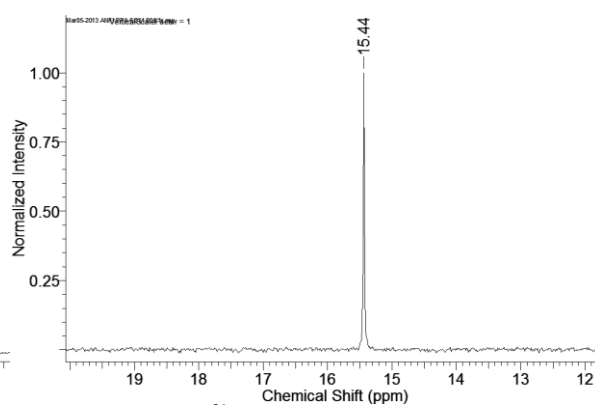
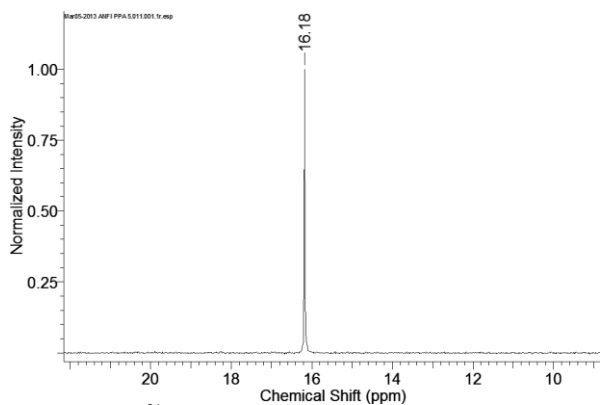
**S 16:** Washing solution:  $^{13}\text{C}$  NMR (75 MHz,  $\text{D}_2\text{O}$ ,  $25^\circ\text{C}$ ):  $\delta = 131.27$  (d,  $^4J = 3.30$  Hz, 1 C),  $130.27$  (d,  $^3J = 10.45$  Hz, 2 C),  $128.44$  (d,  $^2J = 14.30$  Hz, 2 C) ppm, the doublet for the last carbon atom disappears in the background due to the poor concentration



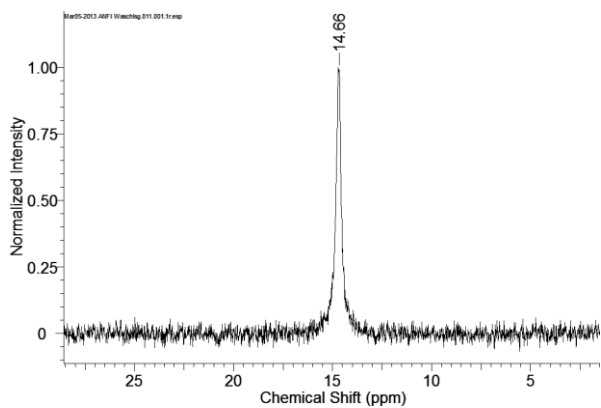
**S 17:** PPA\_1:  $^{31}\text{P}$ -NMR (120 MHz,  $\text{D}_2\text{O}$ ,  $25^\circ\text{C}$ ):  $\delta = 17.09$  ppm (left) and PPA\_2:  $^{31}\text{P}$ -NMR (120 MHz,  $\text{D}_2\text{O}$ ,  $25^\circ\text{C}$ ):  $\delta = 17.03$  ppm (right)



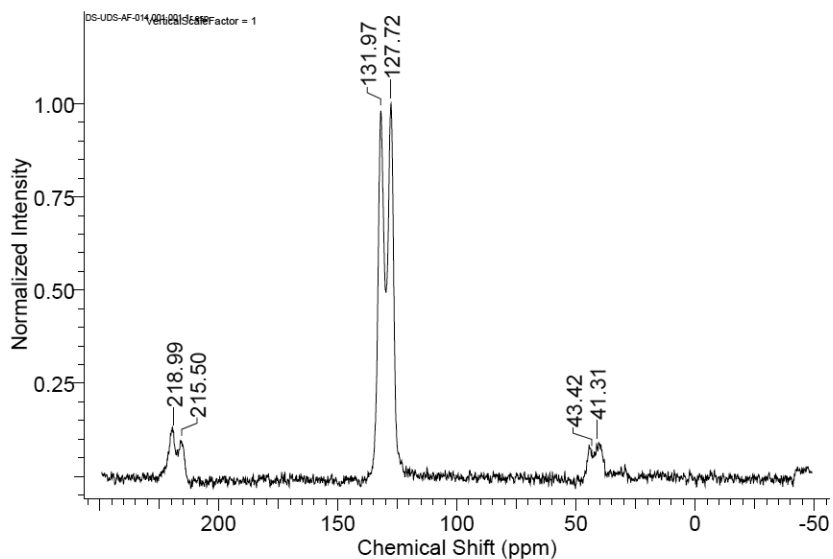
**S 18:** PPA\_3:  $^{31}\text{P}$ -NMR (120 MHz,  $\text{D}_2\text{O}$ ,  $25^\circ\text{C}$ ):  $\delta = 16.91$  ppm (left) and PPA\_4:  $^{31}\text{P}$ -NMR (120 MHz,  $\text{D}_2\text{O}$ ,  $25^\circ\text{C}$ ):  $\delta = 16.64$  ppm (right)



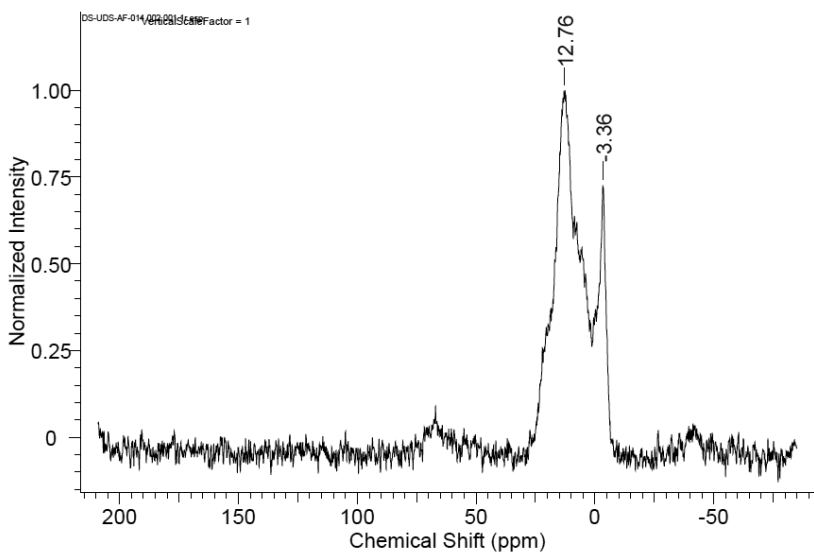
**S 19:** PPA\_5:  $^{31}\text{P}$ -NMR (120 MHz,  $\text{D}_2\text{O}$ ,  $25^\circ\text{C}$ ):  $\delta = 16.18$  ppm (left) and PPA\_6:  $^{31}\text{P}$ -NMR (120 MHz,  $\text{D}_2\text{O}$ ,  $25^\circ\text{C}$ ):  $\delta = 15.44$  ppm (right)



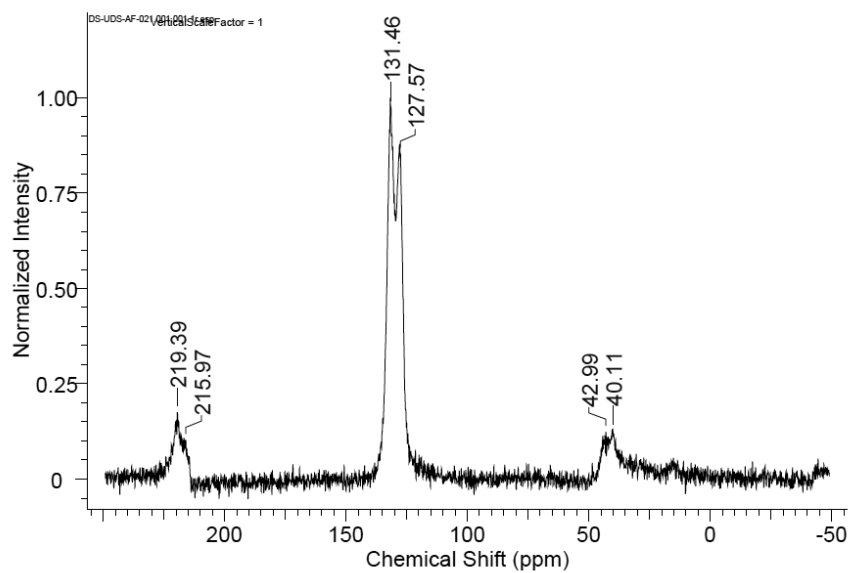
**S 20:** Washing solution:  $^{31}\text{P}$ -NMR (120 MHz,  $\text{D}_2\text{O}$ ,  $25^\circ\text{C}$ ):  $\delta = 14.66$  ppm



S 21:  $^{13}\text{C}$  CP-MAS NMR spectrum, titania milled with phenylphosphonic acid at 200 rpm for 12 h



S 22:  $^{31}\text{P}$  CP-MAS NMR spectrum, titania milled with phenylphosphonic acid at 200 rpm for 12 h



S 23:  $^{13}\text{C}$  CP-MAS NMR spectrum, titania milled with phenylphosphonic acid at 300 rpm for 48 h

**7.2 IMPORTANT REACTION PARAMETERS IN THE  
SYNTHESIS OF PHENYLPHOSPHONIC ACID  
FUNCTIONALIZED TITANIA PARTICLES BY REACTIVE  
MILLING**

Supporting Information belonging to the following publication:

A. Betke, G. Kickelbick, Important reaction parameters in the synthesis of phenylphosphonic acid functionalized titania particles by reactive milling, *New J. Chem.*, **2014**, 38, 1264-1270.

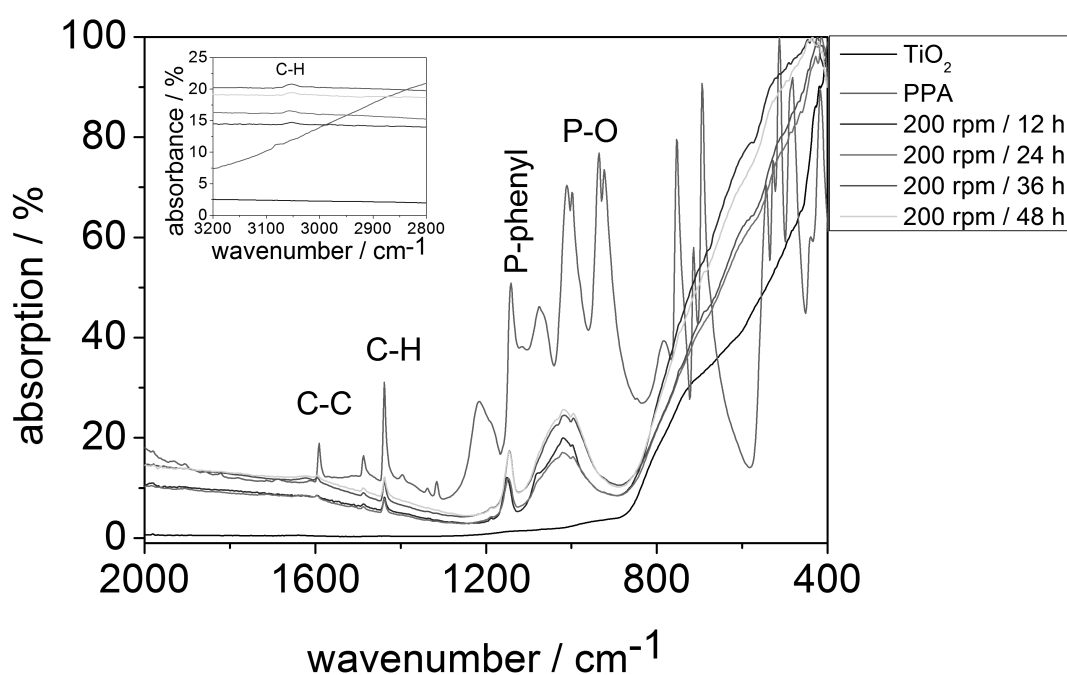
## Supporting Information

# Important Reaction Parameters in the Synthesis of Phenylphosphonic Acid Functionalized Titania Particles by Reactive Milling

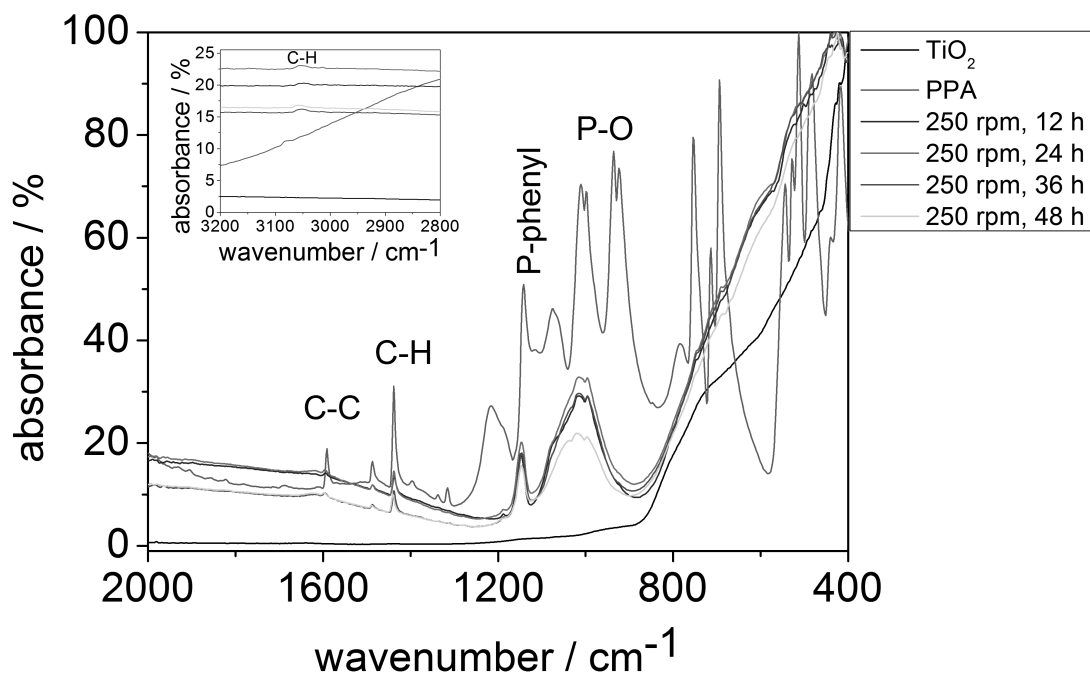
Annika Betke, Guido Kickelbick

Saarland University, Inorganic Chemistry, Am Markt Zeile 3, 66125 Saarbrücken, Germany.

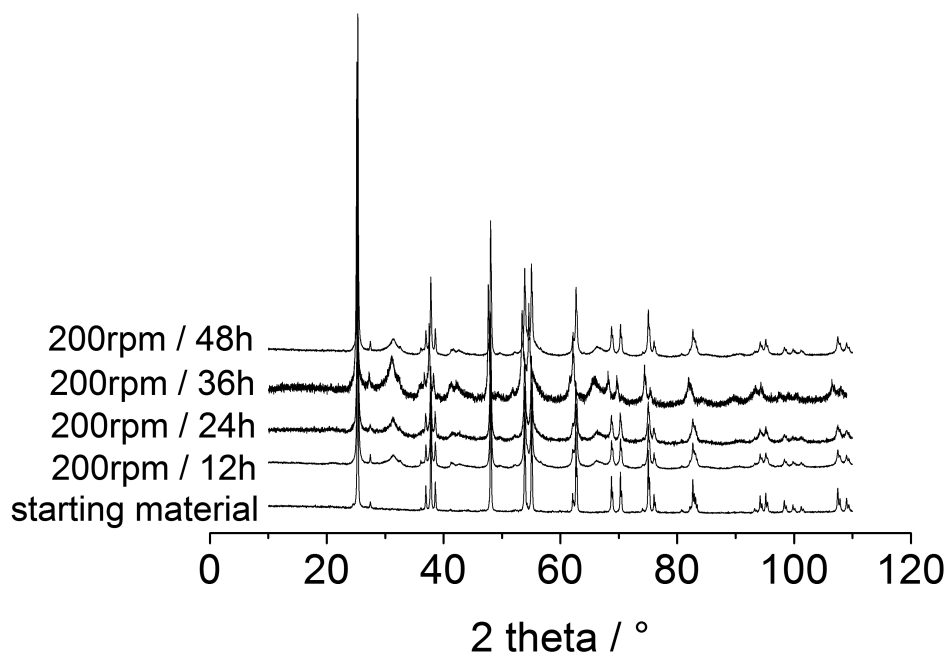
E-Mail: guido.kickelbick@uni-saarland.de



S 1: FTIR-spectra: starting material titania, coupling agent phenylphosphonic acid and samples after the milling process: 200 rpm / 12 h, 200 rpm / 24 h, 200 rpm / 36 h, 200 rpm / 48 h; surface modification has taken place after the milling process, which is indicated by the characteristic bands for aromatic C-C oscillation (1600 cm<sup>-1</sup>), the C-H oscillation (1440 cm<sup>-1</sup>), P-phenyl vibrations (1150 cm<sup>-1</sup>), the wide band at 1000 cm<sup>-1</sup> (P-O region) and the aromatic C-H oscillation at 3050 cm<sup>-1</sup>.

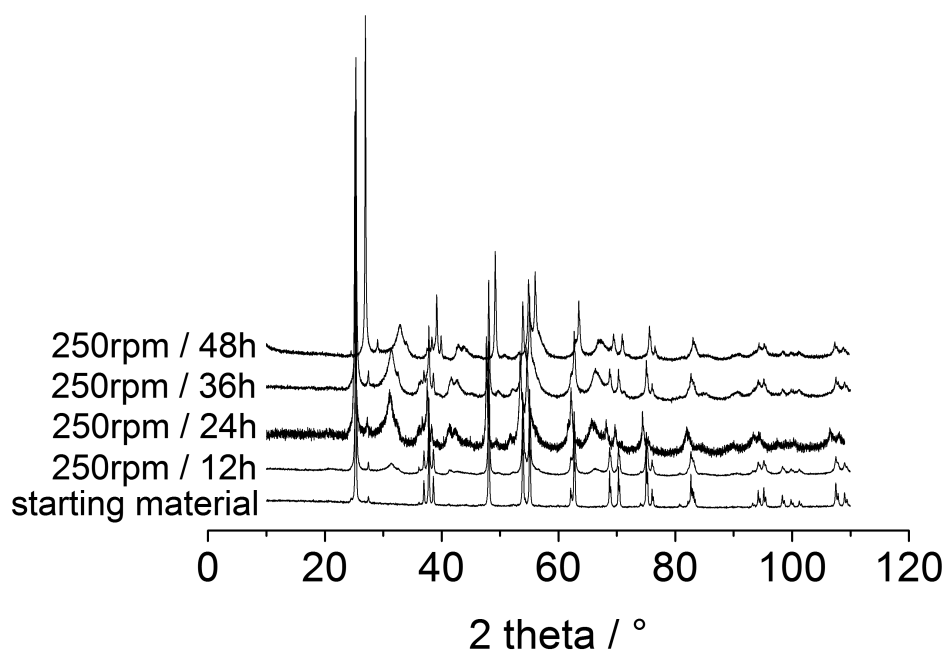


S 2: FTIR-spectra: starting material titania, coupling agent phenylphosphonic acid and samples after the milling process: 250 rpm / 12 h, 250 rpm / 24 h, 250 rpm / 36 h, 250 rpm / 48 h; surface modification has taken place after the milling process, which is indicated by the characteristic bands for aromatic C-C oscillation ( $1600\text{ cm}^{-1}$ ), the C-H oscillation ( $1440\text{ cm}^{-1}$ ), P-phenyl vibrations ( $1150\text{ cm}^{-1}$ ), the wide band at  $1000\text{ cm}^{-1}$  (P-O region) and the aromatic C-H oscillation at  $3050\text{ cm}^{-1}$ .

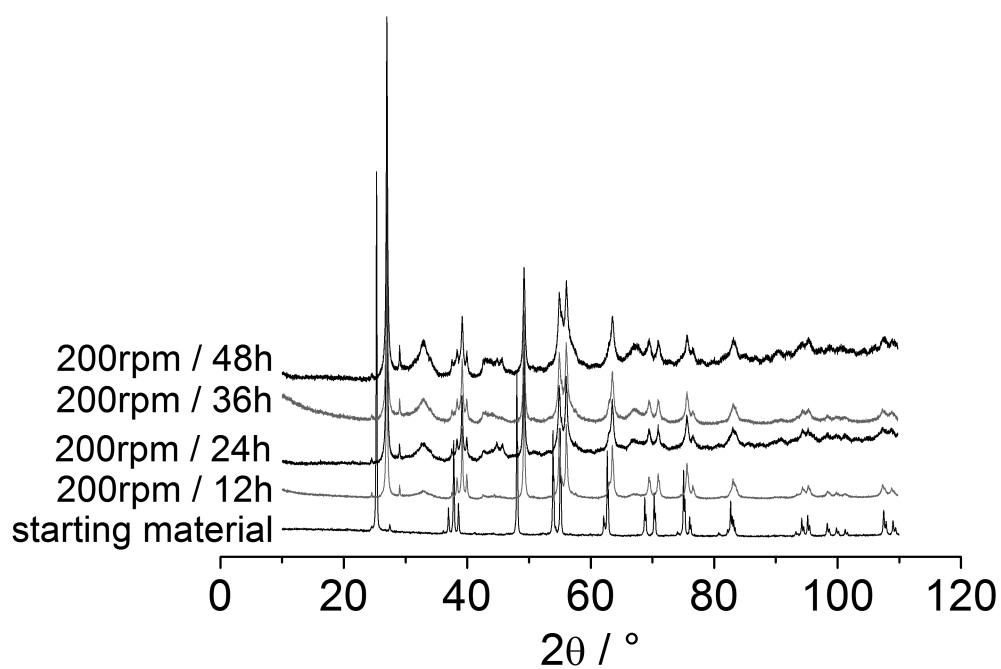


S 3: XRD patterns of the starting material anatase and the samples after milling with phenylphosphonic acid at 200 rpm with different durations. After the milling the presence of high pressure  $\text{TiO}_2$  ( $2\theta = 31^\circ, 42^\circ$  and  $66^\circ$ ) and rutile ( $2\theta = 27^\circ$ ) is indicated by additional reflections.

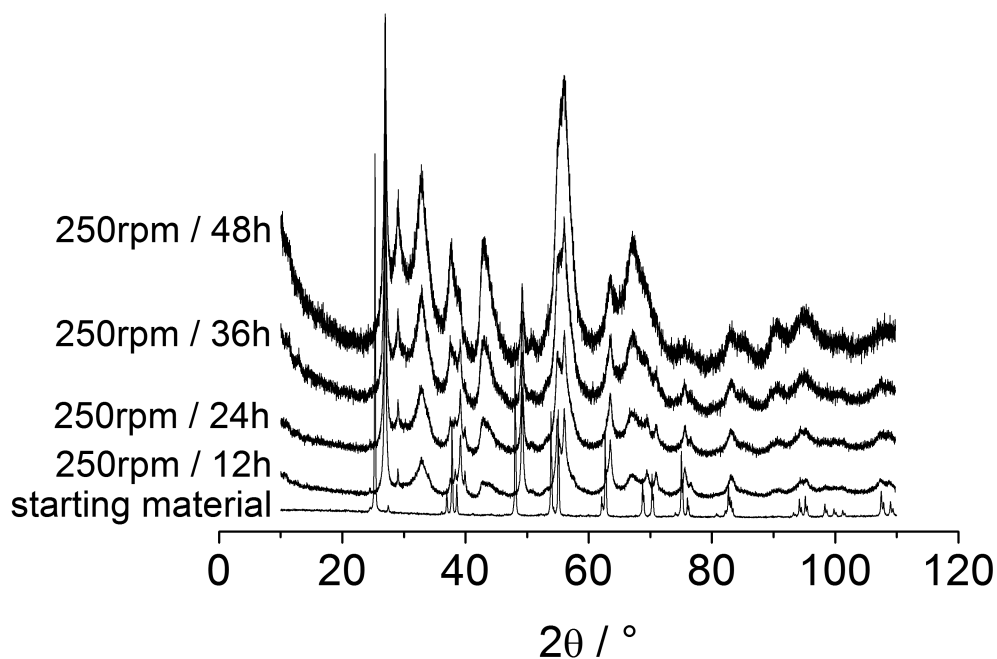




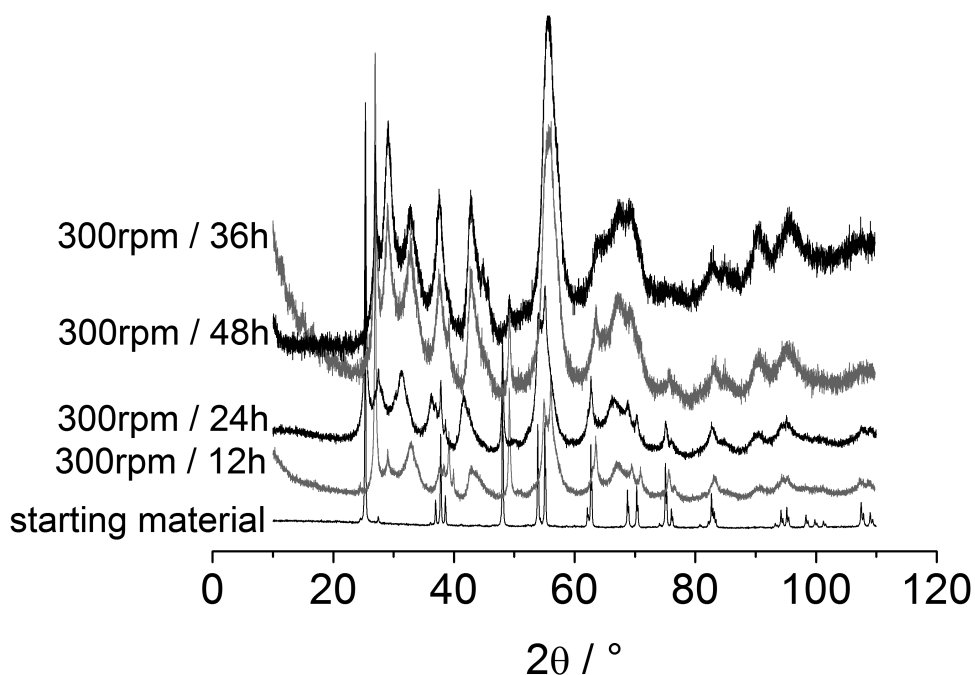
S 4: XRD patterns of the starting material anatase and the samples after milling with phenylphosphonic acid at 250 rpm with different durations. After the milling the presence of high pressure TiO<sub>2</sub> ( $2\theta = 31^\circ$ ,  $42^\circ$  and  $66^\circ$ ) and rutile ( $2\theta = 27^\circ$ ) is indicated by additional reflections.



S 5: XRD patterns of the starting material anatase and the samples after milling without any additive at 200 rpm with different durations. After the milling the presence of high pressure TiO<sub>2</sub> ( $2\theta = 31^\circ$ ,  $42^\circ$  and  $66^\circ$ ) and rutile ( $2\theta = 27^\circ$ ) is indicated by additional reflections.



S 6: XRD patterns of the starting material anatase and the samples after milling without any additive at 250 rpm with different durations. After the milling the presence of high pressure  $\text{TiO}_2$  ( $2\theta = 31^\circ$ ,  $42^\circ$  and  $66^\circ$ ) and rutile ( $2\theta = 27^\circ$ ) is indicated by additional reflections.



S 7: XRD patterns of the starting material anatase and the samples after milling without any additive at 300 rpm with different durations. After the milling the presence of high pressure  $\text{TiO}_2$  ( $2\theta = 31^\circ$ ,  $42^\circ$  and  $66^\circ$ ) and rutile ( $2\theta = 27^\circ$ ) is indicated by additional reflections.

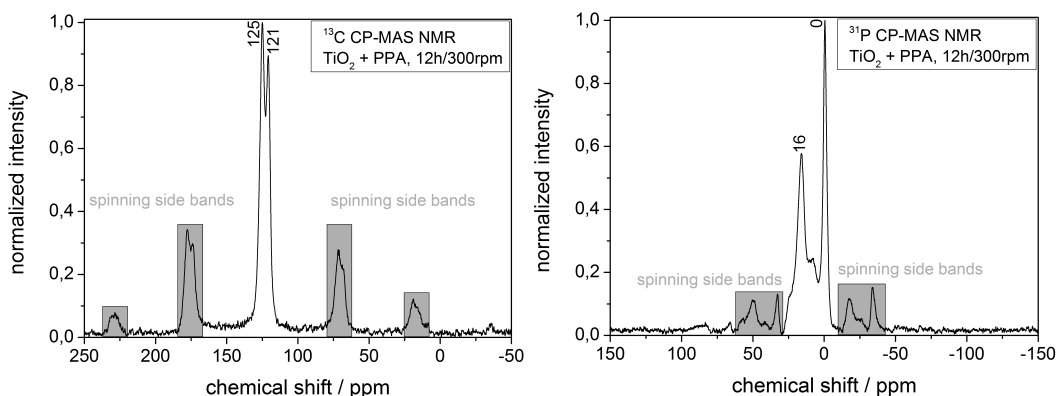
Table S 1: Composition of titania milled with phenylphosphonic acid as coupling agent at specific process parameters

Process parameters	anatase / wt%	rutile / wt%	high pressure / wt%
starting material	$98.2 \pm 0.1$	$1.8 \pm 0.1$	0
200 rpm / 12 h	$69.1 \pm 0.2$	$2.9 \pm 0.1$	$28.0 \pm 0.2$

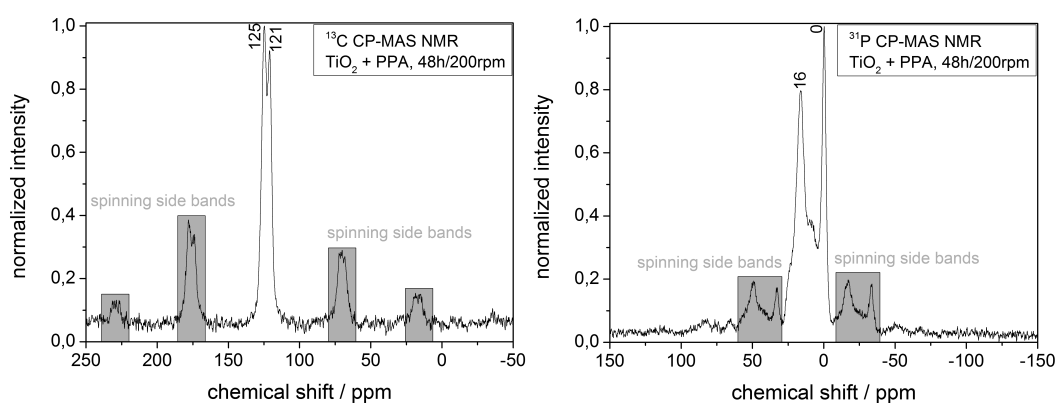
200 rpm / 24 h	64.4 ± 0.3	2.3 ± 0.2	33.3 ± 0.3
200 rpm / 36 h	42.5 ± 0.3	3.8 ± 0.2	53.7 ± 0.3
200 rpm / 48 h	62.4 ± 0.2	3.0 ± 0.1	34.6 ± 0.2
250 rpm / 12 h	71.9 ± 0.2	2.6 ± 0.1	25.5 ± 0.2
250 rpm / 24 h	36.7 ± 0.3	4.1 ± 0.2	59.2 ± 0.3
250 rpm / 36 h	36.9 ± 0.2	3.9 ± 0.1	59.2 ± 0.2
250 rpm / 48 h	41.2 ± 0.3	4.3 ± 0.2	54.2 ± 0.4
300 rpm / 12 h	41.3 ± 0.2	4.3 ± 0.2	54.4 ± 0.2
300 rpm / 24 h	18.3 ± 0.2	4.1 ± 0.1	77.6 ± 0.2
300 rpm / 36 h	13.4 ± 0.2	6.0 ± 0.2	80.6 ± 0.3
300 rpm / 48 h	18.3 ± 0.2	4.1 ± 0.1	77.6 ± 0.2

**Table S 2: Composition of titania milled without any coupling agent at specific process parameters**

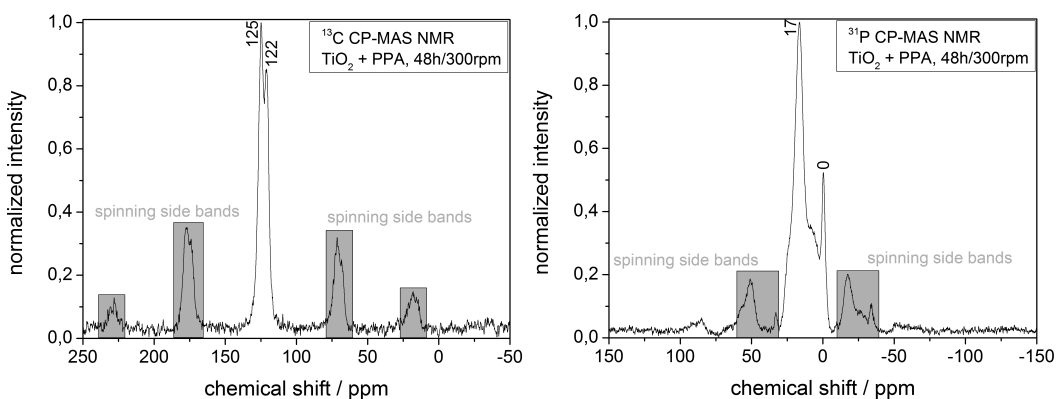
Process parameters	anatase / wt%	rutile / wt%	high pressure / wt%
starting material	98.2 ± 0.1	1.8 ± 0.1	0
200 rpm / 12 h	78.1 ± 0.3	2.4 ± 0.1	19.5 ± 0.3
200 rpm / 24 h	51.9 ± 0.6	2.0 ± 0.1	46.1 ± 0.6
200 rpm / 36 h	50.1 ± 0.4	3.1 ± 0.1	46.8 ± 0.4
200 rpm / 48 h	37.1 ± 0.4	3.8 ± 0.2	59.1 ± 0.4
250 rpm / 12 h	40.7 ± 0.4	3.3 ± 0.2	56.0 ± 0.4
250 rpm / 24 h	23.0 ± 0.3	11.0 ± 0.3	66.0 ± 0.4
250 rpm / 36 h	12.4 ± 0.2	18.0 ± 0.5	69.6 ± 0.5
250 rpm / 48 h	6.1 ± 0.1	26.6 ± 0.5	67.3 ± 0.5
300 rpm / 12 h	23.6 ± 0.2	14.5 ± 0.4	61.9 ± 0.4
300 rpm / 24 h	14.6 ± 0.3	19.0 ± 0.6	66.4 ± 0.6
300 rpm / 36 h	6.4 ± 0.1	36.1 ± 0.5	57.5 ± 0.5
300 rpm / 48 h	2.4 ± 0.1	38.0 ± 0.6	59.6 ± 0.6



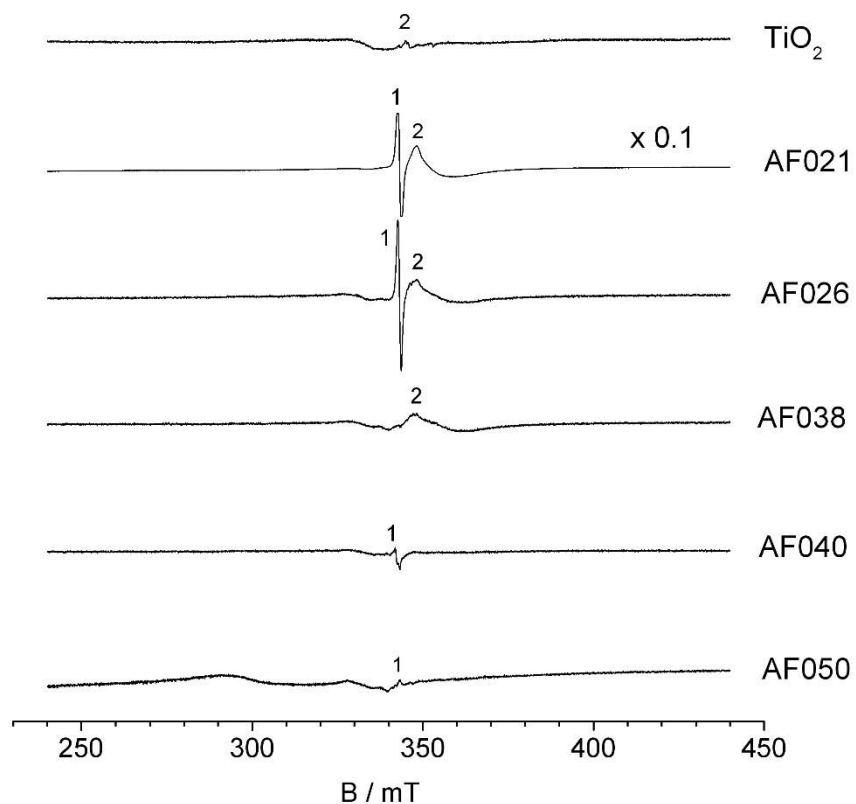
**S 8: Titania milled with phenylphosphonic acid for 12 h at 300 rpm,  $^{13}\text{C}$  solid state NMR (left) and  $^{31}\text{P}$  solid state NMR (right)**



**S 9: Titania milled with phenylphosphonic acid for 48 h at 200 rpm,  $^{13}\text{C}$  solid state NMR (left) and  $^{31}\text{P}$  solid state NMR (right)**



**S 10: Titania milled with phenylphosphonic acid for 48 h at 300 rpm,  $^{13}\text{C}$  solid state NMR (left) and  $^{31}\text{P}$  solid state NMR (right)**



**S 11: ESR spectra of the starting material  $\text{TiO}_2$  and samples after the milling process. Titania milled with phenylphosphonic acid in a WC/Co-hard metal grinding bowl (AF021) and in a zirconia grinding bowl (AF026), titania milled with dodecylphosphonic acid in a zirconia grinding bowl (AF038), titanina milled without any additive in a WC/Co-hard metal grinding bowl (AF050) and in a zirconia grinding bowl (AF040).**

**7.3 LONG ALKYL CHAIN ORGANOPHOSPHORUS COUPLING  
AGENTS FOR *IN SITU* SURFACE FUNCTIONALIZATION BY  
REACTIVE MILLING, *INORGANICS***

Supporting Information belonging to the following publication:

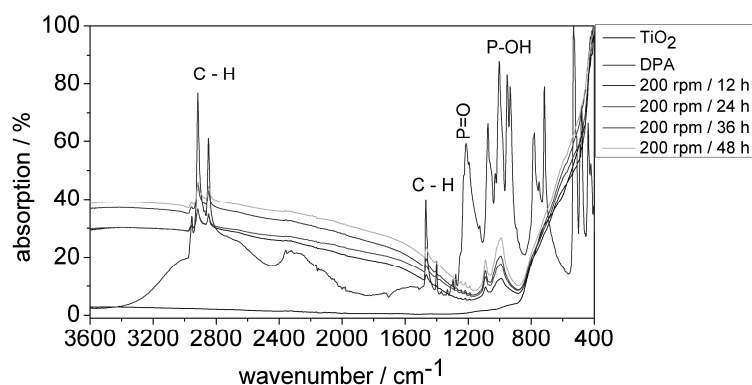
A. Betke, G. Kickelbick, Long alkyl chain organophosphorus coupling agents for *in situ* surface functionalization by reactive milling, *Inorganics*, **2014**, *submitted*.

## Supporting Information

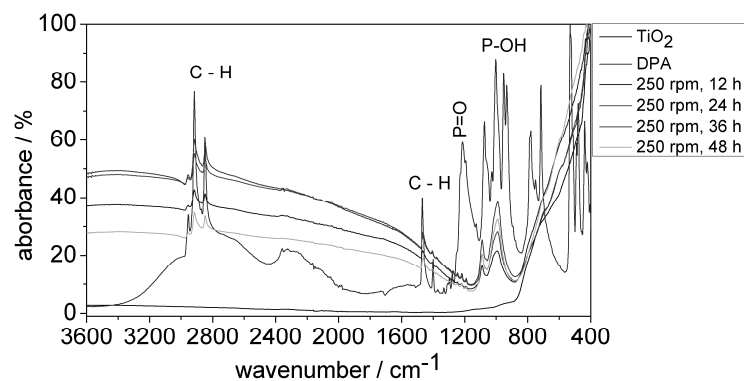
### Long alkyl chain organophosphorus coupling agents for *in situ* surface functionalization by reactive milling

Annika Betke, Guido Kickelbick\*

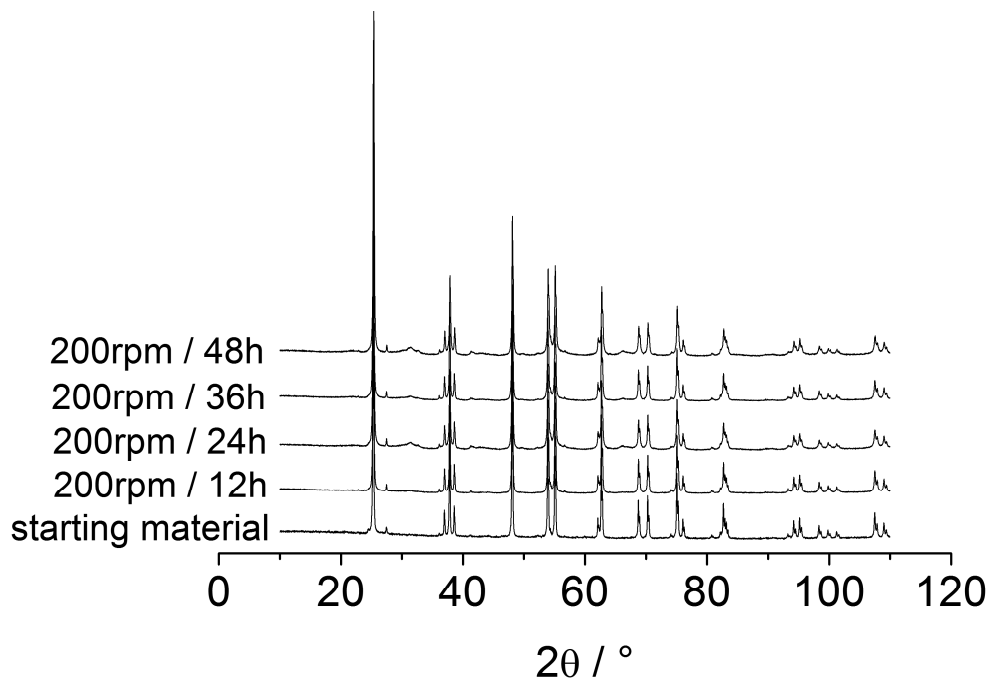
Inorganic Chemistry, Saarland University, Am Markt Zeile 3, 66125 Saarbrücken, Germany;  
E-Mail: guido.kickelbick@uni-saarland.de



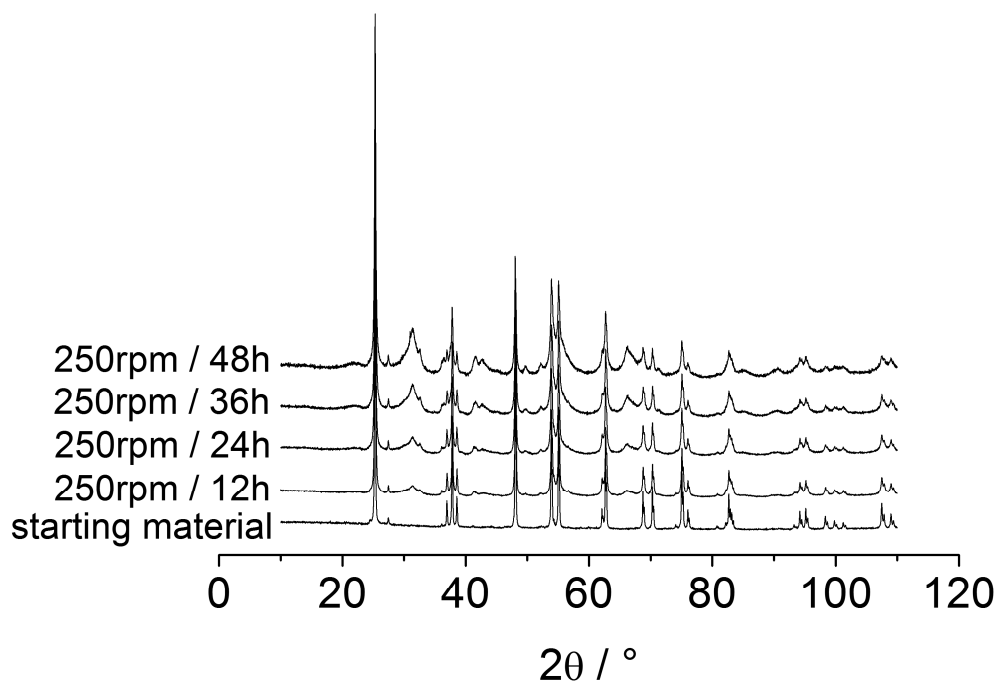
S 1: FTIR-spectra of the starting material titania, coupling agent dedecylphosphonic acid and samples after the milling process at 200 rpm; surface modification has taken place after the milling process, which is indicated by the characteristic bands for the C-H oscillation ( $1440 \text{ cm}^{-1}$  and  $2900 \text{ cm}^{-1}$ ) and the wide band at  $1000 \text{ cm}^{-1}$  (P-O region).



S 2: FTIR-spectra of the starting material titania, coupling agent dedecylphosphonic acid and samples after the milling process at 250 rpm; surface modification has taken place after the milling process, which is indicated by the characteristic bands for the C-H oscillation ( $1440 \text{ cm}^{-1}$  and  $2900 \text{ cm}^{-1}$ ) and the wide band at  $1000 \text{ cm}^{-1}$  (P-O region).



S 3: XRD patterns of the starting material anatase and the samples after milling with dedecylphosphonic acid at 200 rpm with different durations. After the milling the presence of high pressure  $\text{TiO}_2$  ( $2\theta = 31^\circ$ ,  $42^\circ$  and  $66^\circ$ ) and rutile ( $2\theta = 27^\circ$ ) is indicated by additional reflections.



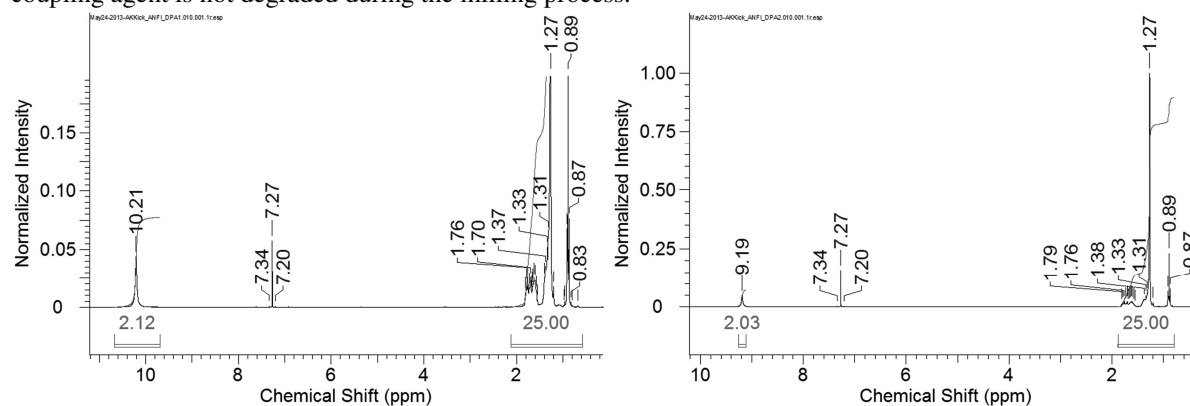
S 4: XRD patterns of the starting material anatase and the samples after milling with phenylphosphonic acid at 250 rpm with different durations. After the milling the presence of high pressure  $\text{TiO}_2$  ( $2\theta = 31^\circ$ ,  $42^\circ$  and  $66^\circ$ ) and rutile ( $2\theta = 27^\circ$ ) is indicated by additional reflections.



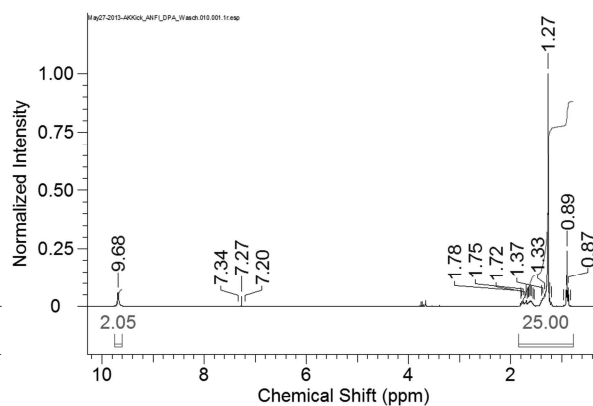
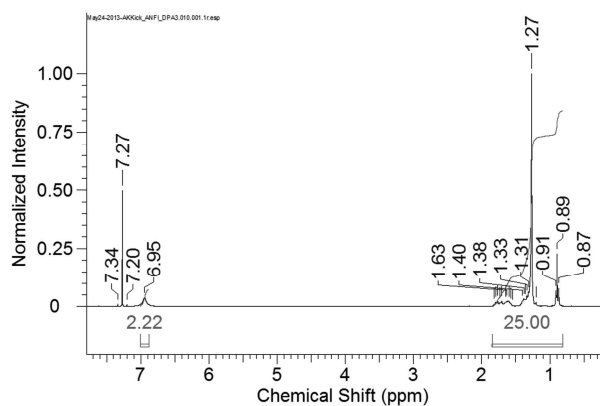
**Table S 1: Composition of titania milled with dodecylphosphonic acid as coupling agent at specific process parameters**

Process parameters	anatase / wt%	rutile / wt%	high pressure / wt%
starting material	98.2 ± 0.1	1.8 ± 0.1	0
200 rpm / 12 h	91.9 ± 0.2	1.8 ± 0.1	6.3 ± 0.2
200 rpm / 24 h	80.6 ± 0.2	2.4 ± 0.1	16.9 ± 0.2
200 rpm / 36 h	86.8 ± 0.2	1.9 ± 0.1	11.3 ± 0.2
200 rpm / 48 h	77.8 ± 0.3	2.6 ± 0.1	19.6 ± 0.3
250 rpm / 12 h	73.9 ± 0.2	2.5 ± 0.1	23.6 ± 0.2
250 rpm / 24 h	64.9 ± 0.2	3.0 ± 0.1	32.1 ± 0.2
250 rpm / 36 h	50.8 ± 0.2	3.6 ± 0.1	45.6 ± 0.2
250 rpm / 48 h	40.6 ± 0.2	3.9 ± 0.2	55.5 ± 0.2
300 rpm / 12 h	66.5 ± 0.2	2.9 ± 0.1	30.6 ± 0.2
300 rpm / 24 h	55.0 ± 0.2	3.5 ± 0.1	41.5 ± 0.2
300 rpm / 36 h	41.3 ± 0.2	3.4 ± 0.1	55.3 ± 0.2
300 rpm / 48 h	24.9 ± 0.2	3.5 ± 0.2	71.6 ± 0.2

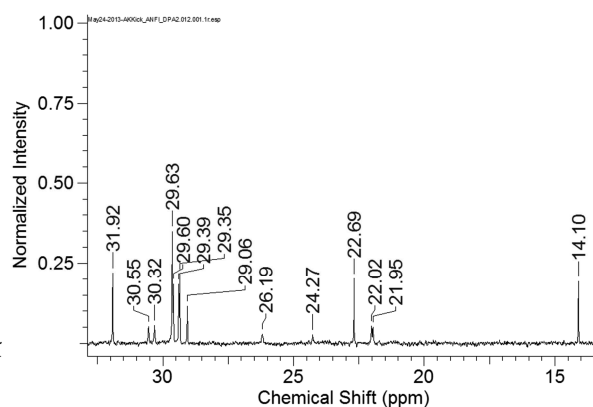
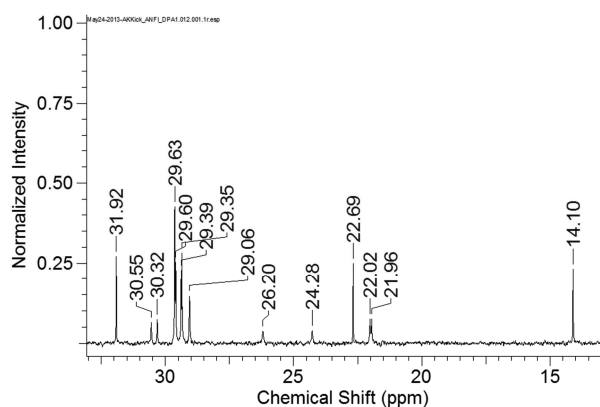
The washing solution of the sample which was exposed to the strongest conditions was analyzed to clarify whether changes occurred at the dodecylphosphonic acid due to the milling process. It turned out that the NMR spectra depend on the concentration of the dodecylphosphonic acid. For this reason a serial dilution was prepared and analyzed by NMR spectroscopy. The concentration decreases from sample DPA\_1 to DPA\_3. At the end the washing solution was analyzed (Figure S9 – S20). <sup>1</sup>H-, <sup>13</sup>C- and <sup>31</sup>P-NMR spectra show the phenyl phosphonic acid being the only species present in the washing solution, no side or decomposition products were detected. The few additional peaks are due to residues of the washing agent ethanol. Therefore it can be assumed that the coupling agent is not degraded during the milling process.



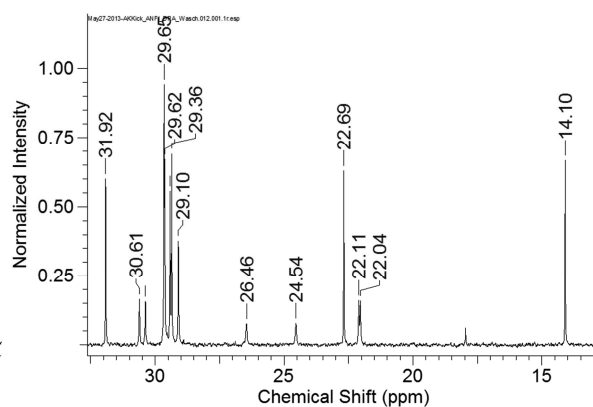
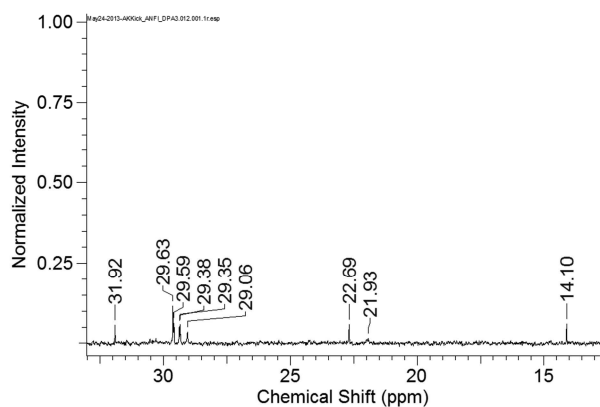
**S 5: DPA\_1: <sup>1</sup>H-NMR (300 MHz, CDCl<sub>3</sub>, 25°C): δ = 1.76 – 0.83 (25 H), 10.21 (2 H) ppm (left) and DPA\_2: <sup>1</sup>H-NMR (300 MHz, CDCl<sub>3</sub>, 25°C): δ = 1.79 – 0.87 (25 H), 9.19 (2 H) ppm (right).**



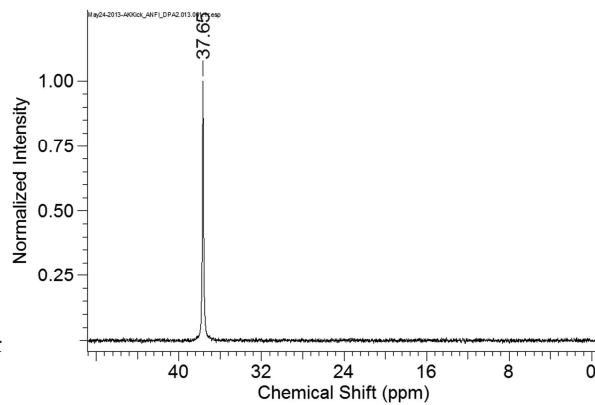
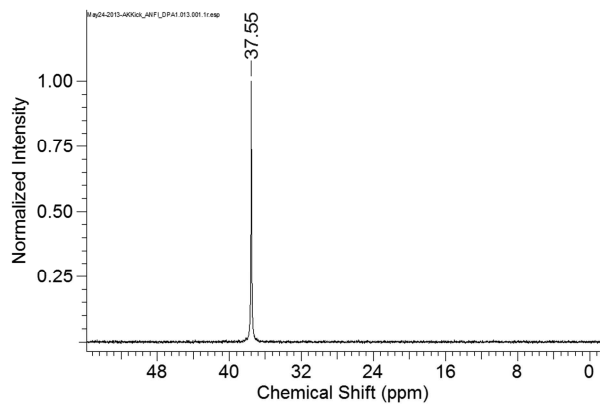
**S 6: DPA\_3:  $^1\text{H}$ -NMR (300 MHz,  $\text{CDCl}_3$ ,  $25^\circ\text{C}$ ):  $\delta = 1.63 - 0.87$  (25 H),  $6.95$  (2 H) ppm (left) and washing solution:  $^1\text{H}$ -NMR (300 MHz,  $\text{CDCl}_3$ ,  $25^\circ\text{C}$ ):  $\delta = 1.78 - 0.87$  (25 H),  $9.68$  (2 H) ppm (right)**



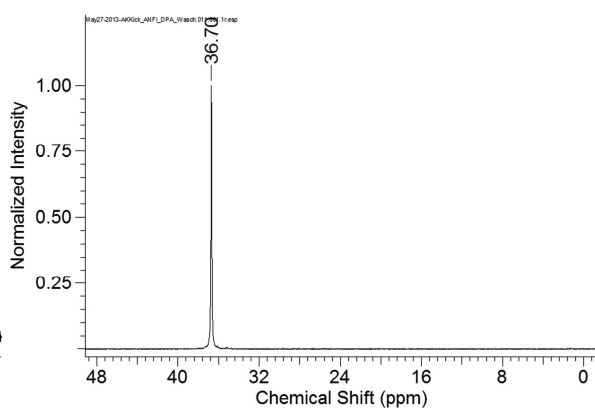
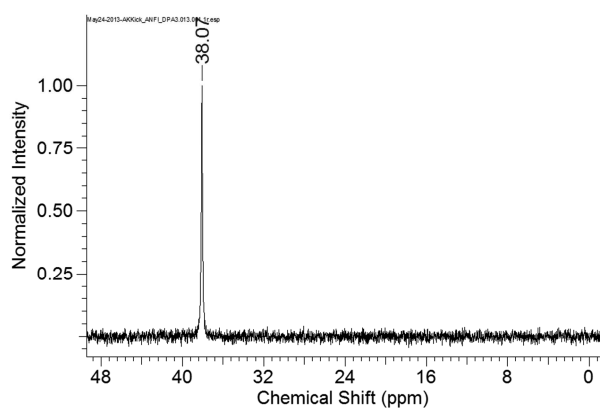
**S 7: DPA\_1:  $^{13}\text{C}$  NMR (75 MHz,  $\text{CDCl}_3$ ,  $25^\circ\text{C}$ ):  $\delta = 25.24$  (d,  $^1J = 145.25$  Hz, 1 C),  $30.44$  (d,  $^2J = 17.06$  Hz, 1 C),  $14.10$  (1 C),  $21.96$  (1 C),  $22.02$  (1 C),  $22.69$  (1 C),  $29.06$  (1 C),  $29.35$  (1 C),  $29.39$  (1 C),  $29.60$  (1 C),  $29.63$  (1 C),  $31.92$  (1 C) (left) and DPA\_2:  $^{13}\text{C}$  NMR (75 MHz,  $\text{CDCl}_3$ ,  $25^\circ\text{C}$ ):  $\delta = 25.23$  (d,  $^1J = 145.25$  Hz, 1 C),  $30.44$  (d,  $^2J = 17.06$  Hz, 1 C),  $14.10$  (1 C),  $21.95$  (1 C),  $22.02$  (1 C),  $22.69$  (1 C),  $29.06$  (1 C),  $29.35$  (1 C),  $29.39$  (1 C),  $29.60$  (1 C),  $29.63$  (1 C),  $31.92$  (1 C) (right)**



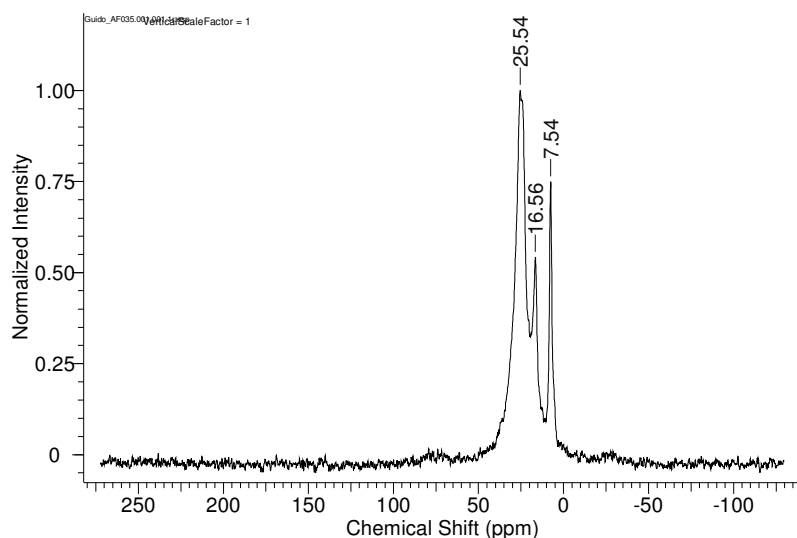
**S 8: DPA\_3:  $^{13}\text{C}$  NMR (75 MHz,  $\text{CDCl}_3$ ,  $25^\circ\text{C}$ ):  $\delta = 14.10$  (1 C),  $21.93$  (1 C),  $22.69$  (1 C),  $29.06$  (1 C),  $29.35$  (1 C),  $29.38$  (1 C),  $29.59$  (1 C),  $29.63$  (1 C),  $31.92$  (1 C), there are some peaks missing which is due to the poor concentration of the solution (left) and washing solution:  $^{13}\text{C}$  NMR (75 MHz,  $\text{CDCl}_3$ ,  $25^\circ\text{C}$ ):  $\delta = 25.50$  (d,  $^1J = 144.70$  Hz, 1 C),  $30.50$  (d,  $^2J = 17.06$  Hz, 1 C),  $14.10$  (1 C),  $22.04$  (1 C),  $22.11$  (1 C),  $22.69$  (1 C),  $29.10$  (1 C),  $29.36$  (1 C),  $29.42$  (1 C),  $29.62$  (1 C),  $29.65$  (1 C),  $31.92$  (1 C) (right)**



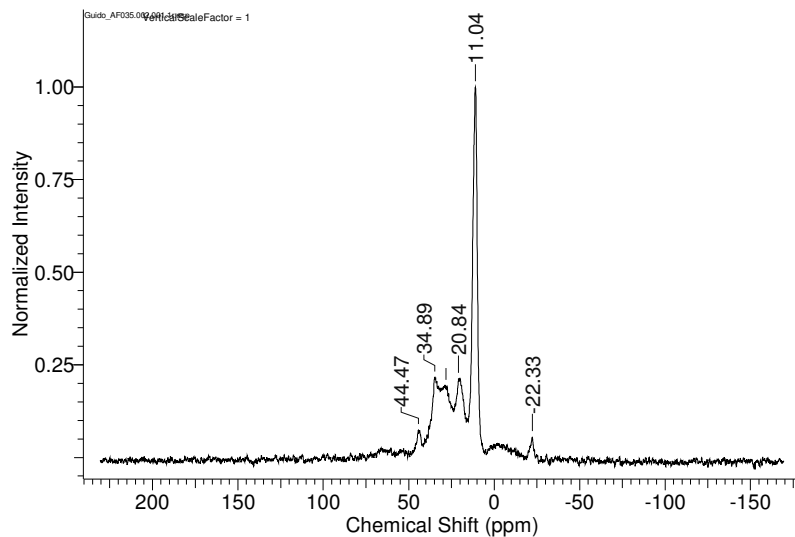
**S 9: DPA\_1:  $^{31}\text{P}$ -NMR (120 MHz,  $\text{CDCl}_3$ ,  $25^\circ\text{C}$ ):  $\delta = 37.55$  ppm (left) and DPA\_2:  $^{31}\text{P}$ -NMR (120 MHz,  $\text{CDCl}_3$ ,  $25^\circ\text{C}$ ):  $\delta = 37.65$  ppm (right)**



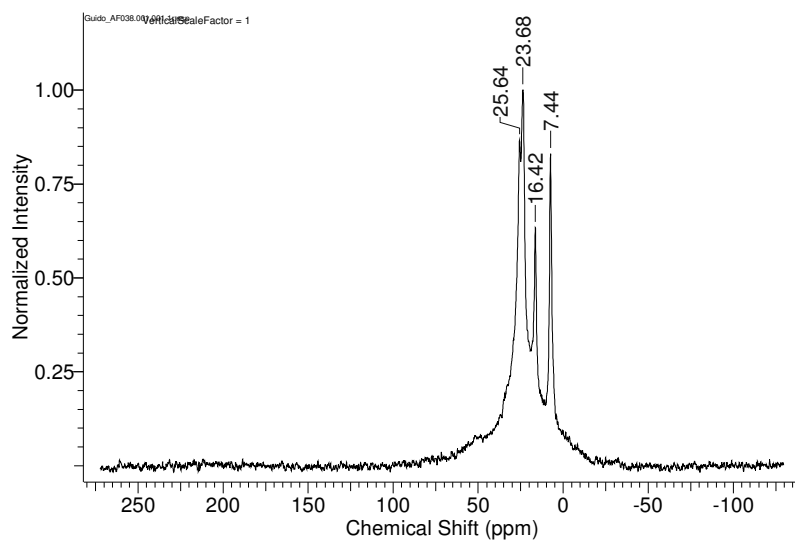
**S 10: DPA\_3:  $^{31}\text{P}$ -NMR (120 MHz,  $\text{CDCl}_3$ ,  $25^\circ\text{C}$ ):  $\delta = 38.07$  ppm (left) and washing solution:  $^{31}\text{P}$ -NMR (120 MHz,  $\text{CDCl}_3$ ,  $25^\circ\text{C}$ ):  $\delta = 36.70$  ppm (right)**



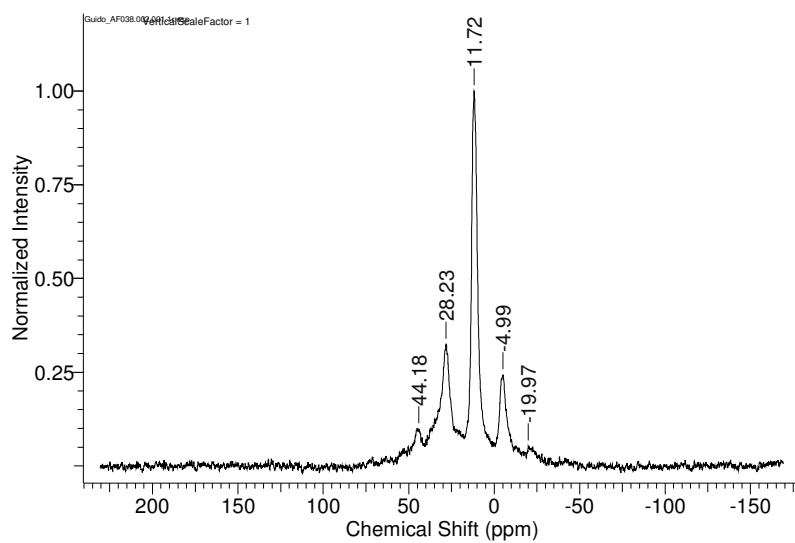
**S 11:  $^{13}\text{C}$  CP-MAS NMR spectrum, titania milled with dodecylphosphonic acid at 300 rpm for 12 h**



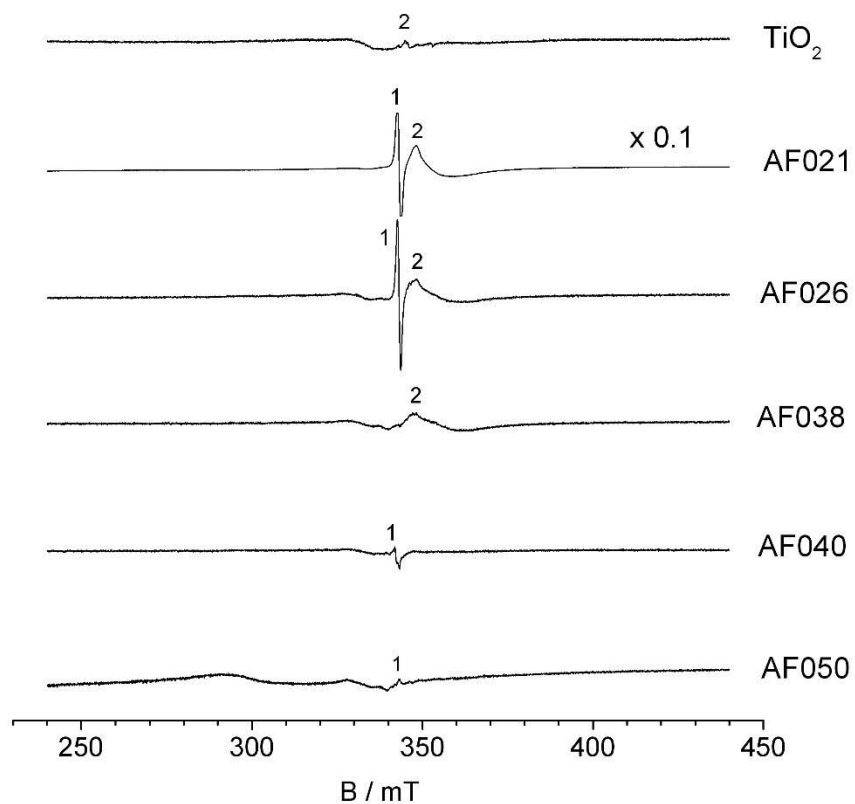
S 12:  $^{31}\text{P}$  CP-MAS NMR spectrum, titania milled with dodecylphosphonic acid at 300 rpm for 12 h



S 13:  $^{13}\text{C}$  CP-MAS NMR spectrum, titania milled with dodecylphosphonic acid at 300 rpm for 48 h



S 14:  $^{31}\text{P}$  CP-MAS NMR spectrum, titania milled with dodecylphosphonic acid at 300 rpm for 48h



**S 15: ESR spectra of the starting material  $\text{TiO}_2$  and samples after the milling process. Titania milled with phenylphosphonic acid in a WC/Co-hard metal grinding bowl (AF021) and in a zirconia grinding bowl (AF026), titania milled with dodecylphosphonic acid in a zirconia grinding bowl (AF038), titanina milled without any additive in a WC/Co-hard metal grinding bowl (AF050) and in a zirconia grinding bowl (AF040).**

## **8. ACKNOWLEDGMENT**

First of all, I would like to thank my Ph.D. supervisor Prof. Dr. G. Kickelbick for providing me the opportunity to undertake my Ph.D. thesis in his research group. Furthermore, I would like to thank him for the very interesting and ongoing research topic as well as for the constant support and assistance.

In addition I would like to thank PD Dr.-Ing. habil. G. Falk for the friendly acquisition of the second report.

I would also like to thank Sylvia Beetz and Hermann Recktenwald for the installation of the microjet reactor system and for solving every kind of technical problems. Furthermore, I would like to thank Dr. Robert Haberkorn for the patient assistance regarding to the X-ray powder measurements and analysis as well as for the assistance relating to the RFA and REM measurements, Susanne Harling for the CHN analysis and Nina Zahn for the TEM measurements. In addition, I would like to thank Tom Engel for the admission and qualified advices to every kind of arising problems regarding to the all instruments of the working group.

I would like to thank Matthias Gasthauer for the nice society in the laboratory and the whole working group for the enjoyable collaboration during my time there.

Last but not least I would like to thank Dr. Ulf Betke for the thoroughly proofreading of this work.

Finally, I would like to express special thanks to my whole family, especially to my husband, for their throughout loving support and encouragement during my complete Ph.D. studies.